

**The Potential of Vortex Amplifiers to  
Improve Mixture Preparation in Spark  
Ignition Engines**

*A thesis submitted for the degree of Doctor of Philosophy*

at

**The University of Sheffield**

**Department of Mechanical Engineering**

**T.J. Scanlon**

**November 1997**



## IMAGING SERVICES NORTH

Boston Spa, Wetherby  
West Yorkshire, LS23 7BQ  
[www.bl.uk](http://www.bl.uk)

**BLANK PAGE IN ORIGINAL**



## IMAGING SERVICES NORTH

Boston Spa, Wetherby  
West Yorkshire, LS23 7BQ  
[www.bl.uk](http://www.bl.uk)

**ORIGINAL COPY TIGHTLY  
BOUND**



## IMAGING SERVICES NORTH

Boston Spa, Wetherby  
West Yorkshire, LS23 7BQ  
[www.bl.uk](http://www.bl.uk)

**BEST COPY AVAILABLE.**

**VARIABLE PRINT QUALITY**

## **I. ACKNOWLEDGEMENTS**

My thanks go to:-

My supervisor Robin Saunders for his tireless support during the duration of this work. He was constantly available to offer help and advice throughout the project.

The technical staff in the Department of Mechanical Engineering at Sheffield University, and in particular to Malcolm Nettleship for his work on my test rig.

The Department of Mechanical and Process Engineering at Sheffield University for funding this research.

And finally my family, friends and fellow students who have helped and supported me in ways too numerous to list here.

## II. SUMMARY

Spark ignition engines are a significant source of air pollution. Emissions are most severe in the period after the engine has been started from cold. This is because fuel enrichment is needed to ensure reliable combustion in the cold cylinder. The problem is compounded by the exhaust treatment catalyst not reaching operating temperature until some minutes after starting. As the majority of car usage is for short journeys, engines spend much of their time in this high emission operating regime.

One route to reducing emissions is to improve mixture preparation. This is particularly effective after a cold start as less enrichment is required to ensure combustion. The aim of this project has been to evaluate a Vortex Amplifier as a route to improving mixture preparation.

The vortex amplifier is a no moving parts fluidic control device. It regulates a large volume supply flow by imparting swirl to it with a small volume control flow. The control flow vortex creates a region of highly turbulent flow at the device outlet which possesses the potential to atomise a fuel spray.

The VA has been tested experimentally. The sprays produced by the vortex amplifier were measured by a laser diffraction technique. Numerical analysis has also been undertaken to determine the motion of droplets within the vortex chamber and the potential of the flow to disrupt a fuel spray.

The vortex amplifier has been found to be a highly effective atomiser. It produces sprays with a Sauter mean diameter approximately half the size of the best current technology. However the spray impacts on the walls of any pipework downstream of the VA due to the high tangential velocities in the flow exiting the VA. This problem currently precludes engine use, but suggestions for improving the situation are contained in the recommendations for future work.

### III. NOMENCLATURE

Many subsidiary variables are defined locally and are not included in this list.

#### Variables

|          |                                       |
|----------|---------------------------------------|
| A        | area                                  |
| $C_D$    | discharge coefficient                 |
| $c_p$    | specific heat at constant pressure    |
| $d_e$    | VA throat diameter                    |
| h        | VA chamber height                     |
| $R$      | density                               |
| $R_e$    | Reynolds number                       |
| $\Gamma$ | specific heat ratio $\frac{c_p}{c_v}$ |
| $P_{co}$ | control to outlet pressure difference |
| $P_{so}$ | supply to outlet pressure difference  |
| $P_{cs}$ | control to supply pressure difference |
| Q        | volume flow rate                      |
| $Q_s$    | supply flow rate                      |
| $Q_c$    | control flow rate                     |
| $Q_T$    | outlet flow rate                      |

#### Abbreviations

|      |                                 |
|------|---------------------------------|
| BDC  | bottom dead centre              |
| BMEP | brake mean effective pressure   |
| BSFC | brake specific fuel consumption |
| CPR  | control pressure ratio          |
| EVC  | exhaust valve closing           |
| EVO  | exhaust valve opening           |
| IVC  | inlet valve closing             |
| IVO  | inlet valve opening             |

|      |                                    |
|------|------------------------------------|
| TDC  | top dead centre                    |
| TDR  | turn down ratio                    |
| VA   | vortex Amplifier                   |
| VGVA | variable geometry vortex amplifier |



## IV. CONTENTS

|  |           |
|--|-----------|
| <b>1 Introduction.....</b>   | <b>12</b> |
| I. Introduction.....   | 13        |
| II. Mixture Preparation.....   | 15        |
| III. Improving Mixture Preparation.....  | 16        |
| III.i Target droplet sizes. ....   | 16        |
| III.ii Devices to improve atomisation.....                                     | 17        |
| III.iii Previous attempts to use a Vortex to improve mixture preparation. .... | 19        |
| <b>2 Review of Vortex Amplifiers .....</b>                                     | <b>22</b> |
| I. Introduction.....   | 23        |
| II. Steady State Flow Visualisation.....                                       | 27        |
| III. Steady Flow Characteristics .....   | 31        |
| IV. Effect of Geometry on Vortex Amplifier Characteristics .....               | 33        |
| V. Vortex Amplifier Instability.....   | 35        |
| VI. VA Modelling. ....   | 38        |
| VII. Practical Applications of Vortex Amplifiers .....                         | 40        |
| <b>3 Measuring droplet sizes.....</b>  | <b>43</b> |
| I. Spray Characteristics and methods of measurement. ....                      | 44        |
| II. The Malvern Particle sizer.....  | 46        |
| III. Experimental Technique. ....  | 50        |
| III.i Choice of fuel.....  | 50        |
| III.ii Preventing lens cut off .....   | 51        |
| III.iii Measuring the spray.....   | 52        |
| III.iv Possible sources of error .....   | 53        |
| <b>4 Designing and Evaluating a Vortex Amplifier .....</b>                     | <b>56</b> |
| I. Introduction.....   | 57        |
| II. Design of a variable geometry VA.....                                      | 57        |
| III. Measuring the steady state characteristics of the VGVA.....               | 60        |
| IV. Results of steady flow tests.....  | 62        |
| V. Discussion .....  | 65        |
| VI. Design of a fuel injection system.....                                     | 67        |
| VII. Photographing the spray .....   | 69        |
| VII.i Photographs in the VA body. ....   | 69        |
| VII.ii Photographs in the exit pipe. ....                                      | 69        |
| VIII. Results of particle sizing .....   | 72        |
| VIII.i Experimental method .....   | 72        |
| VIII.ii Spray Measurements .....   | 73        |
| IX. Discussion of results .....  | 78        |
| <b>5 Designing a VA optimised for atomisation .....</b>                        | <b>80</b> |
| I. Criteria for design of new VA .....   | 81        |
| II. Steady flow performance of VA.....   | 81        |
| <b>6 Modelling droplet motion.....</b>   | <b>91</b> |
| I. Introduction.....   | 92        |
| II. VA data.....   | 93        |

|   |            |
|---|------------|
| III. Droplet motion in the VA .....                                     | 98         |
| IV. Results and Discussion .....  | 100        |
| IV.i Limitations of modelling .....                                     | 102        |
| <b>7 Modelling droplet breakup.....</b>                                 | <b>104</b> |
| I. Droplet break-up in turbulent flows.....                             | 105        |
| II. Weber number criteria .....   | 105        |
| III. Turbulent flow.....  | 106        |
| III.i The breakup of drops smaller than the turbulent microscale .....  | 108        |
| III.ii The break up of drops larger than the turbulent microscale.....  | 109        |
| IV. Modelling turbulent flows.....                                      | 111        |
| <b>8 Experimental results from optimised VA .....</b>                   | <b>117</b> |
| I. Malvern Particle Sizer measurements on new VA .....                  | 118        |
| I.i Droplet sizes produced by the VA with control flow .....            | 118        |
| I.ii Effect of varying the VA outlet diffuser.....                      | 120        |
| I.iii Effect of varying injector position.....                          | 121        |
| I.iv Results with supply flow and mixed control and supply flow through |            |
| the VA .....  | 123        |
| I.v Effect of varying pipework downstream of the VA.....                | 125        |
| II. Photographs of sprays from the new VA.....                          | 127        |
| III. Discussion .....   | 128        |
| III.i Accuracy of results.....  | 128        |
| III.ii Overview of results .....  | 130        |
| III.iii Attempts to prevent droplet deposition.....                     | 130        |
| <b>9 Fuel injection into unsteady airflow.....</b>                      | <b>136</b> |
| I. Introduction.....  | 137        |
| II. Test rig for pulsed flow through the VA .....                       | 137        |
| III. Simple Lumped Capacitance model of flow through VA test rig.....   | 140        |
| IV. Transmission Line Modelling of flow through VA test rig. ....       | 142        |
| V. Experimental drop size measurements with pulsed airflow through the  |            |
| VA.....   | 147        |
| VI. Conclusions.....  | 150        |
| <b>10 Overall Discussion .....</b>                                      | <b>151</b> |
| I. Project Overview .....   | 152        |
| II. Choosing a VA geometry .....  | 152        |
| III. Droplet formation in steady air flows .....                        | 155        |
| IV. Effect of pulsed airflow.....                                       | 156        |
| V. Modelled behaviour.....  | 157        |
| VI. Reliability and Applicability of Results.....                       | 157        |
| VII. Application of work to Spark Ignition engines.....                 | 158        |
| <b>11 Conclusions.....</b>  | <b>160</b> |
| I. Summary of conclusions by chapter .....                              | 161        |
| I.i Chapter 1.....  | 161        |
| I.ii Chapter 2.....   | 161        |
| I.iii Chapter 3 .....   | 162        |
| I.iv Chapter 4.....   | 162        |
| I.v Chapter 5.....  | 162        |

|  |            |
|--|------------|
| I.vi Chapter 6.....                                      | 163        |
| I.vii Chapter 7.....                                     | 163        |
| I.viii Chapter 8 .....                                   | 163        |
| I.ix Chapter 9.....                                      | 164        |
| I.x Chapter 10.....                                      | 165        |
| II. Overview .....                                       | 165        |
| <b>12 Recommendations for future work .....</b>          | <b>166</b> |
| I. Introduction.....                                     | 167        |
| II. Changing the VA diffuser geometry .....              | 167        |
| III. CFD analysis of two phase flow through the VA ..... | 168        |
| IV. Engine Testing of VA .....                           | 169        |
| V. Close coupling of VA and engine cylinder. ....        | 170        |
| VI. Conclusion .....                                     | 170        |
| <b>References .....</b>                                  | <b>171</b> |

## V. LIST OF FIGURES

|  |     |
|--|-----|
| Figure 1 Emissions Legislation in Europe and California.....   | 14  |
| Figure 2 Hartmann whistle atomiser .....   | 18  |
| Figure 3 Results from engine tests with a vortex inducing manifold.....  | 20  |
| Figure 4 Schematic of a Vortex Amplifier.....  | 24  |
| Figure 5 Proportional VA Characteristics .....   | 25  |
| Figure 6 Bistable Vortex Amplifier Characteristics .....   | 26  |
| Figure 7 VA Performance .....  | 27  |
| Figure 8 Representation of Flow Pattern within a VA (from Asquith <sup>16</sup> ).....   | 29  |
| Figure 9 Contour plots of velocity components within a VA at cut off (from King <sup>17</sup> ).....   | 30  |
| Figure 10 Steady Flow Characteristics for a VA under a range of control to outlet pressure drops <sup>19</sup> .....                             | 31  |
| Figure 11 Normalised Steady Flow Characteristics <sup>19</sup> .....   | 33  |
| Figure 12 Negative Resistance Surge.....   | 36  |
| Figure 13 Transport Delay Surge.....   | 38  |
| Figure 14 Cycle for combined early inlet valve closing and VA throttling.....  | 40  |
| Figure 15 Accuracy of D32 Measurement .....  | 45  |
| Figure 16 Summary of non-intrusive particle sizing techniques.....   | 46  |
| Figure 17 Light energy distributions produced by monodisperse sprays.....  | 47  |
| Figure 18 Malvern Particle Sizer.....  | 48  |
| Figure 19 Detector Element Geometry .....  | 48  |
| Figure 20 Size ranges measured by different lenses .....   | 49  |
| Figure 21 Properties of Gasoline and n-Heptane .....   | 51  |
| Figure 22 Lens Cut Off.....  | 52  |
| Figure 23 Results from Malvern particle sizer spray measurement (Control Flow through the VA = 200<br>li/min, time after injection = 14ms) ..... | 53  |
| Figure 24 Scattered light data with and without beam steering .....  | 54  |
| Figure 25 Geometry of variable vortex amplifier .....  | 59  |
| Figure 26 Test rig for flow measurement.....   | 61  |
| Figure 27 Steady flow data for VGVA with radius set at 70mm.....   | 63  |
| Figure 28 Steady flow data for VGVA with radius set at 30mm .....  | 64  |
| Figure 29 Table of VA performance indices from VGVA.....   | 67  |
| Figure 30 Fuel injector specifications .....   | 68  |
| Figure 31 Circuit controlling injection timing.....  | 68  |
| Figure 32 Time Sequence of spray injected into Control Flow=100li/min. T=1,2,3 and 5ms.....  | 71  |
| Figure 33 Spray in the measurement zone 12ms after injection into still air .....  | 72  |
| Figure 34 Variation of spray SMD with time after injection .....   | 73  |
| Figure 35 Volume Distribution 13ms after injection into still air .....  | 74  |
| Figure 36 Volume Distribution 17ms after injection into still air.....   | 74  |
| Figure 37 Volume Distribution 13ms after injection into Control Flow =100li/min .....  | 75  |
| Figure 38 Volume Distribution 15ms after injection into Control Flow=150li/min .....   | 76  |
| Figure 39 Summary of SMD data .....  | 77  |
| Figure 40 Volume Distribution 13ms after injection into Supply Flow=200li/min and Supply<br>Flow=200li/min, Control Flow=50li/min.....           | 77  |
| Figure 41 SMD measurements with supply flow through the VA .....   | 78  |
| Figure 42 Geometric Ratios for best performance of a VA .....  | 82  |
| Figure 43 Photograph of VA installed in test rig .....   | 83  |
| Figure 44 Geometry of VA .....   | 85  |
| Figure 45 Steady Flow Characteristics of new VA.....   | 86  |
| Figure 46 Data Plotted from three different VAs using dimensionless ratios.....  | 89  |
| Figure 47 Steady Flow Data from PhD thesis by King.....  | 93  |
| Figure 48 VA geometry and grid of air velocity.....  | 97  |
| Figure 49 Outlets for the vortex amplifier.....  | 97  |
| Figure 50 Flowchart describing program to solve motion of a droplet within an experimentally<br>determined VA flow field.....                    | 99  |
| Figure 51 X-Z motion with droplet diameter 50µm.....   | 100 |
| Figure 52 X-Z motion with droplet diameter 150µm.....  | 101 |
| Figure 53 X-Z motion with droplet diameter 50µm, off centre injection .....  | 101 |

|   |     |
|---|-----|
| Figure 54 X-Y motion with Droplet diameter 50 $\mu$ m, off centre injection.....  | 102 |
| Figure 55 Maximum stable drop sizes ( $\mu$ m) in outlet flow from the VA at control flow = 400 li/min.....               | 116 |
| Figure 56 Measured SMDs with control flow through the VA.....   | 119 |
| Figure 57 Measured SMDs with different outlet diffusers.....  | 121 |
| Figure 58 Comparison of results for axial and offset injector positions.....  | 122 |
| Figure 59 Comparison of measured SMD for supply and control flow.....   | 124 |
| Figure 60 Measured SMDs for mixed mode flow through the VA.....   | 125 |
| Figure 61 SMD measurements with a tube outlet attached to the VA (viewing chamber results included<br>for comparison..... | 126 |
| Figure 62 Spray Photograph. Control Flow = 100 li/min. Orifice plate attached to VA exit.....                             | 132 |
| Figure 63 Spray Photograph. Control Flow = 400 li/min. Orifice plate attached to VA exit.....                             | 133 |
| Figure 64 Spray Photograph. Control Flow = 400 li/min. Short diffuser attached to VA exit.....                            | 134 |
| Figure 65 Spray Photograph. Control Flow = 400 li/min. Long diffuser attached to VA exit.....                             | 135 |
| Figure 66 Schematic diagram of chopping valve.....  | 138 |
| Figure 67 Comparison of chopping valve and engine inlet valve opening profiles.....                                       | 139 |
| Figure 68 Schematic of test rig adapted for pulsed flow.....  | 139 |
| Figure 69 Schematic layout of test rig for pulsed flow.....   | 141 |
| Figure 70 Comparison of measured pressures in test rig and results from lumped capacitance model.....                     | 142 |
| Figure 71 The pulsed flow test rig as modelled by the SUNAS programme.....  | 144 |
| Figure 72 Comparison of measured pressures in test rig and results from TLM model.....                                    | 146 |
| Figure 73 Air flow rates through the VA with chopping valve speed of 400 rpm (TDC=1.95s).....                             | 146 |
| Figure 74 Measured spray SMDs in pulsed airflow.....  | 147 |
| Figure 75 Measured spray SMDs vs. Predicted flowrate in pulsed flow.....  | 149 |
| Figure 76 Comparison of VA performance.....   | 155 |
| Figure 77 Schematic of a VA fitted with a Radial diffuser.....  | 168 |

# **CHAPTER 1**

## **Introduction**

*A summary of the emission problems of the Spark Ignition Engine, and the potential for enhanced mixture preparation to improve performance.*

## I. Introduction

The environmental impact of the motor vehicle has been of increasing concern since the arrival of mass motor manufacture in the 1950s and 1960s. It has been estimated that cars account for 10000 billion cubic metres of exhaust fumes world-wide annually (Nieuwenhuis *et al.*<sup>1</sup> p. 20). Although more than 97% of vehicle exhaust emissions consists of non toxic substances (e.g. water, carbon dioxide, oxygen and nitrogen), the large volume of exhaust emitted means that the remaining 2-3% can have significant environmental impact. In view of this most governments have introduced legislation to control vehicular emissions.

Californian legislation, passed in 1990, requires progressively higher proportions of new cars to be Low Emission Vehicles (LEV) and Ultra Low Emission Vehicles (ULEV) in the period 1994-2003. Additionally, from 1998, a steadily increasing proportion of vehicles must produce no emissions at the point of use, which will require the introduction of electric vehicles. As an indication of the stringency of these limits, laboratories have encountered problems measuring emissions from prototype ULEVs as they are often lower than the background pollution.

The climate of California, which promotes the occurrence of atmospheric smog, has meant that the Californian legislation has tended to lead the world. However the requirements of European legislation are now approaching those of California. The EC introduced limits that required all new cars registered in the region after December 1992 to be equipped with three way catalytic converters. These limits were updated in 1996 and will be again in 2000. As European legislation includes methane emissions in the Hydrocarbon (HC) content, the European 2000 limits may be as challenging to manufacturers as meeting the Californian ULEV targets (Hadded *et al.*<sup>2</sup>). Emission limits in the EC and California are summarised in Figure 1.

---

<sup>†</sup> Documents are referenced in this thesis in numerical order of appearance and listed in the references at the rear.

Note:- Californian legislation has separate limits for hydrocarbons and NOx. These are combined in this graph.

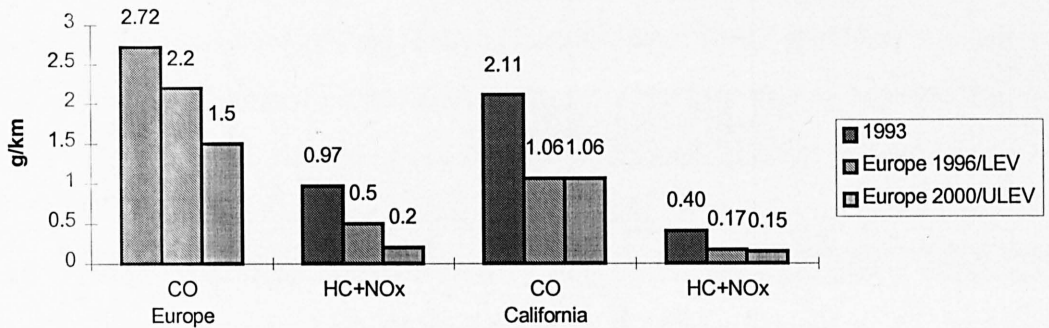


Figure 1 Emissions Legislation in Europe and California

Emission limits are now one of the major factors influencing engine design. Three way catalysts will only operate effectively if the engine burns a stoichiometric mixture so their introduction meant that all cars had to be fitted with engine management systems and electronic fuel injection. Meeting future emission limits is likely to require the introduction of further new technology.

One of the largest challenges facing manufacturers is the expected inclusion of the initial warm up phase, currently unmeasured, in the measurement cycle in the new European standards for the year 2000. Results from the American test cycle FTP75 show that approximately 80% of unburned hydrocarbon emissions occur during the first 125 seconds of warm up, and only 20% occur in the remaining 2375 seconds (quoted in Ashley<sup>3</sup>). Clearly reducing emissions during warm up is essential if engines are to meet future limits.

Several methods for achieving this are under consideration. During warm up, exhaust gas after-treatment could be improved with an electrically heated or close coupled catalyst. More sophisticated engine management systems could reduce air-fuel ratio excursions during engine transients. Extremely retarded ignition could produce hot exhaust gases to bring the catalyst to working temperature rapidly. It is likely that some combination of measures will be required, and the performance of any such strategy would be enhanced by improving the preparation of the air-fuel mixture.

Good mixture preparation is essential for low emission combustion. Current fuel injectors are low pressure (typically 2 bar) pintle designs. These produce droplets with a Sauter mean diameter (SMD) of 100-150 $\mu$ m, which can be improved to around



50 $\mu$ m at part load by manifold driven air shrouding. Further improvement would seem to require a new method of atomisation. However the current pintle injectors are reasonably cheap to manufacture and are easily incorporated within an electronic engine management system. The current project aims to evaluate the potential to improve the atomisation of a fuel jet from this design of injector by directing it into an extremely turbulent air flow. This airflow will be produced by a fluidic control device known as a Vortex Amplifier (VA). This device is being used as previous work has shown that it can improve fuel consumption by reducing pumping work (Abdul-Wahab<sup>4</sup>). If it can also improve mixture preparation it could be used to enhance the performance of SI engines in terms of both efficiency and emissions.

## II. Mixture Preparation.

In a spark ignition (SI) engine, fuel enters the cylinder in three forms: as a vapour, as fine liquid droplets carried in the air-stream, and as a film of liquid from the manifold wall. The relative amount of fuel in each form varies depending on engine temperature, speed, and manifold vacuum, but under cold starting conditions the fuel entrained from the manifold wall is highly significant. It is this poor mixture distribution that necessitates the use of low air-fuel ratios to ensure combustion when starting from cold, with the attendant problems of low economy and high emissions. In carburetted and Single Point Injection (SPI) systems the problem is exacerbated by fuel maldistribution to the cylinders. At cold start this cylinder to cylinder variability is increased due to:

- i) The manifold handling large quantities of liquid fuel.
- ii) Low engine speed leading to low gas velocities for mixing.

The maldistribution makes necessary a further decrease in air to fuel ratio to prevent misfiring in the weaker cylinders. Thus after cold start, low fuel economy and high emissions, particularly of unburned hydrocarbons, are unavoidable in a carburetted engine.

The situation is better with multi-point fuel injection (MPI). The effects of fuel maldistribution are almost eliminated, as the fuel is metered into the intake port. This means that the degree of enrichment required to give reliable starting is lower. In addition fuel injection gives the advantage of higher maximum power, as the pressure

drop across the carburettor is eliminated. It also allows closed loop control of air to fuel ratios (necessary for the use of catalytic converters), as the injector can be incorporated into an engine management system, with feedback from an oxygen sensor in the exhaust. However numerical simulation shows that significant amounts of fuel are still impacted onto the inlet port walls during injection (Bland and Saunders<sup>5</sup>). Thus some degree of mixture enrichment is still required whenever the engine is started. The emission problems associated with this are compounded by the fact that the exhaust system takes some time to reach the operating temperature of the catalyst.

As car usage is frequently for short journeys, the increased emissions caused by mixture enrichment and cold catalysts contribute significantly to the total pollution caused by automobiles. Clearly there is potential for significant emissions and economy benefits to be obtained from improved mixture preparation, even considering only the enhancement this would provide at start up. If fuel-air mixing is improved, there is also the potential to utilise the resulting ability of the engine to burn leaner mixtures, to further improve economy.

### III. Improving Mixture Preparation

#### III.i Target droplet sizes.

Improving atomisation has the potential to reduce droplet sizes to such an extent that no fuel is deposited on the intake port walls and all the fuel is carried along in the air-stream. The equation of motion for an individual droplet in a flowing gas stream is (from Heywood<sup>6</sup>):

$$\left(\frac{1}{6}\pi D_d^3 \rho_f\right) \bar{a} = m_d \bar{g} - \frac{1}{2}(v_d - v_g)|v_d - v_g| \rho_g C_D \frac{\pi D_d^2}{4}$$

where  $D_d$  is the droplet diameter,  $\rho_f$  and  $\rho_g$  are the liquid and gas densities,  $v_d$  and  $v_g$  are the droplet and gas velocities,  $\bar{a}$  is the droplet acceleration,  $\bar{g}$  the acceleration due to gravity, and  $C_D$  the drag coefficient. For  $6 < \text{Re} < 500$  the drag coefficient is a strong function of Reynolds number,  $\text{Re}$ :

$$C_D = 27 \text{Re}^{-0.84}$$

where  $\text{Re} = (\rho_g D_d |v_d - v_g| / \mu_g)$ .

For 90° bends, drops of 10 µm diameter are basically carried by the air stream (<10 % impacting); practically all droplets larger than 25 µm impact on the walls. The target is clearly to have an injector capable of producing a spray in which all the droplets are 10µm or less in size. Current low pressure manifold fuel injectors do not achieve this. The range of droplet sizes produced by current fuel injectors is ill-defined as it varies with manifold vacuum, air flow rate, and injection timing. The finest sprays are produced by air-shrouded injectors producing a conical spray. The atomisation achieved is strongly dependent on the pressure difference between the intake manifold and the atmosphere. SMDs of 50 µm are achievable under idle conditions but increase to above 100 µm at wide open throttle. This is the same as an unshrouded injector, which is the technology currently used on most production vehicles (Lenz<sup>7</sup>). Injectors without air shrouding have less variation in SMD with manifold vacuum, a slight increase being noticeable as vacuum increases, due to the decreasing air density.

Whilst a target droplet size of 10µm is desirable, any reduction in droplet sizes will tend to improve the mixture preparation, and hence the engine performance. For example, reducing the SMD of the spray produced by an injector from 176µm to 85µm gave a 3% improvement in fuel economy and an 8% reduction in HC emissions in engine tests (Kashiwaya and Kosuge<sup>8</sup>).

### III.ii Devices to improve atomisation.

Many devices exist to improve mixture preparation. The aim of such devices is either to supply heat to the intake manifold to increase the proportion of evaporated fuel, or to increase the shearing forces on the droplets to reduce their size. Using the turbulent flow in a VA to improve atomisation falls into the second category. Both these strategies have drawbacks associated with them. Supplying extra heat to the manifold decreases the density of the charge drawn into the cylinder. Thus the volumetric efficiency of the engine is reduced, lowering the maximum power. Additionally the time taken for the fuel to evaporate introduces a time lag during engine transients, making control of air to fuel ratio difficult. The disadvantage of atomising devices is that most impose a pressure drop on the intake flow, which also reduces volumetric efficiency.

Several methods of decreasing spray SMD by shattering the droplets in a high velocity air stream exist, though only the air shrouded injector has gained widespread acceptance. Two examples of devices that aim to improve mixture preparation by reducing droplet size are Hartmann whistle atomisers and sonic throat carburettors.

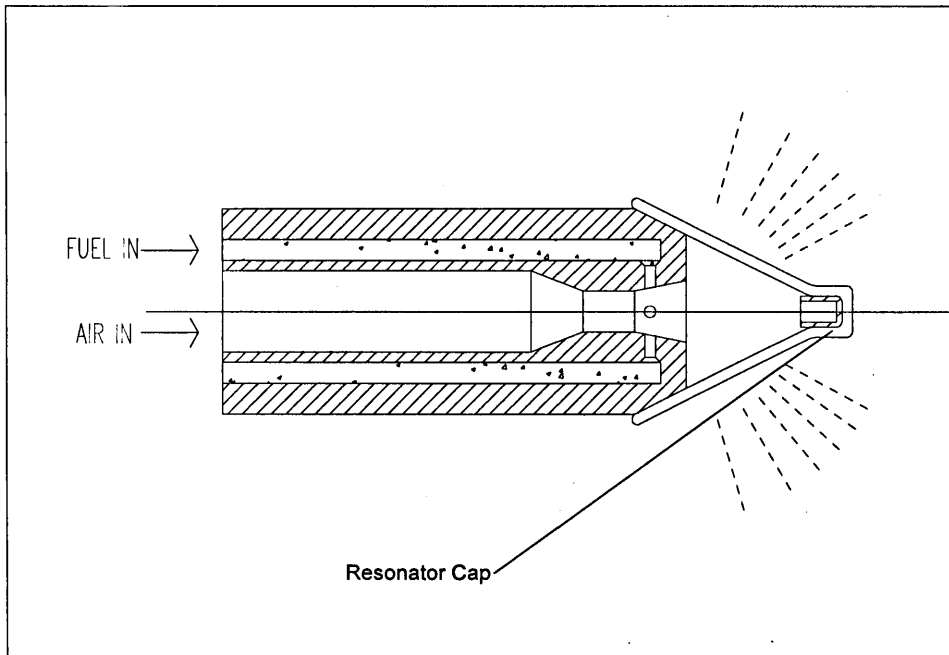


Figure 2 Hartmann whistle atomiser

These devices were tested and compared with conventional manifolds (Nightingale and Tsatsami<sup>9</sup>). In the Hartmann whistle a standing wave is set up in the device by directing high-pressure air into a cap at the end of the nozzle. This can give excellent atomisation, producing droplets with a characteristic size of less than  $10\ \mu\text{m}$  for a supply pressure of  $140\ \text{kN/m}^2$ , which is superior to more conventional air-blast atomisers ( $15\text{-}30\ \mu\text{m}$ ). However this atomisation was negated by the spray impacting with the throttle plate, and it is not practicable to mount the Hartmann whistle downstream of the throttle.

The sonic throat carburettor is a converging-diverging nozzle that maintains sonic velocity at the throat over a wide range of operating conditions. Introducing the fuel near the throat produces droplet sizes around the value of  $10\ \mu\text{m}$  for any rig depression over  $50\ \text{mm Hg}$ . As the throat area can be varied to throttle the flow, there is no problem with droplets impacting on the throttle plate. However it was found that the velocity of the droplets meant that, unless an extension tube was added after the sonic throat carburettor to allow deceleration of the flow, then the spray impacted on the

manifold wall opposite the carburettor. Under bonnet space restrictions mean that the extension tube is impracticable.

It is clear that the energy used in throttling the air for part load operations could atomise the spray effectively. Indeed characteristic droplet sizes produced in the flow past a partially closed throttle plate are frequently of the order of 5  $\mu\text{m}$ . However the butterfly type of throttle valve means that the mixture passes it in two high velocity streams. The general turbulence of these streams together with their proximity to the walls leads to the droplets being deposited. In addition their velocity makes subsequent changes in direction difficult to accomplish without significant numbers of droplets impacting.

In the VA the same turbulent flow, with rapid shearing between layers of fluid, exists, but it is in a much more self contained form. It is hoped that the air flow through the VA could atomise droplets in the same way as the flow past a butterfly valve or through a sonic throat carburettor. However the lower axial velocity of the airflow will allow the mixture to navigate changes of direction downstream without droplets being deposited on the walls.

### **III.iii Previous attempts to use a Vortex to improve mixture preparation.**

In an undergraduate project at Sheffield University (Acton and Allen<sup>10</sup>), a vortex inducing manifold was placed downstream of the carburettor. It was hoped that the vortex flow in this manifold would atomise the fuel supply from the carburettor. Engine tests showed improvement in Brake Specific Fuel Consumption (BSFC) at some engine conditions, compared with the normally carburetted engine. The improved mixture preparation also extended the engines lean mixture limit. The improvement in BSFC at a Brake Mean Effective Pressure (BMEP) is shown in Figure 3.

## Engine test results from full throttle tests at 3000 rpm

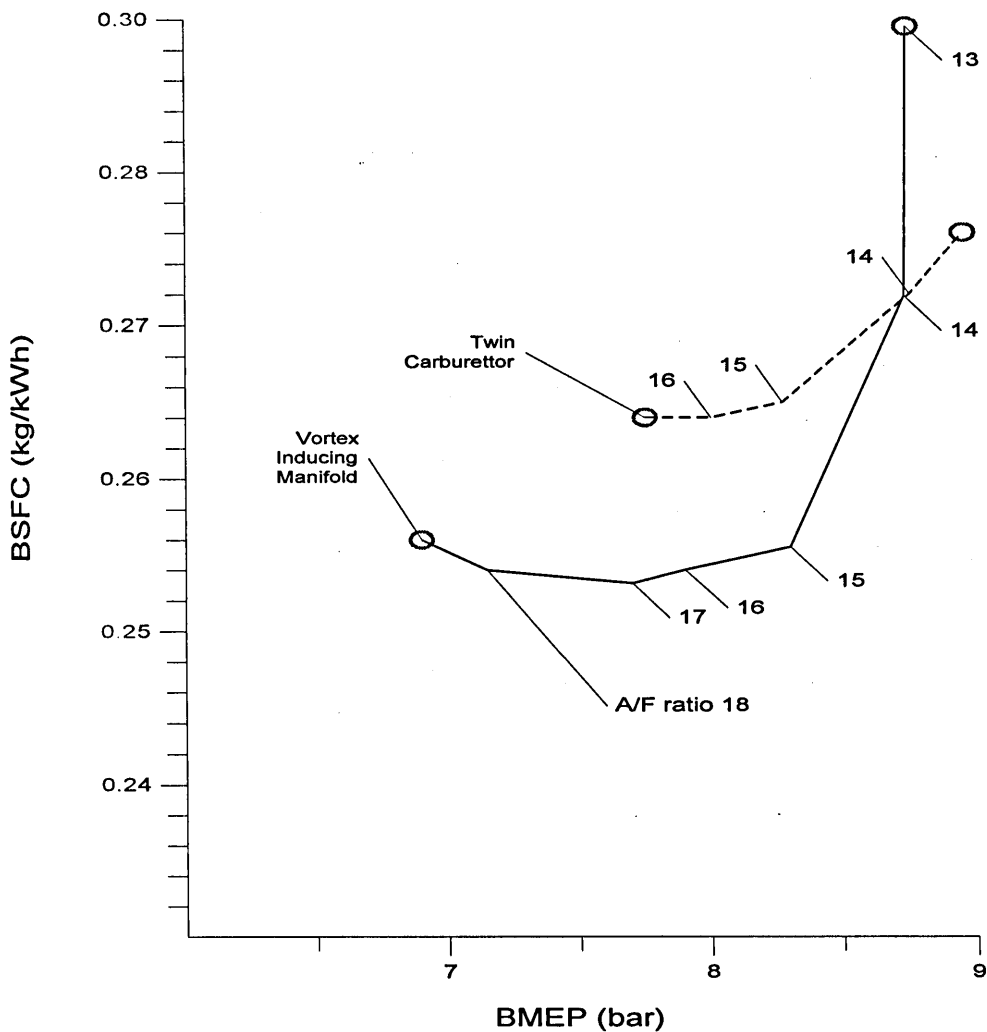


Figure 3 Results from engine tests with a vortex inducing manifold

Unfortunately this improvement could not be sustained across the engine's whole operating range. Significant quantities of fuel were observed being centrifuged against the wall of the manifold. Also any mixture distribution problems at the carburettor persisted into the chamber. Even allowing for these obvious shortcomings the results are reasonably encouraging.

The current project works on the same principle of using a vortex flow to atomise a spray. It is hoped that injecting the spray directly into the centre of the vortex will extend this improvement in mixture preparation to all engine operating conditions. By introducing the fuel into the most turbulent part of the flow opportunity for

atomisation is maximised, and the risk of centrifugal effects depositing the droplets on chamber walls is minimised.

The VA has the potential to improve mixture preparation, and thus improve BSFC and reduce emissions, particularly in the cold start regime. Also as the pressure drop across the VA can be varied it should achieve this improvement with a minimal loss in power output.

## **CHAPTER 2**

### **Review of Vortex Amplifiers**

*Chapter 2 reviews the literature on characteristics and behaviour of Vortex Amplifiers. It also summarises the factors that indicate the Vortex Amplifier could be used to improve mixture preparation.*



## I. Introduction

The Vortex Amplifier (VA) is a no-moving-part fluidic device, which controls flow. It is designed to modulate a large volume supply flow with a smaller control flow. This is achieved by using the control flow, which is at a higher pressure, to impart tangential momentum to the supply flow as it passes through a cylindrical chamber. The tangential momentum sets up a vortex flow within the chamber, which increases the flow resistance, and thus reduces the flow. By varying the amount of control flow the intensity of the vortex can be regulated. This controls the amount of flow through the chamber.

The most common design of VA is the radial vortex amplifier. It consists of a short cylindrical chamber with three ports: an axial outlet, a radial entrance for supply flow and a tangential entrance for the control flow. This design is shown in Figure 4. The axial vortex amplifier works on the same principle but has an axial supply flow inlet. Although only one supply and control port are illustrated in Figure 4, in practice multiple supply and control ports are used to ensure good radial distribution of the flow.

When the control flow is zero then the supply flow passes through the vortex chamber to the outlet with a negligible pressure drop. This is termed the normal state. When the control flow is increased a vortex flow field forms inside the chamber. This reduces the supply flow rate. When the control flow is increased sufficiently the vortex resistance will completely stop the supply flow. This is termed the vortex state. This is the minimum flow through the chamber for a given supply-to outlet pressure drop. Any further increase in control flow will cause the outflow to rise again. The minimum control flow required to reduce the supply flow to zero is called the cut-off flow.

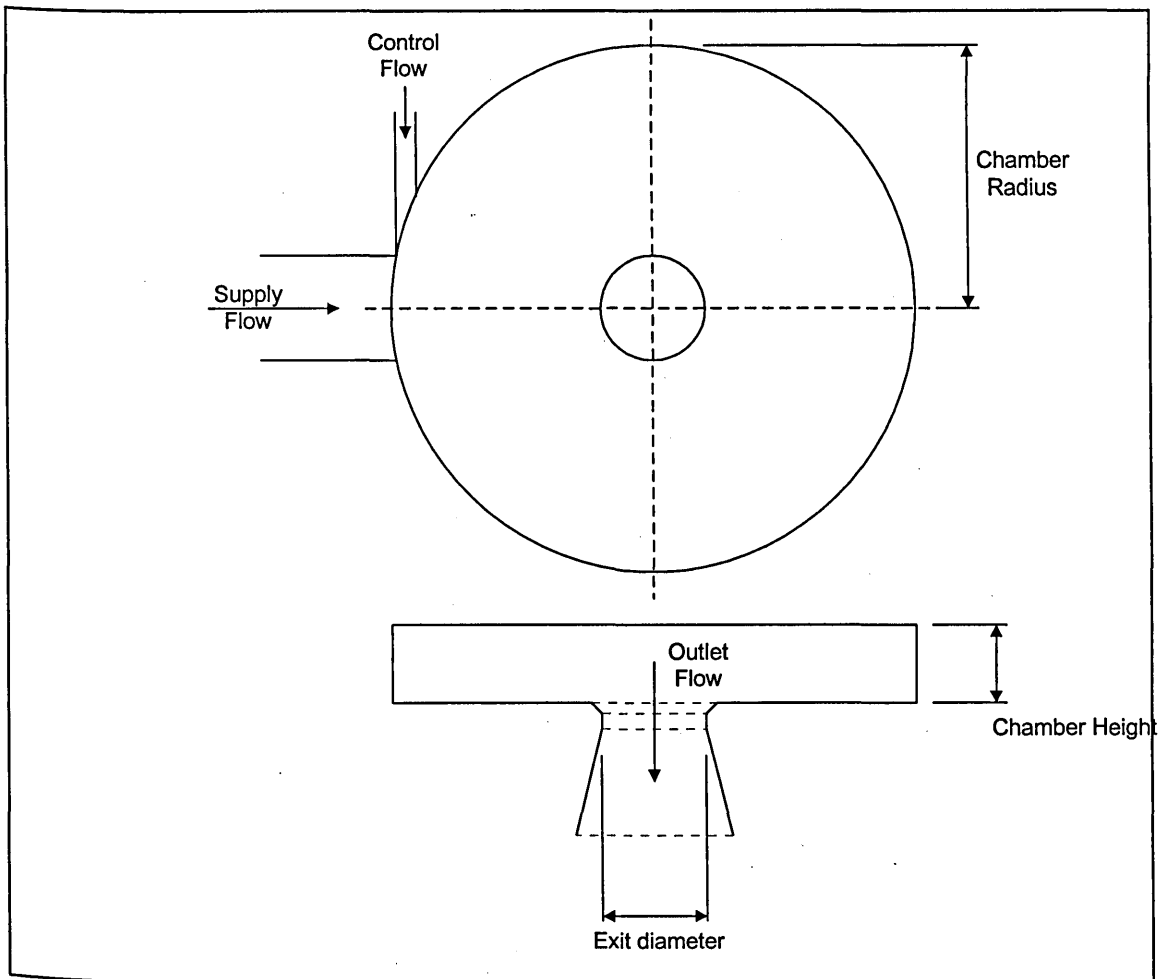


Figure 4 Schematic of a Vortex Amplifier

Two ratios that are used to evaluate VA performance are:

i) The turndown ratio (TDR):

$$\text{TDR} = \frac{Q_{\text{MAX}}}{Q_{\text{CC}}} = \frac{\text{Maximum flow rate}}{\text{Cutoff control flow rate}}$$

ii) The cut-off control pressure ratio (CPR):

$$\text{CPR} = \frac{P_{\text{CCO}}}{P_{\text{SO}}} = \frac{\text{Control to outlet pressure at cut off}}{\text{Supply to outlet pressure}}$$

The TDR measures how much the VA can reduce the flow through the VA, and the CPR measures the pressure required to achieve this reduction. The CPR of a vortex amplifier will always be greater than one, as control pressure must be greater than supply pressure to achieve cut off.

A typical characteristic for a vortex amplifier, normalised with respect to maximum flow, is shown in Figure 5. This is a proportional type characteristic. The contribution made by the supply and control flows to the total flow is shown.

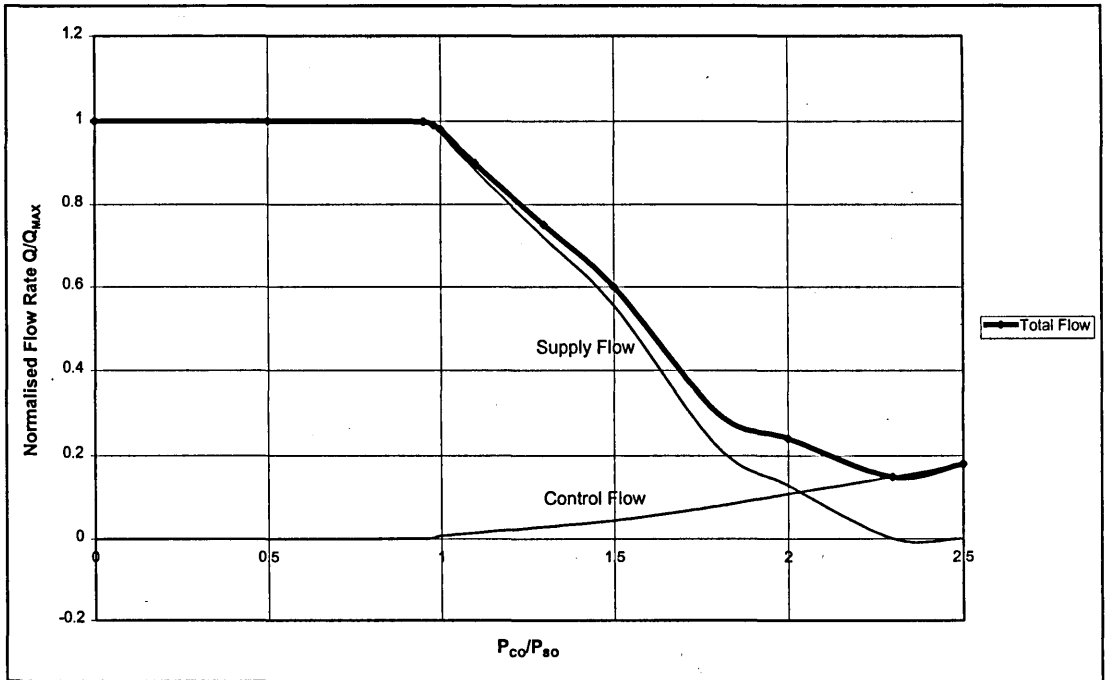


Figure 5 Proportional VA Characteristics

A different type of VA characteristic is shown in Figure 6, which is usually referred to as bistable. It can be seen that a region of the characteristic exists where there are three values of total outflow for each value of the control to supply pressure ratio. Under most conditions the VA will display hysteretic behaviour, jumping from A-B as the control flow is increased, and D-C as it is reduced. This bistability is due to negative resistance surge and transport delay surge, which will be explained later.

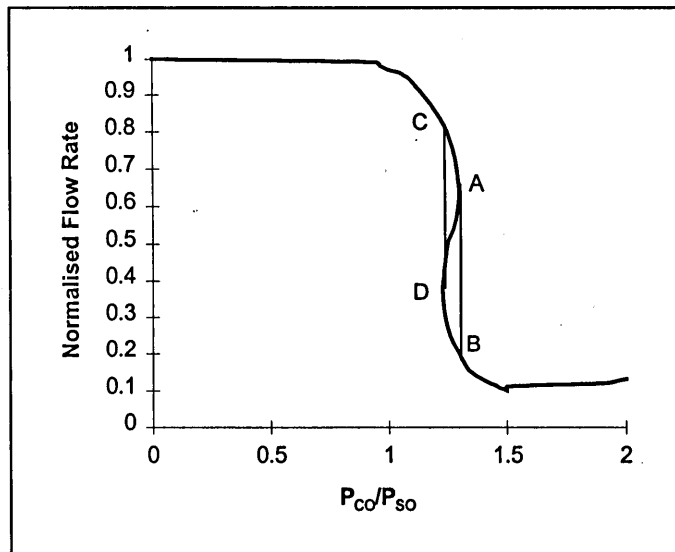


Figure 6 Bistable Vortex Amplifier Characteristics

Although proportional amplifiers have the advantage of being able to control the flow smoothly over a range of flow values it is possible to achieve significantly better TDR and CPR values with bistable amplifiers.

Increasing knowledge of the factors affecting VA behaviour has allowed designers to improve VA performance. Obviously a well designed VA aims at a high TDR in conjunction with a low CPR. Values of TDR = 22 for CPR = 4.0<sup>11</sup>, TDR = 20 for CPR = 3.0<sup>12</sup> and TDR = 8 for CPR = 2.0<sup>13</sup>, have been achieved by Chow, Syred, and Gebben respectively. A few years later Brombach<sup>14</sup> generated an envelope of optimum design. He produced this by gathering results from a wide range of authors, with various authors presenting results lying on the envelope curve for a small length of the envelope. After an extensive study, King<sup>15</sup> produced a design algorithm, and used it to construct a VA that gave a significant improvement on this envelope. These results are summarised in Figure 7.

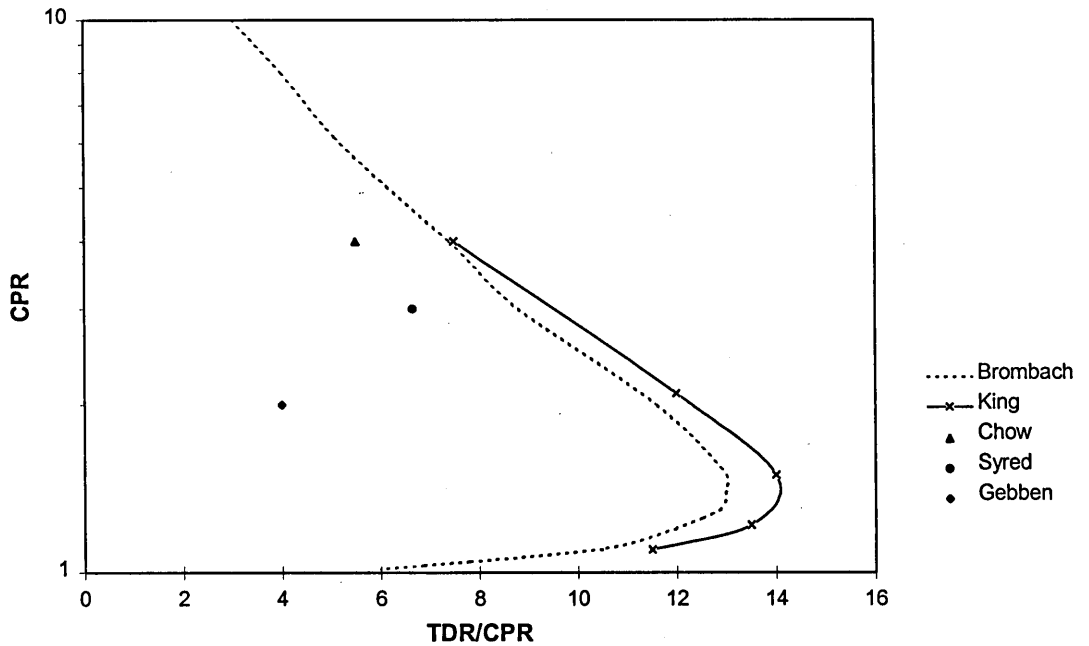


Figure 7 VA Performance

## II. Steady State Flow Visualisation

Flow visualisation work on the VA has shown a complex three-dimensional flow structure in the vortex state. Asquith<sup>16</sup> performed a series of tests on a VA, using water as the working fluid, by injecting ink into various parts of the flow. His representation of the flow at the vortex state is shown in Figure 8. It contains a number of distinct regions. At the outer edge of the VA is a mixing region of the control and supply flows, which depending on the geometry and pressures used in the tests sometimes contained precessing vortices. Along the chamber end walls there is flow towards the centre of the chamber in the boundary layer. Outside the boundary layer there is a region of zero radial flow, which is often termed the 'spinning doughnut'. At the VA exit the flow is highly complex with a core of reversed flow surrounded by a number of precessing vortices.

The reversed flow at the outlet of the VA is extremely important to understanding VA behaviour. The conservation of angular momentum in the vortex flow leads to very high velocities, and thus high dynamic heads, near the centre of the chamber. This leads to the low static pressure that sets up the reversed core.

The reversed core causes a blockage to flow through the chamber, which leads to the high resistance of the VA in the vortex state. In the vortex state shown in Figure 8, the reversed core is attached to the vortex chamber roof. However at lower levels of swirl the reverse flow will form a free stream stagnation point in the VA outlet. As the swirl is increased this stagnation point moves towards the VA chamber roof, reducing the outlet flow area. Thus the resistance of the VA is increased as the swirl level increases. If the rate of this increase in resistance with increased control flow is large enough a negative resistance region is formed. Such a region can be seen in the bistable characteristic shown in Figure 6. The step change in VA resistance observed when measuring bistable characteristics can be understood as the free stream stagnation point jumping to attach to the VA chamber roof.

King<sup>17</sup> studied air flow through a VA by taking velocity measurements with a hot wire probe. His velocity measurements for a VA in the vortex state are shown in Figure 9. They are presented as contour plots of radial, tangential and axial components of velocity.

These velocity measurements largely agreed with the flow structure observed by Asquith. In particular he found a core of reversed flow at the outlet which was attached to the vortex chamber back wall at the vortex state. He also found large velocity fluctuations in the flow in the outlet diffuser, which indicate precessing vortices. Although he found an area of reversed radial flow it was much smaller in extent than the 'spinning doughnut' observed by Asquith and was at a smaller radius in the vortex chamber. Many researchers such as Haider<sup>18</sup> have found no evidence of the 'spinning doughnut', particularly in VAs of low aspect ratio. This is assumed to be due to the boundary layer, which contains radial flow, filling the entire height of the VA. The VA studied by King was a low aspect ratio device. He attributed the reversed radial flow to the presence of the recirculating flow from the reversed flow core at the centre of the VA.

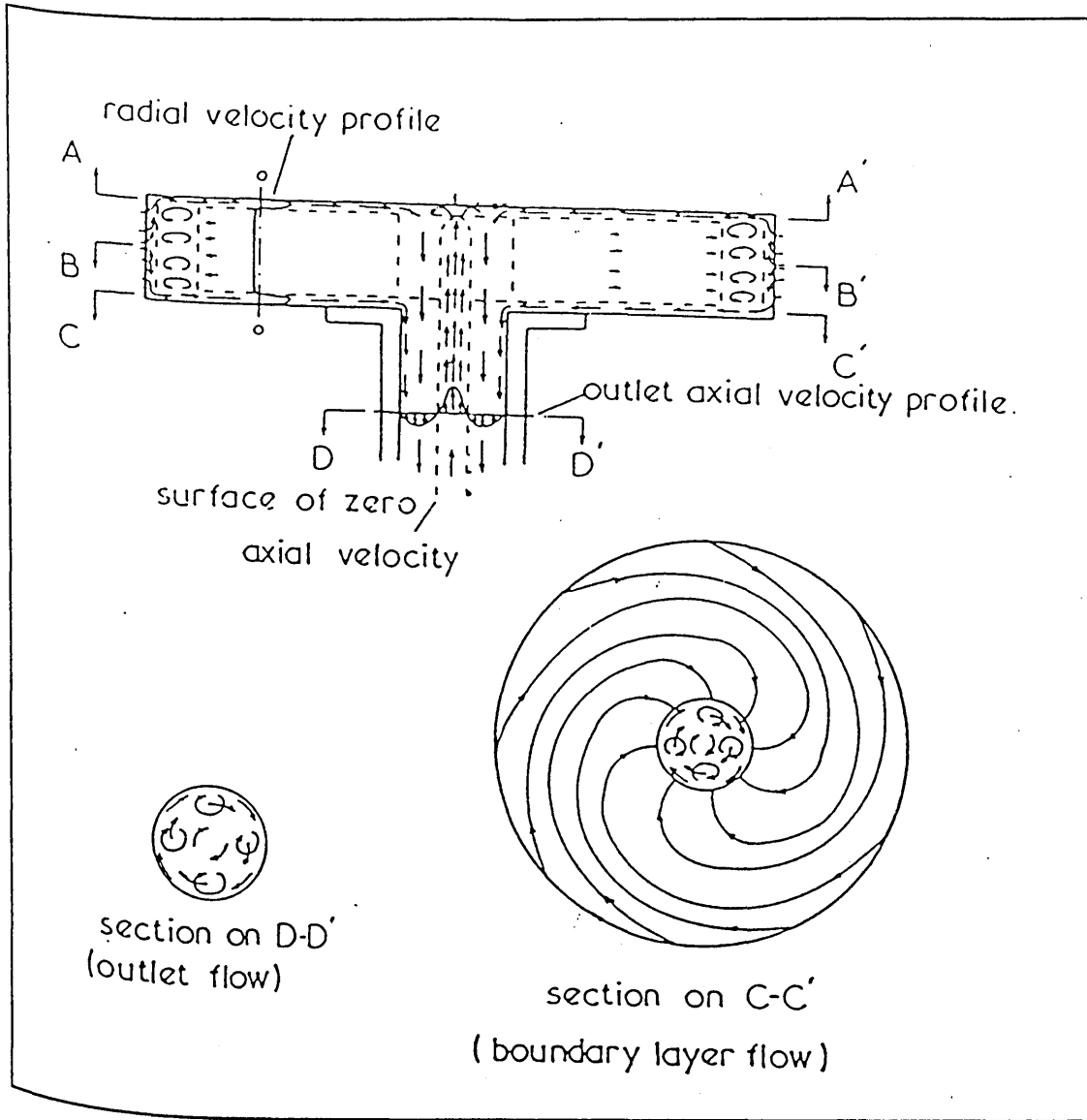


Figure 8 Representation of Flow Pattern within a VA (from Asquith<sup>16</sup>)

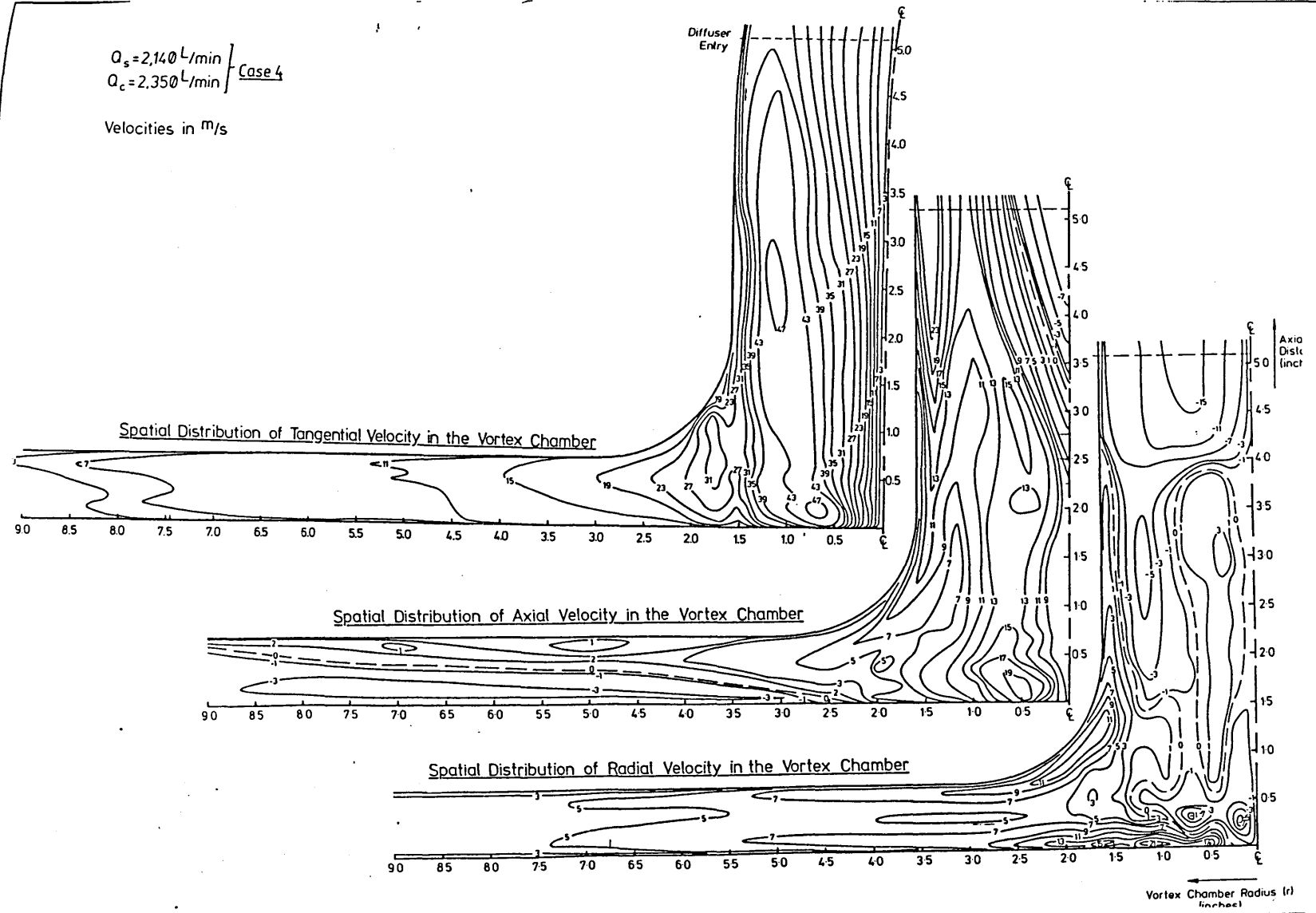


Figure 9 (contour plots of velocity components within a VCA at cut off (from King<sup>17</sup>))



### III. Steady Flow Characteristics

The VA can be viewed as a 3 terminal device (supply inlet, control inlet and outlet). Flow is controlled by three pressure differences (supply to outlet  $\{P_{SO}\}$ , control to outlet  $\{P_{CO}\}$  and control to supply  $\{P_{CS}\}$ ) and three volumetric flow rates (supply flow  $\{Q_S\}$ , control flow  $\{Q_C\}$  and outlet flow  $\{Q_T\}$ ). Due to the requirements of continuity and pressure summation only two of the pressures and two of the flow rates are independent if incompressible flow is assumed.

The steady flow characteristics of the VA are traditionally evaluated by holding one pressure difference constant, usually  $P_{SO}$ , and varying the others. This produces a family of characteristics. Such a family, with constant  $P_{CO}$ , is shown in Figure 10.

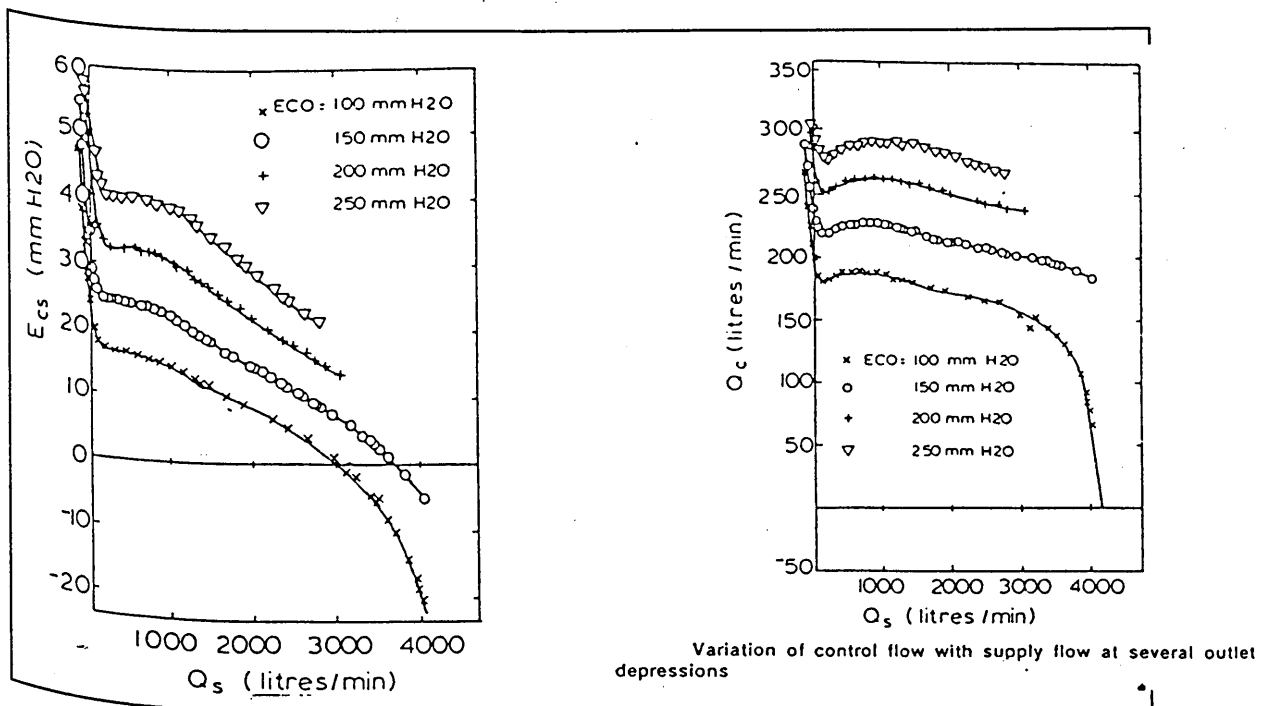


Figure 10 Steady Flow Characteristics for a VA under a range of control to outlet pressure drops<sup>19</sup>.

To perform a dimensional analysis of the VA the required variables are fluid density  $\rho$ , viscosity  $\mu$  and a characteristic length  $l$ , along with the two independent flow rates and two independent pressures. Such an analysis was undertaken by Boucher and Kitsios<sup>19</sup> giving the four following dimensionless groups:-

$$F\left(\frac{(\rho P_{CO})^{1/2} l}{\mu}, \frac{Q_c}{l^2 (P_{CO}/\rho)^{1/2}}, \frac{Q_s}{l^2 (P_{CO}/\rho)^{1/2}}, \frac{P_{CS}}{P_{CO}}\right) = 0$$

Data similar to that presented in Figure 10 was replotted, using the following normalised variables, derived from the dimensionless groups by eliminating  $l$ , and normalising to standard density:-

$$f\left(\frac{(\rho p_{co})^{1/2} l}{\mu}, \frac{q_c}{p_{co}^{1/2}}, \frac{q_s}{p_{co}^{1/2}}, \frac{p_{cs}}{p_{co}}\right) = 0$$

The data plotted using the normalised groups all collapses accurately onto one curve, as shown in Figure 11. This demonstrates independence from the first dimensionless group, which is a form of Reynolds number. Thus only one set of characteristics is required to characterise a VA. This agrees with the experimental data of Wormley and Richardson<sup>20</sup> which shows that VA characteristics are relatively insensitive to Reynolds number (Re):-

$$Re = \frac{Q_{max}}{2 \pi r_c \mu}$$

for  $Re > 750$  for tests up to  $Re = 3300$ . This independence of Reynolds number is perhaps slightly surprising given that the flow in the chamber is dominated by boundary layer effects, and that losses in such flow are Reynolds number dependent. This supports the view that chamber losses are minor in comparison with the energy dissipation in the swirling exit flow. Such flows are relatively insensitive to Reynolds number effects.

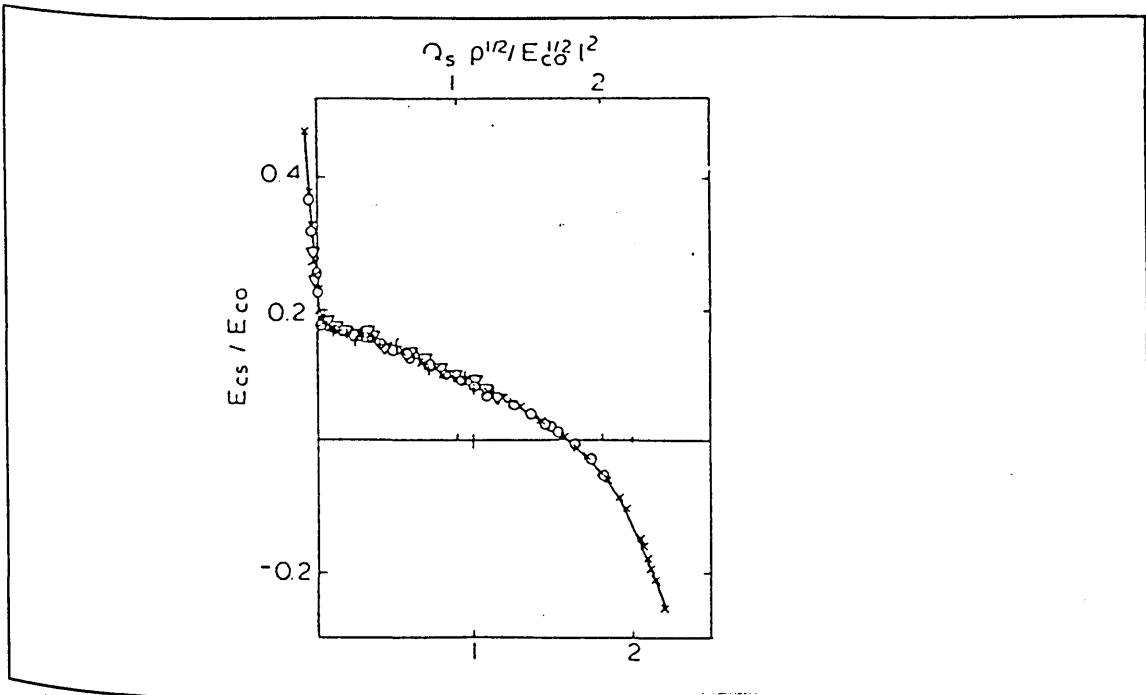


Figure 11 Normalised Steady Flow Characteristics<sup>19</sup>

#### IV. Effect of Geometry on Vortex Amplifier Characteristics

The geometry of a VA is usually defined in terms four dimensionless ratios.

These are:-

$$\text{Height Ratio (H)} = \frac{\text{chamber height}}{\text{exit hole radius}}$$

$$\text{Radius Ratio (R)} = \frac{\text{chamber radius}}{\text{exit hole radius}}$$

$$\text{Control Area Ratio} = \frac{\text{control port area}}{\text{exit hole area}}$$

$$\text{Supply Area Ratio} = \frac{\text{supply port area}}{\text{exit hole area}}$$

Wormley and Richardson<sup>21</sup> evaluated the effect of these ratios upon the VA behaviour. Their conclusions are summarised in the following paragraphs.

The supply area ratio has a negligible effect on amplifier characteristics providing it is greater than three in value. As the supply port acts as a resistance between the supply pressure and the chamber it has no effect at cut-off flow. If the supply area ratio is reduced below three, the effect of the supply port resistance becomes

significant and reduces the supply flow rate, thus limiting the maximum flow rate through the VA. This clearly reduces TDR.

Control area ratio has a strong influence on the VA characteristic. To understand this consider flow through a VA at a constant supply-to-outlet pressure drop. A decrease in control area ratio causes a given control flow to reduce the total flow by a larger amount. This is because for a given control flow a smaller control port area gives a control jet of higher velocity, creating a stronger vortex. The cost is an increase in the control pressure required<sup>20</sup> for a given control flow. Thus, as control area ratio is decreased, both TDR and CPR increase. However, for values of control area ratio less than 0.1, values of TDR become relatively insensitive to the control port area, and may even decrease slightly due to mixing losses.

The radius ratio also exerts a strong influence on the VA characteristic and determines whether its behaviour is proportional or bistable. A VA with a large radius ratio exhibits proportional behaviour. Usually the minimum radius ratio for this to be the case is 14. With decreasing radius ratio, the TDR of the VA increases but at the cost of a larger bistable region in the flow characteristic. This is because in a VA of large radius ratio the chamber end walls have a larger area. The frictional losses in the VA chamber increase, thus damping out the instability effects that lead to bistable behaviour.

As the height ratio is reduced below 2 the chamber turn down ratio increases. This is because the resistance of the chamber to pure control flow increases, reducing the cut off control flow. However decreasing the height ratio tends to increase levels of internally generated noise. Thus the height ratio chosen for a VA will be a trade off between the demands of high TDR and low noise operation. It should be noted that the height should not be reduced to the point where the curtain area around the exit is smaller than the exit hole area. This would mean the exit would not be the primary restriction on outflow. The exit hole curtain area is  $2\pi r_e h$ , the exit hole area is  $\pi r_e^2$ , and so the height ratio must be greater than 0.5.

King<sup>15</sup> describes four other factors that also influence the VA behaviour. These are:

- the length of the parallel section in the outlet throat

- the blending radius between the VA chamber and exit throat
- the area ratio of the outlet diffuser
- the geometry of the VA backwall opposite the VA exit.

A parallel section in the outlet throat increases both the supply and control flow resistance and hence decreases both TDR and CPR. A blending radius reduces the supply flow resistance which increases TDR. However if too large a radius is used the control flow resistance will be affected which reduces this benefit. Manufacturing the VA to include a pip on the backwall of the vortex chamber opposite the outlet has been found to improve performance if the control area ratio is small. All these factors and the four main VA geometric ratios can be optimised for either high TDR, low CPR or low noise by following the design algorithm set out by King.

## **V. Vortex Amplifier Instability.**

Steady flow in the vortex amplifier has often been observed to be very unstable, which has led to difficulties in obtaining complete steady flow characteristics. Tippets<sup>22</sup> identified three causes of instability in VAs. These are:-

- i) Flow field instability.
- ii) Negative resistance surge.
- iii) Transport delay surge.

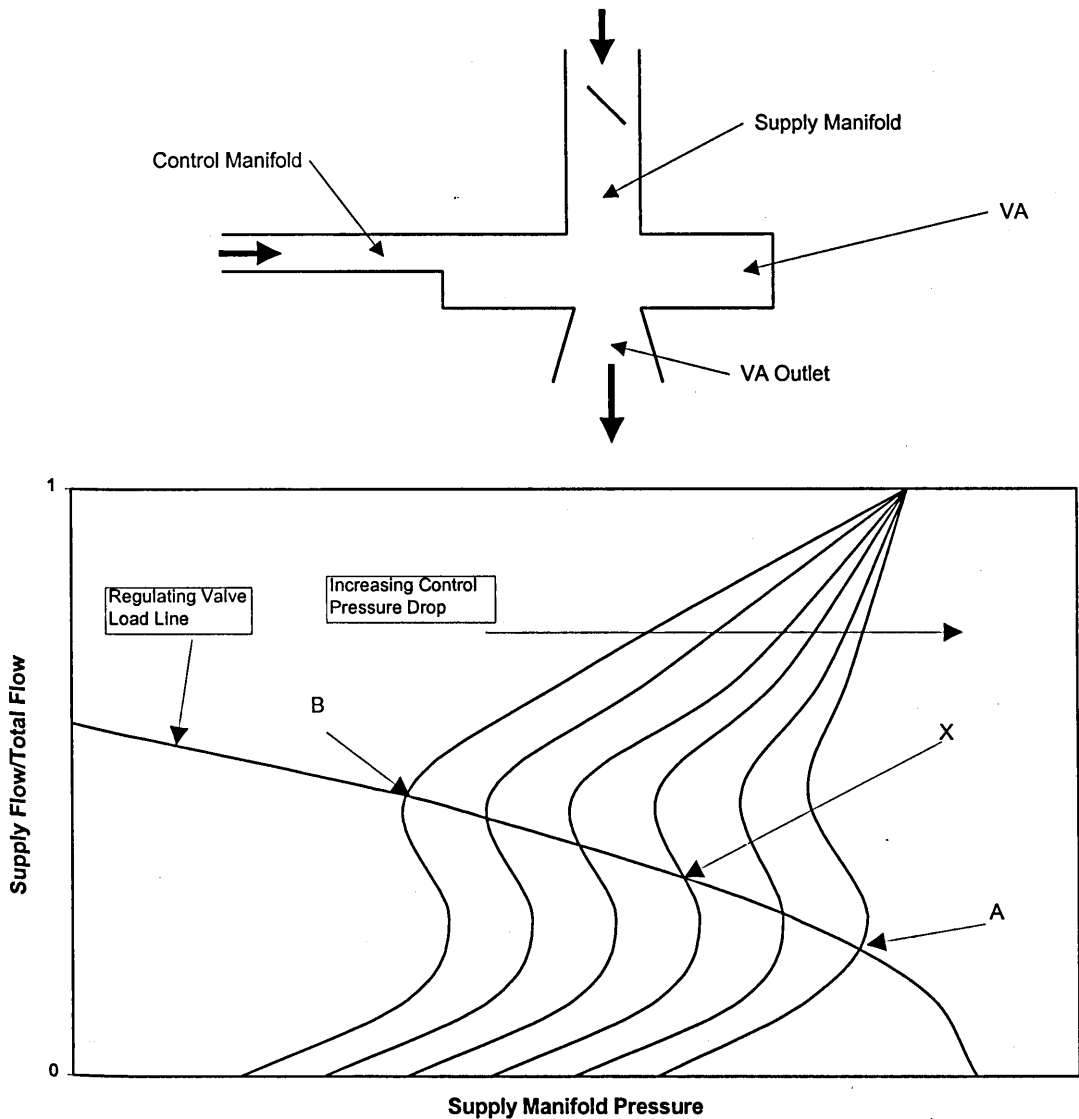


Figure 12 Negative Resistance Surge

Flow field instability in a vortex chamber is due to the oscillating flow structures in the VA such as precessing vortices and vortex breakdown in the exit pipe. The amount of flow instability caused by these effects is small except in the unlikely event that the oscillation occurs at a resonant frequency of the system.

Negative resistance surge is similar to the surge commonly encountered in fans or pumping systems. It is not a property of the VA but of the interaction of the VA and the system in which it is contained. Most VA characteristics have a negative resistance region where the flow increases as the supply pressure decreases. Consider the flow at a point X in Figure 12. This figure shows a family of supply flow characteristics intersecting the load line of a regulating valve. Each characteristic is at constant  $P_{CO}$ .

As the control pressure drop increases it throttles the supply flow, increasing the pressure in the supply manifold. Point X lies in the negative resistance region of one of the constant  $P_{CO}$  characteristics.

In a positive resistance region, such as at point B, a fluctuation causing an increase in supply manifold pressure decreases the flow through the regulating valve and increases the supply flow through the VA. This tends to restore the pressure to its original value. In the negative resistance region at point X, flow is obviously unstable as a slight increase in the supply pressure causes flow through the valve to be greater than that through the supply port. This causes further increase in the supply pressure until point A on the graph is reached, where the control flow characteristic has positive resistance. Flow will then oscillate between points A and B on the regulating valve load line. It can be seen that this instability is strongly dependent upon the interaction with other components in the system as a different valve characteristic would change the conditions where the instability occurred.

Transport delay surge is caused by a mismatch between the rate at which supply and control flows change. For instance, in the series of events depicted in Figure 13, control flow is increased, thus increasing the strength of the vortex in the VA chamber. The inertia of the supply flow means that it does not instantly adjust to the new value and so a surge of supply flow arrives in the chamber, in this case causing negative control flow. This in turn causes the control flow to surge as the supply flow drops, repeating the process.

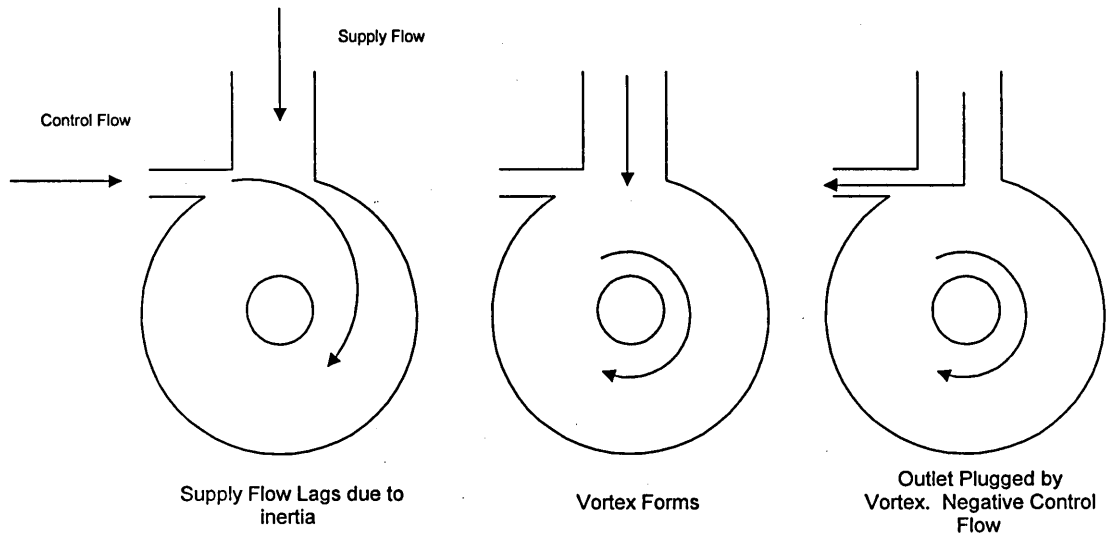


Figure 13 Transport Delay Surge

Both transport delay surge and negative resistance surge are caused by interaction between the VA and the circuit in which it is being used. Both can be prevented around an operating point by making appropriate modifications to the circuit. To prevent transport delay surge, which is the most serious instability there are two strategies:-

i) inertial balancing. Extra control pipe is added to reduce the flow mismatch. The amount of pipe is usually found by cut-and-try methods. Too much pipe reintroduces the surge at a higher frequency.

ii) capacitive decoupling. A large air volume is attached to the supply port.

Although these strategies can give stable VA behaviour around an operating point, it is usually not possible to render a normally bistable VA stable across its entire operating range.

## VI. VA Modelling.

Wormley<sup>23</sup> describes a steady state model for a VA. He considered the chamber flow field as three separate regions:- an inlet mixing region, a main chamber region and an exit region. He developed both an inviscid and a viscous model. Viscous behaviour is simulated by a boundary layer coefficient. The geometrical effects predicted by his model are much the same as those observed experimentally.



Much work (Kitsios<sup>24</sup>, Mo<sup>25</sup>) has been done at Sheffield University in developing a lumped parameter dynamic model for predicting the small signal response of a VA. This work models the VA circuit using transition line modelling in which all the losses in pipes are modelled as lumped resistance and the dynamic response is modelled as lumped capacitance and inertia.

Kitsios followed Anderson's<sup>26</sup> approach. He modelled the VAs response as a combination of two time delays. The first was a pure time delay,  $T_1$ , representing the transport of the new conditions to the chamber exit. The second was a first order lag,  $T_2$ , arising from driving the spinning doughnut inertia to a new state. Therefore the transfer function of the chamber was:-

$$G(s) = K_1 \frac{e^{-sT_1}}{1 + sT_2}$$

Mo used a vortex chamber of very low aspect ratio and found no evidence of a spinning doughnut. He used only a pure time delay to model the chamber.

A complete solution to the flow field within a VA using a CFD technique is very difficult to achieve. This is because the flow in the exit region contains highly curved streamlines and very rapid shear. These conditions violate the assumptions that are normally made to achieve closure of the equations for turbulent flow.

## VII. Practical Applications of Vortex Amplifiers

The VA has been used as a flow controller in applications where the inherent reliability of its no moving parts construction is perceived as an advantage. This is particularly the case in the nuclear industry. As a result VAs have been incorporated in the ventilation systems of nuclear plants. One example of its application has been the pressure regulation of glove boxes (Grant<sup>27</sup>, Balakrishnan<sup>28</sup>). Other applications for the VA include pipeline protection<sup>29</sup>, maintaining constant outflow from a reservoir as the level of water varies<sup>14</sup>, and applying a coating to a round bar<sup>30</sup>. There has also been an effort to improve engine volumetric efficiency by using a VA for intake manifold tuning<sup>31</sup>.

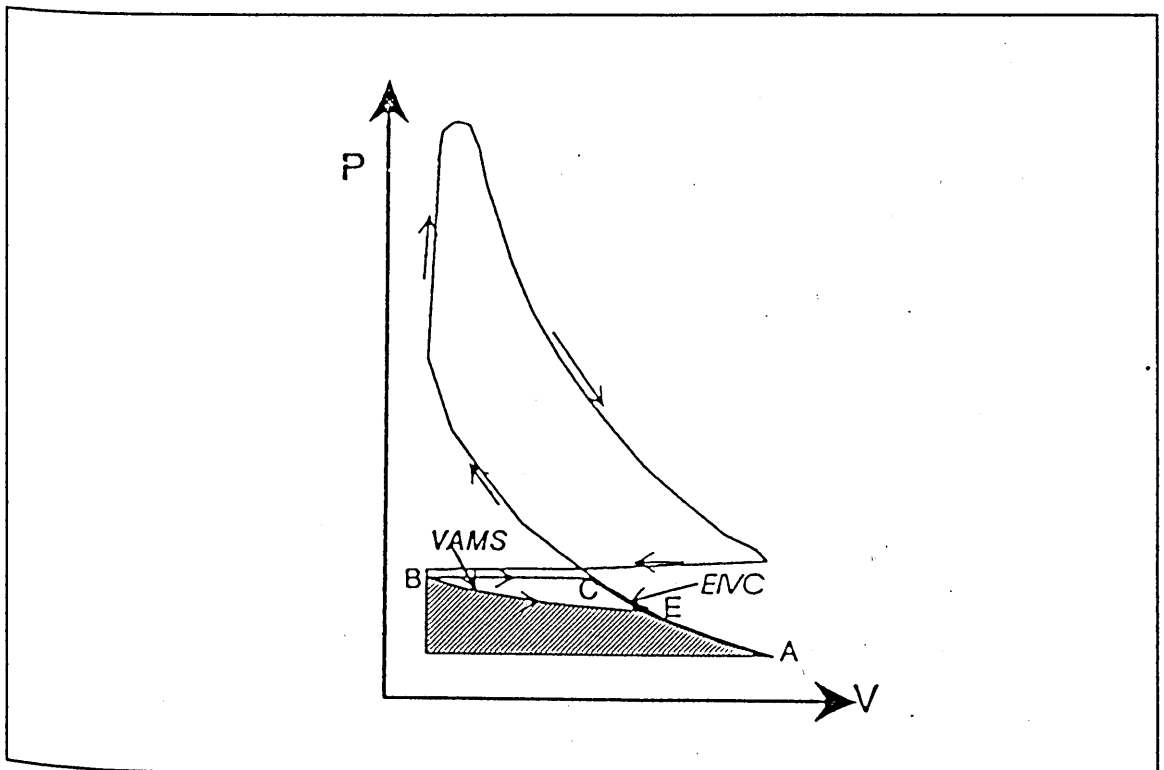


Figure 14 Cycle for combined early inlet valve closing and VA throttling.

A previous study (Abdul-Wahab<sup>4</sup>) evaluated the potential of the VA for controlling the rate of air intake of a spark ignition engine. The primary benefits that were expected were:-

- i) A more linear response than with a conventional throttle valve
- ii) Reduction of pumping losses in the engine
- iii) Improved mixture preparation due to the turbulent exit flow from the VA

The study focused on the reduction of pumping losses. By using individual VAs as intake port throttles it is possible to allow the intake flow to each cylinder to be controlled separately. This means that at part load conditions the intake manifold can remain at almost atmospheric pressure and the required vacuum in the cylinder could be achieved by pressure drop across the VA. The pressure upstream of the intake port can therefore recover between periods of induction. At inlet valve opening (IVO) the cylinder will confront a very small vacuum. Thus the cylinder pressure can decrease progressively during induction. This would reduce pumping losses and minimise exhaust back flow during valve overlap.

This concept was difficult to implement in practice. It was found that it was difficult to achieve the required inlet valve closing (IVC) vacuum for idling conditions. At a typical idling speed of 800 rpm the required cylinder pressure at IVC is around 0.7 bar of vacuum. The VA could not achieve this since suction decreased when the cylinder piston slowed as it approached bottom dead centre. This reduced the intensity of the vortex and thus allowed pressure recovery in the cylinder.

One way to overcome this is to combine the VA with an early inlet valve closing (EIVC) system which could close the cylinder before the piston slowed. Operating in tandem the two systems could provide mutual benefits. The throttling provided by the VA would allow the valve closing to take place later in the cycle than would otherwise be necessary. As considerable charge cooling takes place during expansion if the inlet valve is closed early this would increase the charge temperature at ignition. The use of EIVC would allow less rigid design constraints to be placed on the VA meaning that it could be designed for a good dynamic range. A proposed part load indicator diagram is shown in Figure 14, with the potential pumping savings illustrated.

In the current project it is intended to test the potential of the VA to improve mixture preparation. It is hoped that if a significant improvement in mixture preparation can be demonstrated it will combine with the potential pumping work savings to provide the possibility of significant improvements in engine economy and emissions. It has already been shown in **Chapter 1** that a highly turbulent flow can produce very fine sprays. The VAs ability to dissipate flow energy is due to the high turbulence of the vortex flow field. It also appears that the turbulence is highly concentrated in the VA throat. King<sup>17</sup> estimated that nearly 90% of the pressure drop in the VA at the

vortex state occurs in the throat and diffuser. Fuel injected into this highly turbulent region can reasonably be expected to be atomised into a very fine spray.

## **CHAPTER 3**

### **Measuring droplet sizes**

*An overview of spray measurement techniques is presented, and the operation of the Malvern particle sizer to be used in this project is explained.*

## I. Spray Characteristics and methods of measurement.

The usually accepted definition of a spray is a mechanically produced dispersion of droplets with sufficient momentum to penetrate the surrounding gaseous medium. This implies a large enough mass median diameter to give the spray reasonable momentum. Generally this diameter is greater than 5-10 $\mu\text{m}$ ; droplet dispersions with diameters smaller than these are referred to as aerosols.

Atomisation of sprays is important in many industries, and so experimental studies of sprays have been carried out by many researchers. These usually concentrate on characterising a particular atomiser, and the most important atomiser characteristic is the droplet size distribution. There are several ways of presenting size distributions, for example, Number or Volume distribution, Spatially or Temporally averaged distributions, Overall distributions (for all the droplets in a spray) or Point distributions (for a given position in the spray).

In studies where the evaporation or combustion of a spray is of interest the results are most useful as a volume distribution. This is because a very large number of small droplets can contain a very small proportion of the liquid in the spray. This causes number distributions to be skewed to the smaller droplet sizes, even though the bulk of the spray may be contained in relatively few large droplets. As large droplets will burn or evaporate slowly they are most significant in determining the performance of the atomiser. The volume distribution of a spray can be expressed as a Probability Density Function  $v(D)$  of droplet diameters at the measurement position.

$$v(D) = \lim_{\substack{\Delta D \rightarrow 0 \\ V \rightarrow \infty \\ \Delta A \rightarrow 0}} \left\{ \frac{\text{Vol of Droplets between } D - \frac{\Delta D}{2} \text{ and } D + \frac{\Delta D}{2}}{\Delta D \cdot V} \right\}$$

Where  $V$  is the volume of all the droplets,  $D$  the droplet diameter, and  $\Delta A$  is the elemental area through which the spray passes.

Another useful parameter for the comparison of sprays is the Sauter Mean Diameter of the spray. This is defined as:

$$\text{SMD} = D_{32} = \left\{ \frac{\int_{D_0}^{D_m} D^3 n(D) dD}{\int_{D_0}^{D_m} D^2 n(D) dD} \right\}$$

Where  $n(D)$  is the number distribution of the spray and  $D_m$  and  $D_o$  are the maximum and minimum diameters. The SMD is the diameter of the droplets in a hypothetical mono sized spray having the same volume and surface area as the real spray.

The number distribution, volume distribution and SMD can all be accurately estimated from experimental data if sufficient numbers of droplets are counted. The accuracy of the SMD is the most sensitive of these characteristics to the number of droplets counted, as it is of the highest order.

Figure 15 shows the accuracy with which the SMD can be calculated with 95% confidence limits<sup>32</sup>.

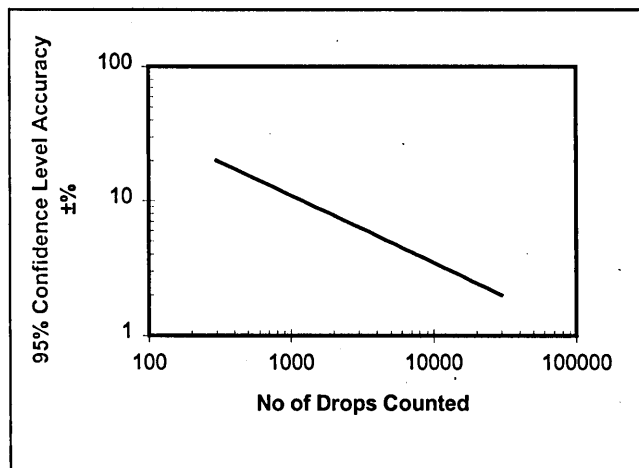


Figure 15 Accuracy of D32 Measurement<sup>32</sup>

Many different methods for measuring the droplets in a spray have been developed. They can be divided into intrusive and non-intrusive techniques. Intrusive techniques generally involve sampling the spray. As they require the insertion of a solid probe into the spray they interfere with the spray prior to measurement. This means they tend to be used only when non-intrusive techniques are impractical. This can be due to either difficulty in gaining access, or high spray density.

Non-intrusive techniques require optical access to the spray. They are subdivided into imaging and optical techniques. A brief summary of the range of options available with some key references are presented in Figure 16.

| Imaging Techniques                  |                                |   |
|-------------------------------------|--------------------------------|---|
| Photography                         | Spark Light Source             | Dombrowski <sup>33</sup> , Yule <sup>34</sup> |
|                                     | Laser Light Source             | Jones <sup>35</sup> , Tishkoff <sup>36</sup>  |
| Velocity and Diameter               | Double Exposure                | McCreath <sup>37</sup>                        |
| Photography                         | Streak                         | Araki <sup>38</sup>                           |
| Video Camera Image<br>Recording     | Semi Automated<br>Analysis     | Markham <sup>39</sup>                         |
|                                     | Automated Analysis             | Simmons <sup>40</sup>                         |
| Holography                          | Manual Analysis                | Thompson <sup>41</sup>                        |
|                                     | Automated Analysis             | Bexon <sup>42</sup>                           |
| Optical Techniques                  |                                |   |
| Single Particle Counting<br>Methods | Single Beam                    | Durst <sup>43</sup>                           |
|                                     | LDA (Diameter and<br>Velocity) | Yule <sup>44</sup> , Farmer <sup>45</sup>     |
| Light Scattering                    | Laser Diffraction              | Swithenbank <sup>46</sup>                     |

Figure 16 Summary of non-intrusive particle sizing techniques

Instruments to implement several particle sizing techniques are commercially available.

The measurement technique chosen for this project is Laser Diffraction. This can be implemented by a Malvern 2600 particle sizer. As it is an optical technique it does not disturb the spray, it allows measurements within a wide size range and automatically produces spray distribution and SMD data. Of all the available techniques it allows the most rapid measurement of sprays, and has shown close agreement with more time consuming imaging techniques<sup>47</sup>. These factors make it suitable for the characterisation of fuel injection sprays and the instrument has been successfully used by other researchers studying low pressure pintle injectors<sup>7,48</sup>.

## II. The Malvern Particle sizer.

When parallel, monochromatic light passes around a small object it creates a pattern of interference fringes. If the shape of the object is known, as in the case of a



spherical droplet, the fringes will produce a characteristic light intensity distribution, dependent on the particle size. When this pattern is focused, the light energy distribution ( $E$ ) at the focal plane from monodisperse spherical particles varies as<sup>46</sup>:

$$E = \frac{2J_1^2(x)}{x}, \text{ where } x = \frac{2\pi as}{\lambda f}$$

Where  $a$  is the particle radius,  $\lambda$  the radiation wavelength,  $f$  the focal length of the lens,  $s$  the radius of the light pattern at the focal plane and  $J_1$  is the first order Bessel function. This equation describes an infinite number of maxima and zero minima. The patterns produced by two different sizes of droplets, with  $\lambda=632.8\text{nm}$  and  $f=300\text{mm}$ , are shown in Figure 17.

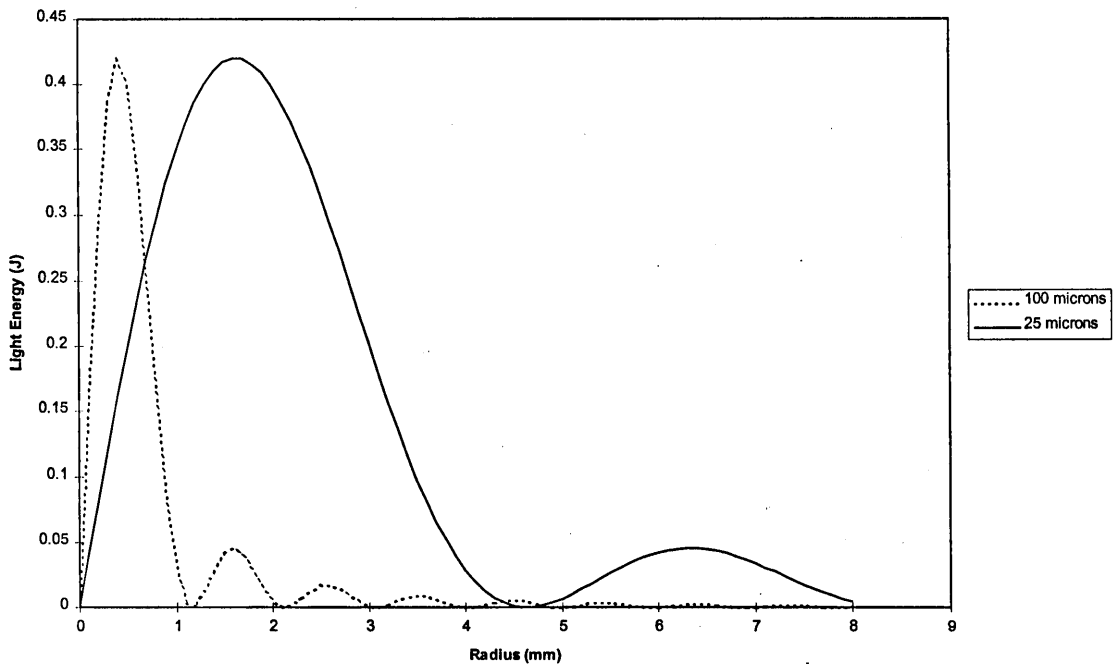


Figure 17 Light energy distributions produced by monodisperse sprays

The Malvern particle sizer uses this effect to measure the sizes of droplets in a spray. A schematic diagram of a Malvern particle sizer is shown in Figure 18.

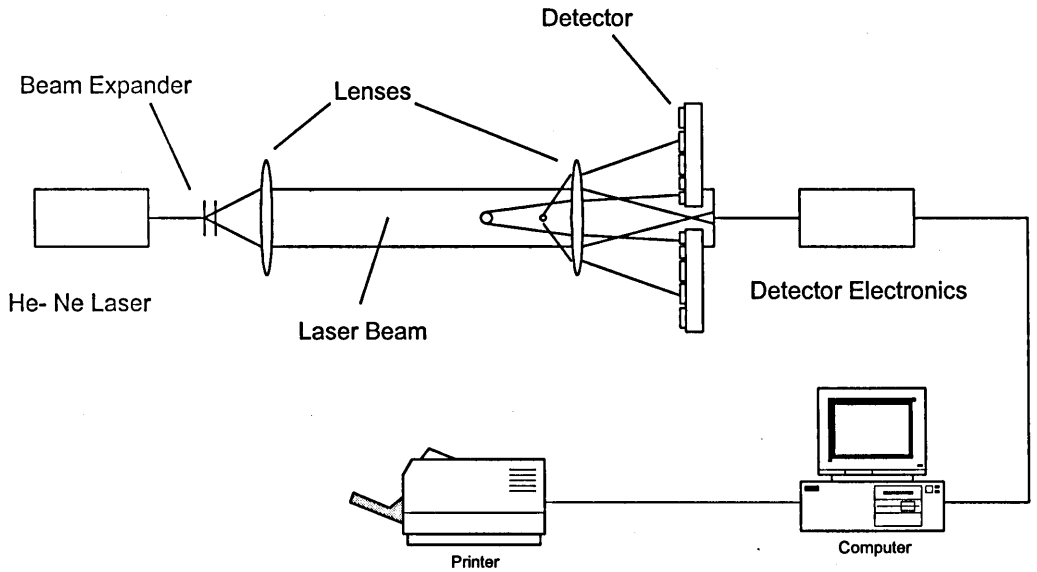


Figure 18 Malvern Particle Sizer

The laser beam is expanded into a collimated, monochromatic beam 9mm in diameter. Any droplets in this beam will scatter light. The peak in the light intensity distribution of the interference fringes depends upon the size of the particle scattering the light. Large droplets scatter most light at low angles and smaller droplets at higher angles. The lens in front of the detector focuses the beam. The detector element is composed of 31 semi-circular photo diodes, the general arrangement of which is shown in Figure 19.

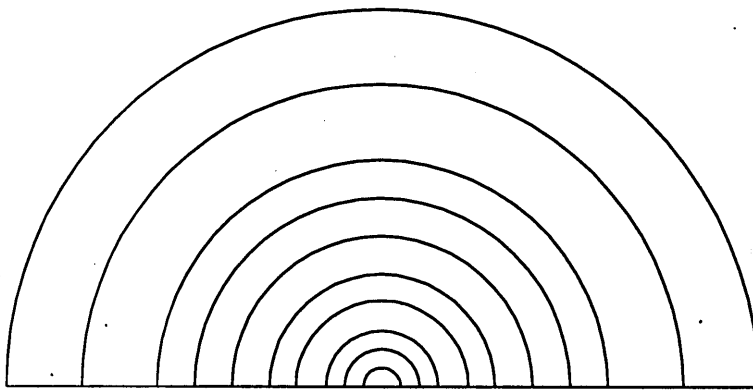


Figure 19 Detector Element Geometry

The undeflected light is focused onto the centre of the detector element, where a small aperture takes it out of the optical system. The volume concentration of the

sample is estimated by measuring the laser energy passing out through the aperture. The lens is a fourier transform lens so that all the light scattered at a particular angle is focused at the same radius. This means the pattern of light detected is not affected by the position within the laser beam of the droplet which scatters it. As the transformation is optical and thus extremely fast, no practically encountered droplet velocities will be high enough to affect the Malvern particle sizer reading.

The light distribution measured by the detector is analysed by the computer to find the volume distribution of the spray. As many droplets are present in the beam the scattered light measured at the detector is the sum of all the individual scattering patterns. The detector provides an electronic output signal proportional to the light energy measured at each of the 31 rings. The computer performs a sweep of the detector rings to find the value of the output signals. This sampling process is extremely rapid, taking approximately 10 $\mu$ s. The software can then calculate the spray volume distribution that would give rise to the observed scattering pattern. The analysis can be constrained to produce a particular form of result, for instance a Rosin-Rammler distribution, but it is usual to perform model independent analysis. This allows resolution of complex distributions, which is important if the measured spray has more than one maxima in its volume distribution. The analysis software contains a table that characterises how a unit volume of material of a given size scatters light. Using this theoretical data the computer estimates the volume distribution that gave rise to the measured light scattering using a process of constrained least squares fitting.

The range of droplet sizes that can be measured by the Malvern particle sizer depends upon the focal length of the lens that focuses light on the detector. Three different choices of range lens are available: 63mm, 100mm and 300mm, and they can measure the size ranges shown in Figure 20.

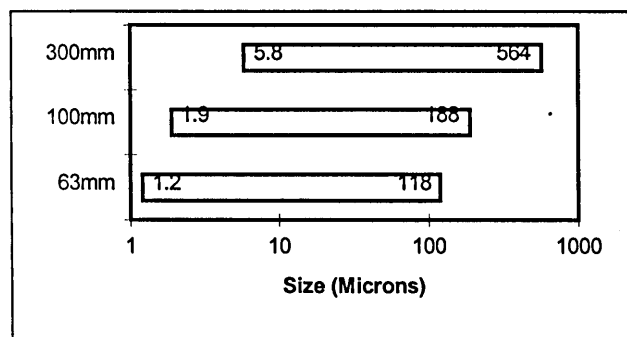


Figure 20 Size ranges measured by different lenses

The spray produced by the pintle injector lies in or below the range measured by the 300mm range lens. The analysis of the scattered light data contains a compensation for undersize particles. As long as there are not many particles below 5.8 $\mu$ m in size, this will mean the 300mm lens is the most appropriate.

### III. Experimental Technique.

#### III.i Choice of fuel

The fuel used in the tests was n-heptane. This has been used successfully by previous researchers with a Malvern particle sizer<sup>7,48</sup>. A gasoline spray is unsuitable for spray measurements. This is because it is difficult to conduct repeatable tests with a mixture such as gasoline, as the proportions of the components change during storage. In addition to this the accuracy of the Malvern particle sizer is adversely affected by the presence of volatile components in the gasoline. The evaporation of the spray creates density gradients along the path of the laser beam. These cause refraction and produce low angle scattering of the light similar to that observed from large droplets. This problem is referred to as 'beam steering'. Use of n-heptane largely eliminates this problem as it has a low saturation pressure at room temperature.

The properties of n-heptane are compared with a typical four star gasoline in Figure 21. Atomisation is mainly controlled by the density, viscosity and surface tension of the liquid. They are sufficiently similar to suppose that results from tests with n-heptane will be similar to those from gasoline sprays. It should be noted gasoline and n-heptane sprays have been observed to behave very differently<sup>48</sup>. This was during injection into a high manifold vacuum with low air-flow, and the difference between the two fuels was attributed to flash boiling of the gasoline when it encountered the manifold vacuum. As the current rig discharges to atmospheric pressure it is expected that this will not be a problem.

| PROPERTY                     | n-HEPTANE | GASOLINE |
|------------------------------|-----------|----------|
| Density (kg/m <sup>3</sup> ) | 684       | 740-760  |
| Boiling Point (°C)           | 98.1      | -        |
| Initial B.P. (°C)            | -         | 28-38    |
| Viscosity (mPa.s) @          |           |          |
| 15.6°C                       | -         | 0.45     |
| 20°C                         | 0.409     | -        |
| 25°C                         | 0.386     | -        |
| 30°C                         | 0.364     | -        |
| 37.8°C                       | -         | 0.38     |
| Surface Tensions (N/m)       | 0.02      | ~0.02    |

Figure 21 Properties of Gasoline and n-Heptane

The spray is introduced into the body of the VA by a pintle injector, and the Malvern particle sizer measures the droplets produced downstream of the VA exit. The spray is contained downstream of the VA as n-heptane is an irritant, and additionally it is desirable to avoid droplet deposition on the lenses of the Malvern particle sizer. To allow optical access to the spray, viewing windows can be fitted to all the various outlets that can be attached downstream of the VA.

### III.ii Preventing lens cut off

Clearly there is a maximum angle of scattered light that the detector lens will focus onto the detector rings. The lens must be close enough to the sample so that all the light scattered at this angle falls within the lens aperture. If the sample is too far away some of the light scattered at the maximum angle will not be collected. This is illustrated in Figure 22 where the maximum scattering angle to be collected is 'a'. The distance within which the sample must lie is referred to as the lens cut off distance, and for the  $f=300\text{mm}$  lens this is 400mm.

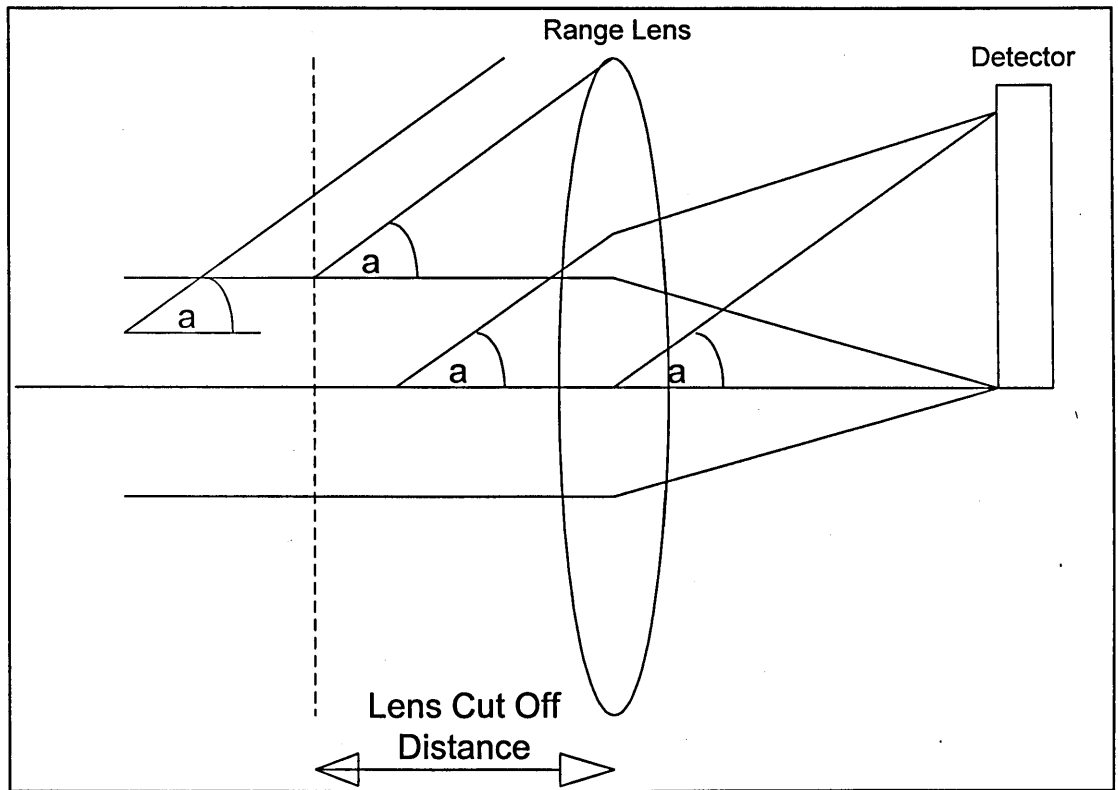


Figure 22 Lens Cut Off

As well as ensuring that the sample lies within 400mm of the lens it is also necessary to take care when designing the windows giving optical access. These must be large enough to allow the light scattered at the maximum angle to pass through them. The lens has an aperture of 50mm, which implies that the highest scattering angle measured is  $3.005^\circ$ . As the maximum distance of the viewing window from the sample is 140mm, the window must be at least 23.8mm in height.

### III.iii Measuring the spray

The Malvern detector will obviously be affected by ambient lighting and any dirt or spray within the beam or deposited on the lenses and viewing windows. It is therefore necessary to measure this background signal before performing any spray measurement. The Malvern particle sizer software then automatically subtracts the background signal from the measured values. When the background signal becomes large due to droplet deposition on the viewing windows they can be removed for cleaning.

As the spray from the injector is a short pulse it is necessary for the computer sweep of the detector rings to be timed relative to the injection pulse. This is possible as the sweep can be triggered externally. Using a single sweep could lead to a lack of statistical significance in the results. This is avoided by repeating the measurement and averaging the results from a number of sweeps. A number of tests were conducted to determine an acceptable number of sweeps to give repeatable results. The data from one such experiment is presented in Figure 23.

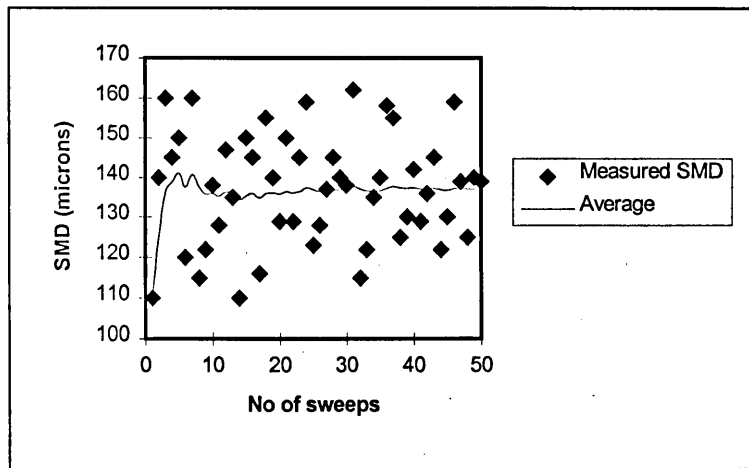


Figure 23 Results from Malvern particle sizer spray measurement (Control Flow through the VA = 200 li/min, time after injection = 14ms)

The data from these tests seem to indicate that the SMD reaches an acceptably stable value after about twenty sweeps. Williams<sup>48</sup> recommends 50 to 100 sweeps, though notes that less can be acceptable. Even when the droplet sizes in the spray are large the laser beam will contain several hundred droplets during any one sweep. Many thousand droplets will be measured with twenty sweeps. With reference to Figure 15 it can be seen that the SMD value should be reasonably free from counting error with this sample size. To allow more experiments to be performed it was decided to use twenty sweeps for all measurements, whilst bearing in mind that this could not guarantee complete confidence in the characterisation of the spray. Further data was gathered for any results that seemed anomalous.

#### III.iv Possible sources of error

Although the Malvern particle sizer allows data to be gathered quickly and easily, it is a non imaging technique and so the results produced must be treated with a

certain amount of caution. Two factors that might conceivably lead to inaccuracy in the results are beam steering and window wetting.

The procedure of measuring the background light scattering prior to every measurement should to a large extent prevent errors due to droplet deposition on the windows. However it would be possible for droplets in advance of the main body of the spray to be deposited on the windows between the fuel injection and the time of measurement. These would then scatter light from the windows and thus affect the results. To minimise this possibility the optical windows were placed some distance from the measurement zone. This strategy appears to have been successful. The increase in the background scatter between two consecutive measurements due to droplets accumulating on the viewing windows was very small.

The mechanism of beam steering by refractive index gradients in the path of the laser beam has already been mentioned in section I. The use of n-heptane as the test fuel should almost completely eliminate this problem. However if good atomisation were achieved the large surface area of very fine sprays will mean that significant evaporation could occur. This would cause refraction of the laser beam. Undelected parallel light could be refracted through a range of small angles, meaning that it is focused on the innermost rings of the detector. Scattered light data that was collected during this research program for measurements with and without beam steering is shown in Figure 24. The additional light focused on the innermost rings can clearly be seen in the left hand chart.

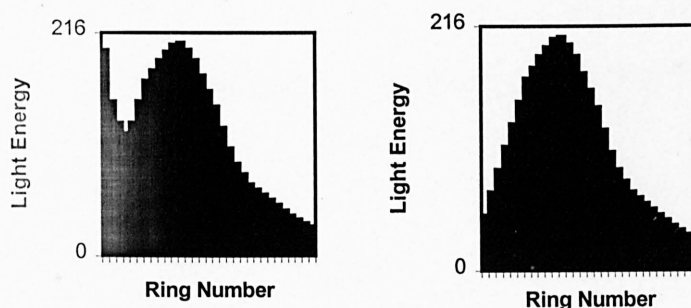


Figure 24 Scattered light data with and without beam steering

This is interpreted by the analysis software as scattered light from large droplets, and distorts the calculated drop size distribution.



Light that has been deflected by droplets can also be steered. However as evaporation is only expected to occur with very fine sprays this will not significantly affect the measurement. There is a logarithmic relationship between drop size and the diffraction angle. This means that for small droplets the beam steering effect is small compared to the diffraction angle.

Another possible problem is that the area of the spray through which the laser beam passes may be unrepresentative of the bulk of the spray. To avoid this the laser beam passes through the axis of the flow out of the VA. As the airflow is axially symmetrical, it is hoped that this means that the laser beam will sample a representative cross section of the spray.

The possibility of these errors occurring make it necessary to validate results obtained with the Malvern particle sizer. The simplest way to do this is by photographing the spray. This allows the size of the largest droplets in the spray to be estimated, and the distribution of the spray to be observed. This data can be used to ascertain whether the Malvern particle sizer is measuring a representative spray sample, and whether beam steering is occurring. The photographs were taken using a conventional 35mm camera with an extension tube. The lighting was provided by a normal camera flash.

As the flash time was approximately 200 $\mu$ s, the definition of many of the photographs was not particularly sharp due to the high speed of the droplets. However to determine the presence of beam steering it is only necessary to see if the scales of the largest droplets in the spray are of the same order as those in the largest size class. If these large droplets are indicated by the Malvern particle sizer measurements, but are not present in the photographs, then evaporation of the droplets is causing refraction of the beam. This problem can be alleviated to some extent by ignoring the data from the innermost rings in the analysis. Clearly this can only be justified if the largest droplets in the spray are sufficiently small for this not to affect the measurement.

As long as these precautions are observed then the Malvern particle sizer will allow rapid measurement of the spray under a wide range of flow conditions. This makes it the ideal instrument for evaluating the VA atomising potential.

## **CHAPTER 4**

### **Designing and Evaluating a Vortex Amplifier**

*To test the effect of Vortex Amplifier geometry on fuel spray atomisation, a Vortex Amplifier with variable geometry was designed and tested. The fuel spray was measured with a Malvern particle sizer and observed photographically.*

## I. Introduction

In determining the effect of a Vortex Amplifier on fuel spray atomisation, it was clearly desirable to investigate how variations in VA geometry can influence spray behaviour. Rather than construct a range of VAs it was decided to design a single VA, for which the main geometrical parameters influencing performance could be varied. This chapter describes the design of this 'Variable Geometry Vortex Amplifier' (VGVA) and presents the results of the tests conducted on it. The first tests determined the steady state characteristics for the range of different VA geometries. It was thought to be important to conduct these tests for a number of reasons. Firstly, several changes had been made to the conventional VA layout to facilitate varying the height and radius (for example two control ports as opposed to the more usual four). The steady state results would check that this did not cause the VGVA to exhibit uncharacteristic behaviour. Secondly, it was hoped that the steady state data would provide insight into the various flow phenomena inside the VA. To test the VA atomising potential a fuel jet was injected into a range of airflow conditions within the body of the VA. The VA geometry was varied throughout the range available with the VGVA. Photographs were taken of the spray and quantitative results were obtained with a Malvern particle sizer.

## II. Design of a variable geometry VA

Although there is a considerable body of literature on designing VAs to achieve a desired steady state performance or stability, this is believed to be the first attempt to utilise the VA as an atomiser. As it is uncertain what effect the geometry of the VA will have upon atomisation, the most thorough approach is to test several different VAs as atomisers. To enable this, a variable geometry VA was designed.

As discussed in the review of literature on Vortex Amplifiers (**Chapter 2, Section IV**), there are four principal geometric ratios that control the flow through a VA. The geometry of a VA is illustrated in **Figure 4**, page 24. Achieving a wide range of VA configurations requires the design of a VA where these ratios can be altered.

The outlet radius is the denominator in all four ratios so it was decided to construct the VGVA with a constant outlet radius. This means that all four ratios can be varied independently by varying the radius, height, supply area and control area of the

VA. The value of the outlet radius determines the pressure drop across the VA with pure supply flow. Abdul-Wahab<sup>4</sup> determined that an outlet radius of 10 mm gives an acceptable pressure drop across the VA (assuming engine speed: 2500rpm, cylinder capacity: 0.5 litre). The eventual aim is to combine throttling and mixture preparation benefits from the VGVA so it was decided to adopt this throat size. This makes the work on these two topics more easily comparable.

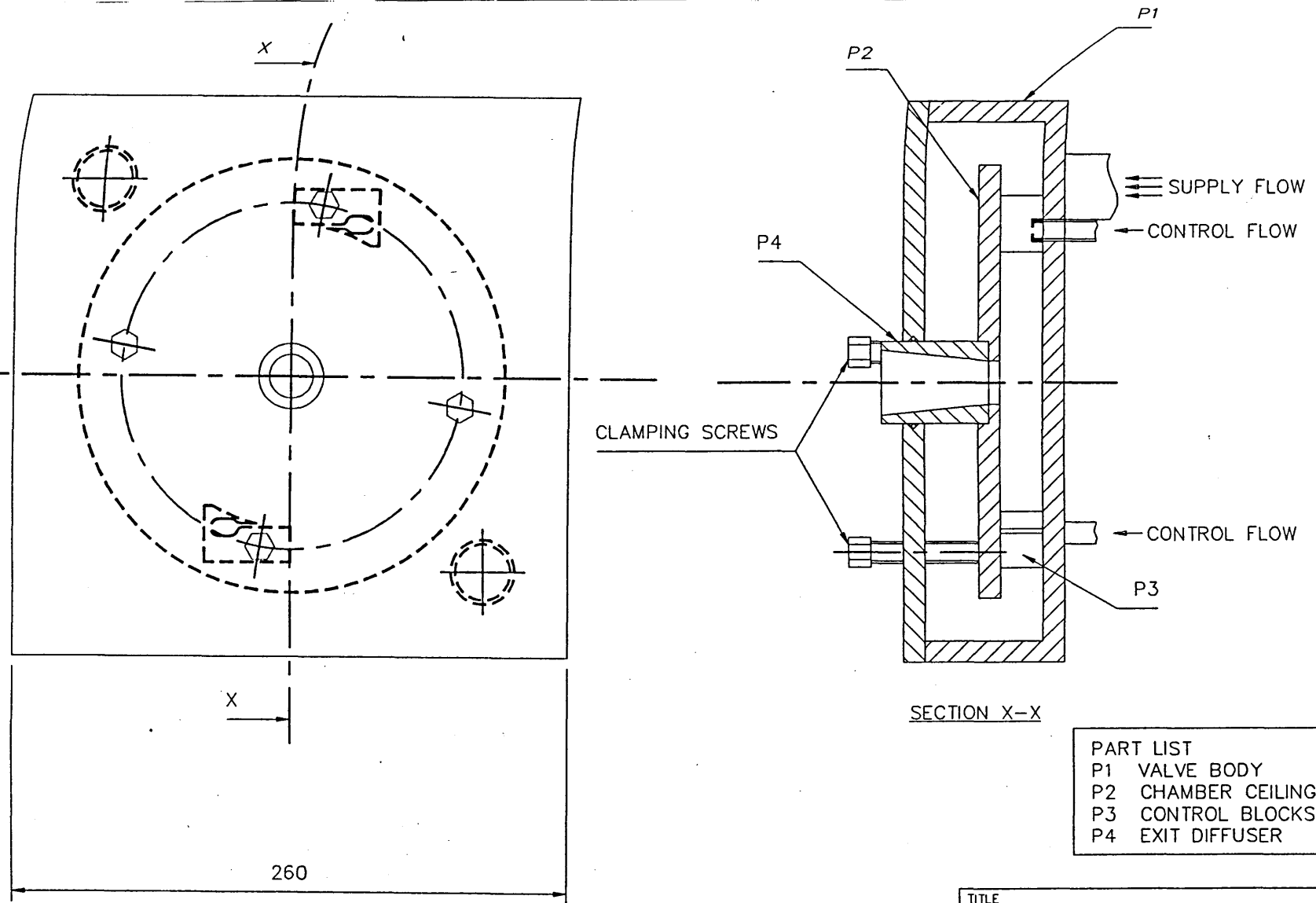
The height area ratio has little effect on the performance of the VA, but can be expected to be significant in atomisation. As the fuel is to be sprayed in from a point on the chamber roof, the chamber height determines the length of fuel jet resident in the chamber. Varying the height of the VA can be achieved through interchangeable control blocks of different heights. However as the control port area is the product of the chamber height and control port width, the different blocks must have different control port widths. This allows the chamber height to be varied independently of the control port area.

The radius ratio will also be significant as it affects flow features such as the 'spinning doughnut' and the precessing vortices in the outlet. The radius of the VA chamber is defined by the radius at which the tangential flow is introduced by the control blocks and can be varied in the VGVA by moving the control blocks. This enables the radius of the VGVA to be varied between 30mm and 70mm.

The VGVA has not been designed to vary the supply or control area ratios. The supply area ratio will vary depending on the position of the control blocks. However this should have negligible effect on the VA performance as the value of the supply area ratio is above 3 for all the VA geometries. The control area ratio is extremely important in determining the steady state performance, but has less effect on the actual flow structure at the VA outlet than the radius ratio. Considering this, it was decided to keep the control area ratio constant.

The variable geometry VA that was designed can be seen in Figure 25. The values of the variable parameters are shown below.

|                    |              |
|--------------------|--------------|
| Height Ratio       | 1,2 or 4     |
| Radius Ratio       | 3,4,5,6 or 7 |
| Control Area ratio | 0.25         |



The control area ratio of 0.25 was chosen based on the results obtained by Abdul-Wahab<sup>4</sup>. It is close to the optimum value he found when using his vortex amplifier manifold system, for throttling the air flow into an engine.

In order to allow optical access for photographs within the VGVA it was mainly constructed from perspex. The exception to this is the control blocks, which due to their intricacy were made by spark erosion from blocks of aluminium.

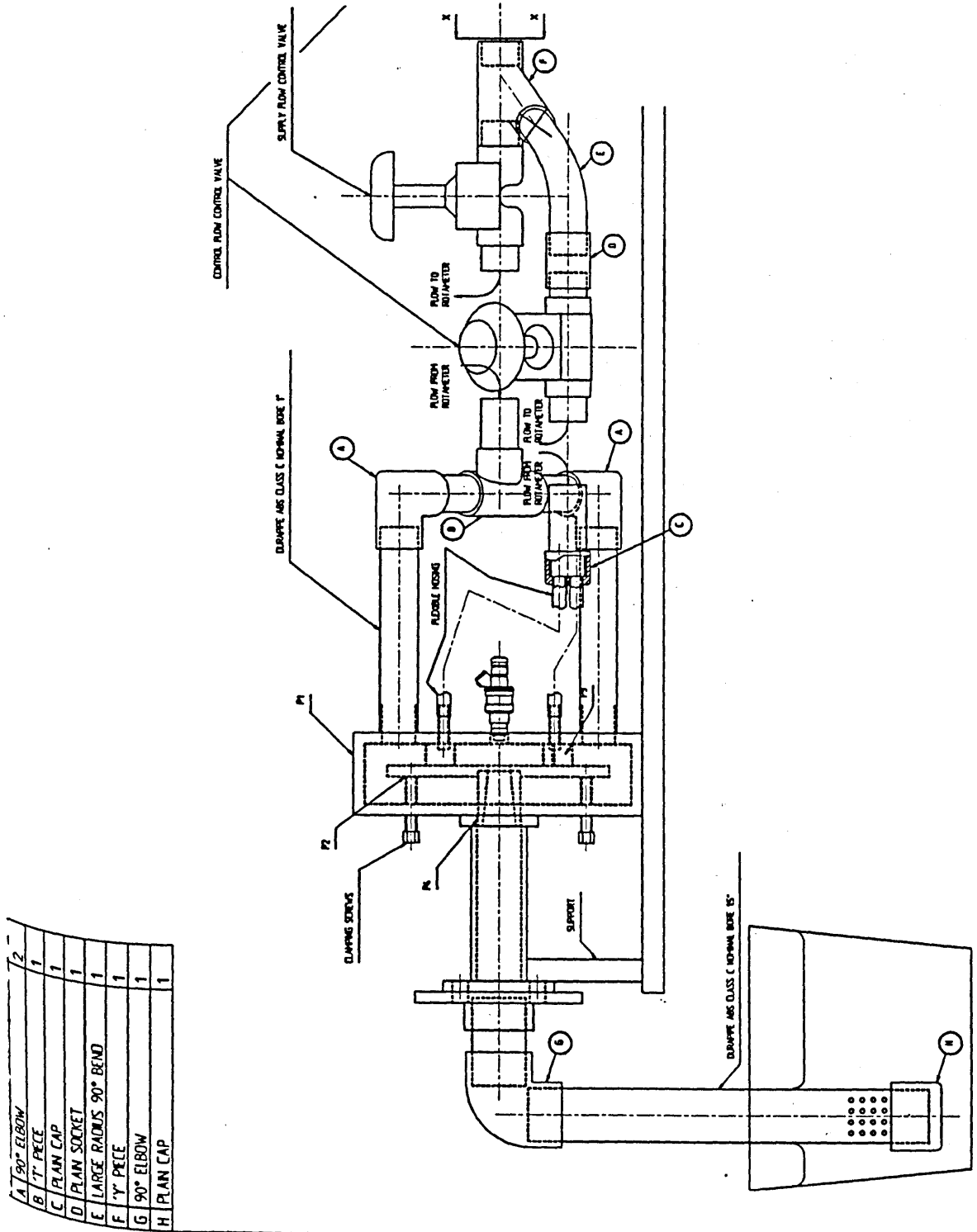
### III. Measuring the steady state characteristics of the VGVA

The VGVA was installed in a test rig. A compressor was used to blow air through the VGVA, and the flow to the supply and control flow inlets could be controlled independently using throttles. The rig was instrumented to allow the steady state characteristics of the various VA configurations to be measured. Due to continuity considerations only two of the three flow rates (i.e.  $Q_T$ ,  $Q_C$ , and  $Q_S$ ) have to be determined. Similarly only two of the three pressures ( $P_{CO}$ ,  $P_{SO}$  and  $P_{CS}$ ) need to be measured.

The test rig was instrumented to measure  $Q_C$  and  $Q_S$ . Downstream of the throttles, rotameters measured the supply and control flow rates. The rotameter for supply flow has a range of 190-2000 li/min; that for control flow, 50-450 li/min.

The pressure drops that were recorded were  $P_{CO}$  and  $P_{CS}$ . Downstream of the control flow rotameter, a pressure transducer measured the gauge pressure. If the VGVA outlet was to atmosphere, then this transducer reading was  $P_{CO}$ . If an outlet plenum was attached then a digital manometer could be used to measure the pressure drop from the plenum to atmosphere, the difference between the transducer reading and this pressure drop being  $P_{CO}$ . It should be noted that, due to the large size of the transducer relative to the control block entrance, the transducer is positioned upstream of the control block. This means that some of the measured pressure drop occurs in the piping. The control to supply pressure drop ( $P_{CS}$ ) was measured by a water manometer. The tapping point for the manometer was upstream of the supply inlet and so includes the pressure drop in the supply plenum.

The remaining flowrate (outlet or total flow) and pressure drop (supply to outlet) required to define the VA state can be calculated from these readings.



|   |                       |   |
|---|-----------------------|---|
| A | 90° ELBOW             | 2 |
| B | 1" PECE               | 1 |
| C | PLAN CAP              | 1 |
| D | PLAN SOCKET           | 1 |
| E | LARGE RADIUS 90° BEND | 1 |
| F | 1" PECE               | 1 |
| G | 90° ELBOW             | 1 |
| H | PLAN CAP              | 1 |

Figure 26 Test rig for flow measurement

The test rig is illustrated in Figure 26.

Steady flow readings were taken for each of the fifteen possible geometries that can be obtained from the VGVA. Readings were taken under supply flow only, control flow only and mixed flow conditions. These readings were then used to plot the steady flow characteristics of the different geometries of the VGVA.

#### **IV. Results of steady flow tests**

Results measured from the test rig were entered directly onto a Microsoft Excel worksheet as this allowed easy manipulation of the data. The results for the largest and smallest VA diameter are presented in Figure 27 and Figure 28 respectively. Each data set represents the measurements taken at one particular height of the vortex chamber. The results for the other VA radii lie within the range bounded by the points plotted on these two graphs.



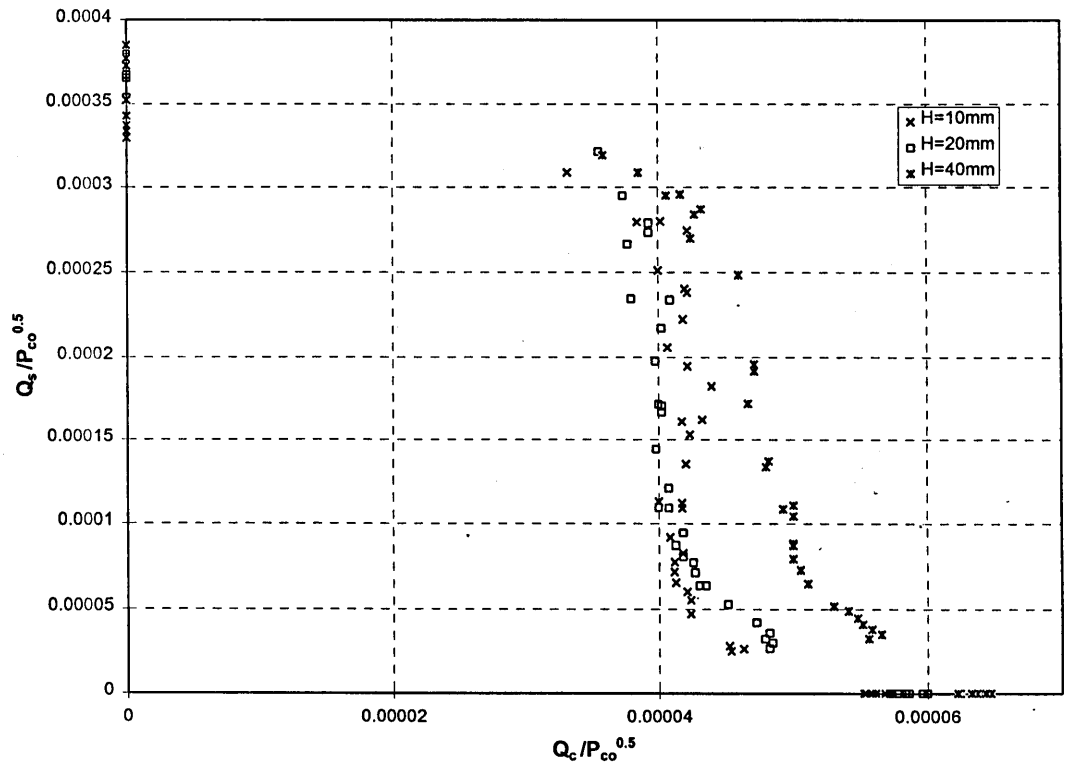
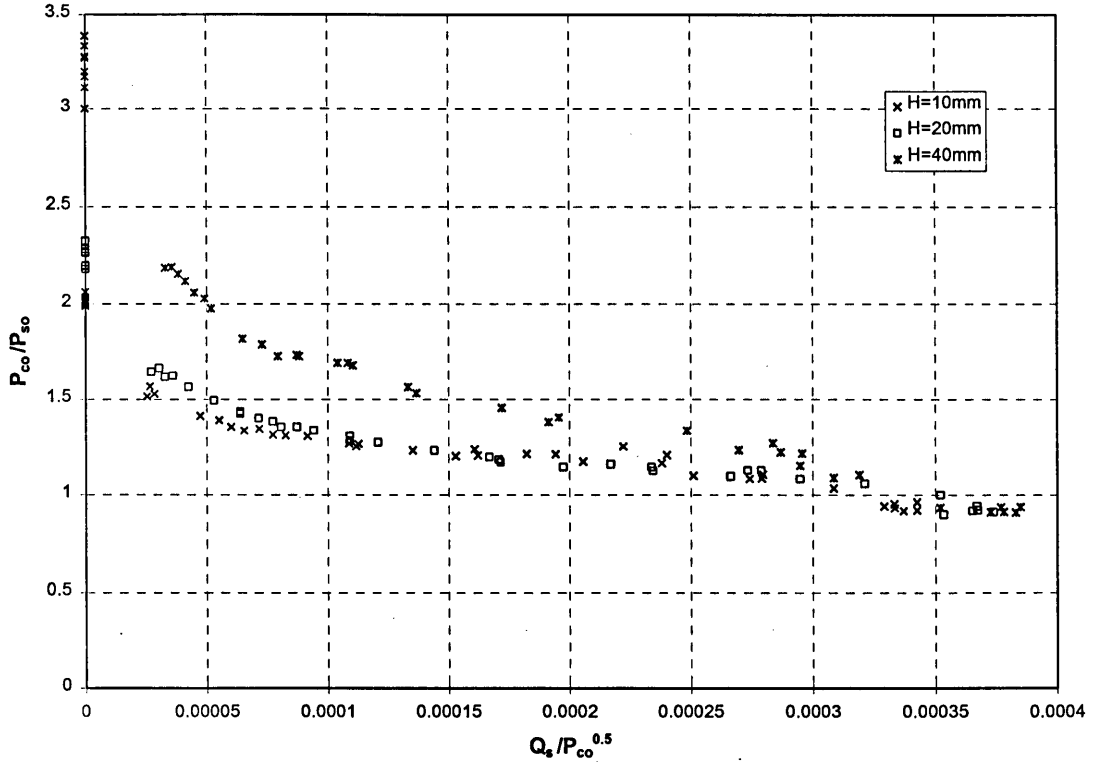


Figure 27 Steady flow data for VGVA with radius set at 70mm.

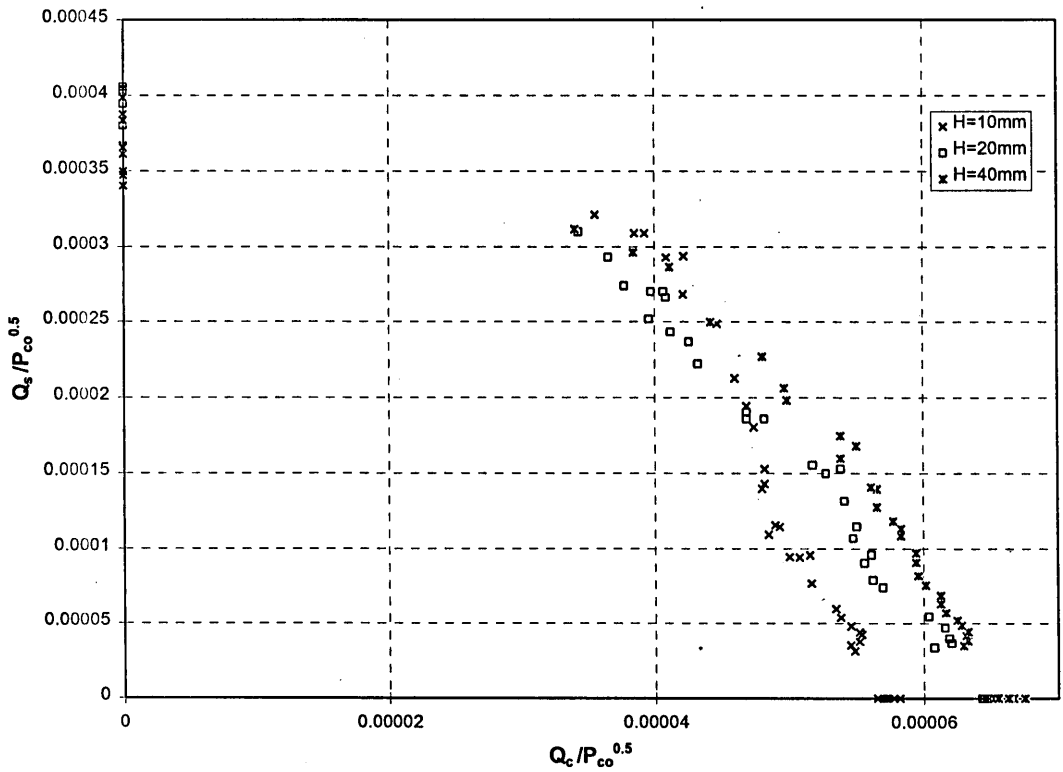
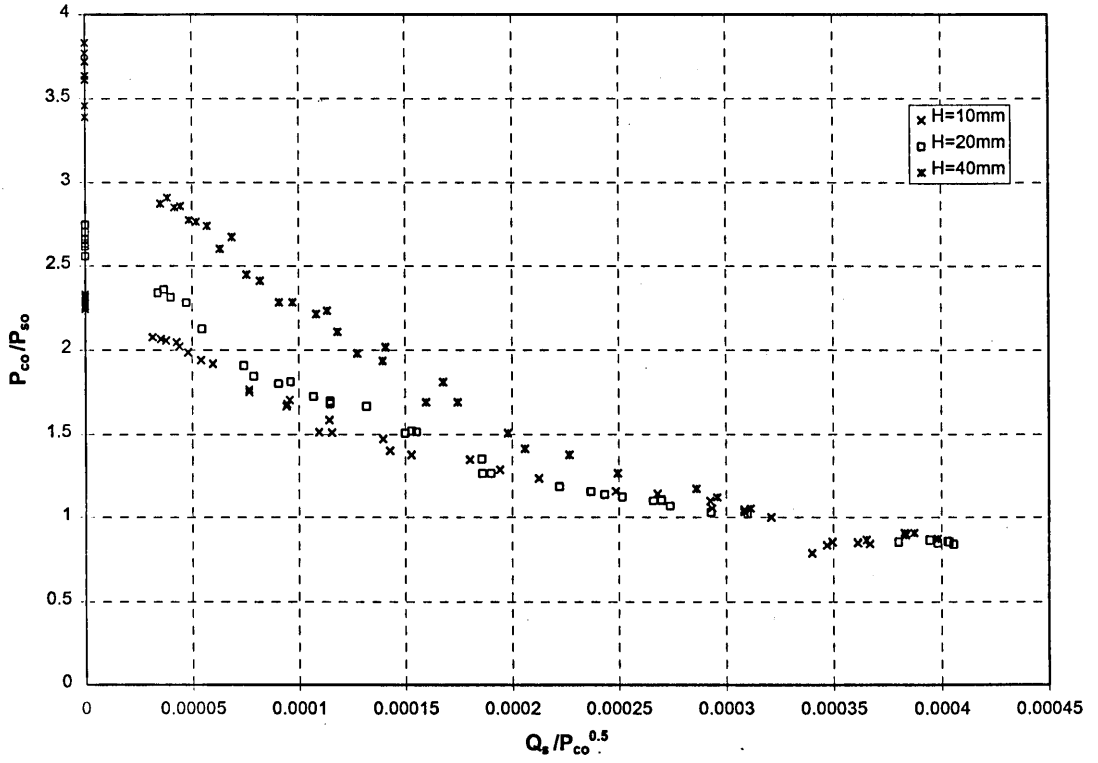


Figure 28 Steady flow data for VGVA with radius set at 30mm

The graphs are plotted with the dimensionless ratios introduced in **Chapter 2**. In the plots of pressure ratio against non dimensional supply flow, the y-axis is the pure control flow state. The proportion of supply flow increases with movement to the right. The second graphs show the non dimensional supply and control flow rates.

## V. Discussion

Typical VA characteristics are depicted in **Chapter 2, Figure 5** and **Figure 6**. There is very little turndown in maximum pressure until the control pressure is equal to supply pressure ( $P_{CS}/P_{CO} = 0$ ). There is then a rapid reduction in outflow as the vortex forms, then a region of less rapid change as the losses due to the high tangential velocities decrease the effect of increasing tangential flow. The characteristics can be of a proportional or bistable form. Measured characteristics often contain discontinuities and jumps.

It can be seen that the results from the VGVA follow this general form well. The characteristic when the height is 40mm is always proportional. All the characteristics from the 30mm radius VA are proportional. The 70mm radius VA produces a bistable characteristic for the two lower VA heights.

Bistable characteristics are produced due to the behaviour of the stagnation point that is located at the outlet of the VA. This stagnation point exists due to the region of negative axial velocity which forms at the centre of the vortex. The step change in the bistable characteristic occurs when this moves suddenly to the backwall of the vortex chamber. This reversed flow zone blocks the VA exit and causes a rapid increase in VA resistance. A proportional characteristic is produced when viscous losses in the body of the VA chamber are significant in the VA resistance.

Many researchers have found that VA characteristics are independent of chamber height. The height dependence shown by the VGVA is probably due to the geometry of the control port in the 40 mm high control block. In order to maintain a constant control to outlet area ratio in the VA at all heights, the control port in the 40 mm high control block was very narrow. The narrow control port width leads to much higher peak velocities in the control jet, and increases the mixing losses as the jet enters the vortex chamber. This imposes a large pressure drop on the control flow, resulting in the much larger  $P_{CO}/P_{SO}$  values observed in the  $H = 40\text{mm}$  plot. Further evidence of the

effect of the control port geometry can be seen from careful study of the  $H = 20\text{mm}$  and  $H = 10\text{mm}$  characteristics. Turndown starts earlier with the 20 mm chamber height as the narrower control port introduces the control flow at a slightly higher average radius, and thus with more angular momentum. However losses, which are caused by the higher velocities in the narrower control port, mean that the 10 mm high chamber achieves cut-off at a slightly lower control pressure.

The proportional characteristic obtained for flow through the 30 mm radius VA implies high viscous losses in the chamber. This is surprising as the 30 mm radius VA clearly has the smallest area of chamber end wall. This means the viscous losses are probably due to high losses in the inlet mixing region between the supply and control flows. Due to the small radius of the VA there is very little room for this mixing region. This means flow from the control jets is likely to spill into the supply plenum, causing high viscous losses. This hypothesis was tested by performing a simple flow visualisation exercise by placing cotton tufts in the supply plenum. These showed there was indeed a high level of turbulence in the supply plenum in the control flow state with the 30 mm radius VA. Although some level of turbulence was present in the supply plenum with all the VA configurations, it was only with the 30 mm radius that it became pronounced.

The pure supply flow condition is practically the same for both radii of VA. This is to be expected due to the fact that in the supply flow condition the VA outlet is the major restriction to flow, and this is the same for both VAs.

Both supply and control flow conditions show considerable scatter on both graphs. As there is no back flow through the VA, all the measurements taken with control flow only correspond to the cut off point. As the  $P_{CO}/P_{SO}$  ratio is theoretically constant at cut off all the control flow only measurements should collapse to a single point. The same should be the case for supply flow.

The scatter in the measured value of  $P_{CO}/P_{SO}$  has no relation to flow velocity. However the deviation of each value from the mean is highest for low flow rates with the higher flow rates usually being reasonably grouped. This means that the primary cause of the scatter is probably due to experimental error. All the pressure gauges used have an accuracy of about  $\pm 1\text{mmH}_2\text{O}$ . At low flow rates, and hence low pressures, this can lead to inaccuracies in calculating pressure ratios. Bearing this in mind, the VA

performance indices have been found from the mean of the closely grouped, high control flow rate data. The best performance is obtained with the VA height set to 10mm. The performance indices for this height at each VA radius are tabulated in Figure 29.

| All heights set at 10mm. |      |      |      |      |      |
|--------------------------|------|------|------|------|------|
| VA Radius                | 30mm | 40mm | 50mm | 60mm | 70mm |
| CPR                      | 2.28 | 1.98 | 1.85 | 1.89 | 2.0  |
| TDR                      | 2.92 | 4.22 | 4.33 | 4.44 | 4.14 |

Figure 29 Table of VA performance indices from VGVA

These results indicate very poor VA performance. This is because the primary aim of the design was to allow variation of the geometry. A VA designed for optimum performance could be expected to achieve a TDR of over 20 at these values of CPR.

It should be born in mind that it is very probable that these results are affected by some VA instability, as no effort has been made to stabilise the test rig. As it is unlikely that the VGVA will be used outside the current test rig it was thought that the considerable effort required to stabilise the VA throughout the operating regime was unnecessary. The results obtained, although not truly static are repeatable as long as the VA remains in the same circuit.

## VI. Design of a fuel injection system

The flow structure in the VA, observed by Asquith<sup>16</sup>, seemed to suggest that the best position for fuel atomisation would be in the highly turbulent exit flow. It was therefore decided to introduce the fuel at the centre of the chamber. This was in the hope that it would be rapidly atomised in the vortex prior to any centrifugal effects flinging the fuel against the chamber walls. The most appropriate form for the fuel spray to take appeared to be a straight jet as this could be accurately directed into the exit flow. Most pulsed fuel injectors for automobile engines are designed to give a wide cone angle. This would increase the likelihood of the fuel being deposited on the walls. To avoid this a Bosch fuel injector, which gave a straight jet, was obtained. The specification of this injector is summarised below.

|                     |                         |
|---------------------|-------------------------|
| Type                | Solenoid Actuated       |
| Car                 | BMW or Rover            |
| Serial Number       | 0280150702              |
| Solenoid Resistance | 15.8 ohms               |
| Solenoid Voltage    | 12 volts                |
| Opening time        | 1ms                     |
| Operating Pressure  | 3 bar                   |
| Flow rate           | 189 to 219 cc/min       |
| or                  | 3.95 cc in 10 2ms shots |

Figure 30 Fuel injector specifications

The timing of the injector was controlled by an electronic clock fitted on a Data Acquisition Board. The 5V pulse from the board was converted to 12V pulse required to power the solenoid by the control circuit shown in Figure 31. The Data Acquisition board could also produce a second 5V pulse which could be used to trigger the Malvern particle sizer measurements, or a camera flash for photographing the spray. This enabled measurements to be synchronised with the fuel injection.

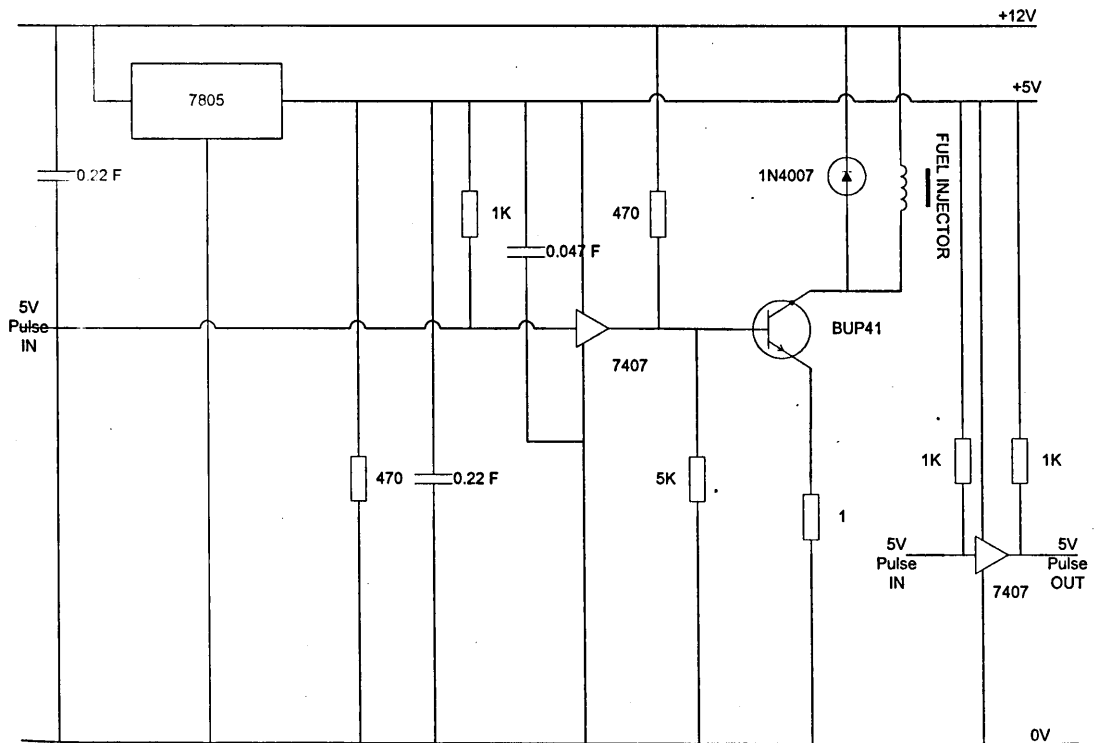


Figure 31 Circuit controlling injection timing

## VII. Photographing the spray

### VII.i Photographs in the VA body.

As it was felt that the complex flow structure in the VA outlet would be significant, it was important to observe the state of the spray entering the exit nozzle. For this purpose a number of photographs of the spray inside the VA body were taken.

Unfortunately it was not possible to photograph the spray within the exit nozzle. To gain an impression of the spray distribution within it the spray was photographed with the chamber set to its maximum height. The cone angle observed within the VA chamber should give some indication of how much spray might be expected to hit the walls in the nozzle. Figure 32 shows a time sequence of injection into a control flow of 100 li/min. The photographs are taken 1ms, 2ms, 3ms and 5ms after the start of a 5ms injection pulse. Clearly when the spray becomes established the cone angle is over 60°. In this case most of the droplets stripped from the jet would hit the walls. However even a modest control flow of 100 li/min is very effective in disrupting the jet. If modifications to the outlet geometry can prevent the spray contacting the chamber walls, then there is potential for excellent fuel and air mixing.

### VII.ii Photographs in the exit pipe.

The photographs taken in the exit pipe were used to corroborate the results from the Malvern particle sizer.

Figure 33 shows the spray in the exit pipe with no air flow 12ms after injection. It is clear, when the spray has just arrived in the measurement zone, that although the spray has broken up considerably after injection the core of the spray still contains many large spray ligaments. This means that the Malvern particle sizer results will be fairly inaccurate. At the later stages of injection, photographs reveal that the spray is more homogenous and the droplets are generally smaller. This is probably due to the larger droplets and ligaments having greater momentum that carries them through the air faster. Thus the size of the droplets in the spray varies with the time after injection. As the spray break up is more complete after the initial large drops and ligaments have passed, the Malvern particle sizer analysis will give a truer picture of the spray. However the presence of the large droplets and ligaments indicate that high readings

upon the inner rings of the Malvern detector are representative of the spray and not due to beam steering.



Figure 32 Time Sequence of spray injected into Control Flow=100li/min.  $T=1,2,3$  and 5ms.

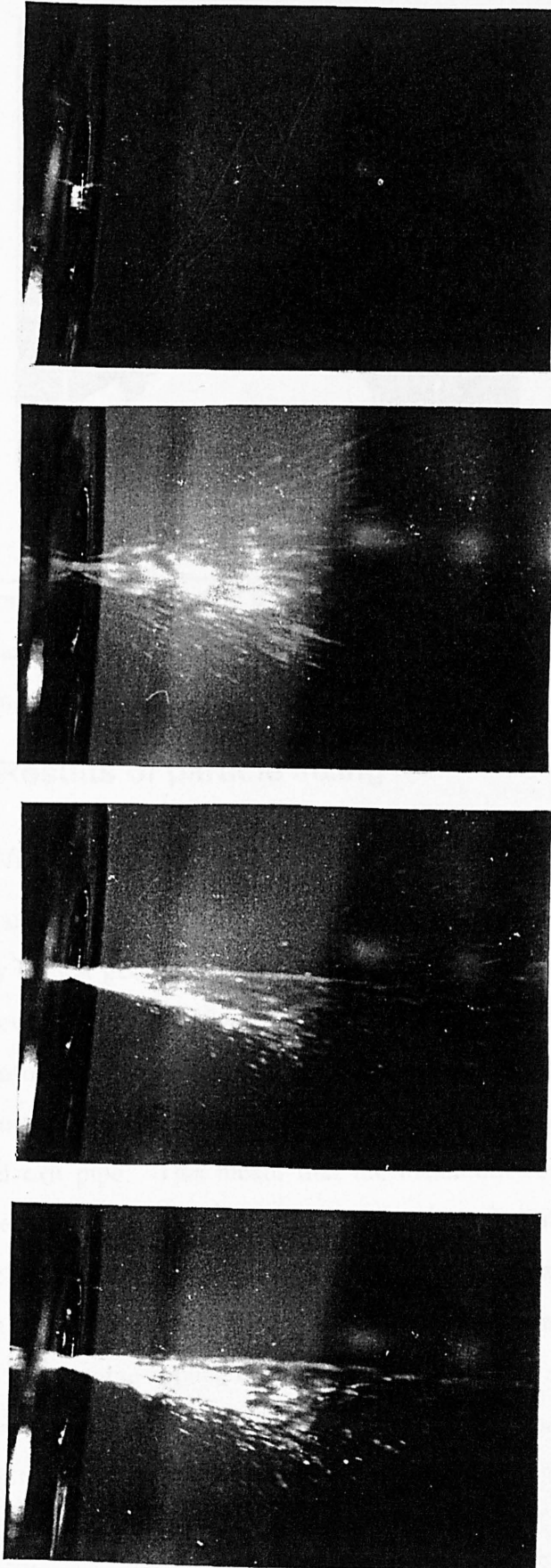
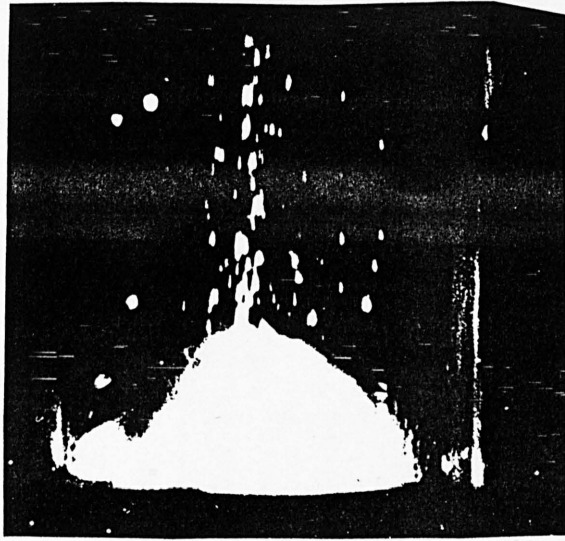


Figure 33 Spray in the measurement zone 12ms after injection into still air



Photographs of the exit pipe for higher control flow rates indicate that no spray reaches the measurement zone for flowrates above 150li/min. This is due to the spray having been flung against the walls of the VA and exit nozzle.

## VIII. Results of particle sizing

### VIII.i Experimental method

Quantitative results describing the spray were obtained with the Malvern particle sizer. A variety of VA geometries were tested over a range of flows. The laser beam was passed through the spray 110mm downstream from the injection position.

The photographs indicated that the range of control flow rates over which valid results could be obtained was limited by droplets hitting the walls of the vortex chamber, exit nozzle and exit pipe. This meant that the maximum control flow rate for which results could be obtained was 150 li/min, as above this value all the spray was impacting on the walls before reaching the measurement zone. The average air flow rate into a 0.5 litre cylinder at idle is around 240 li/min. Clearly the conditions that could be tested had limited relevance to engine applications.

However, it was decided to gather enough data to confirm that the centrifuging action of the vortex was eclipsing any droplet shattering effect. The data could be used to provide some insight into improving the situation.

### VIII.ii Spray Measurements

The first set of tests was undertaken to show any variations in the spray with time from the start of injection. The speed of the spray at injection was determined from the photographs to be around 9 m/s, so spray arrived in the laser beam after approximately 12 ms. Figure 34 shows how the Sauter mean diameter of the spray varies with time from the start of injection over a range of control flow rates.

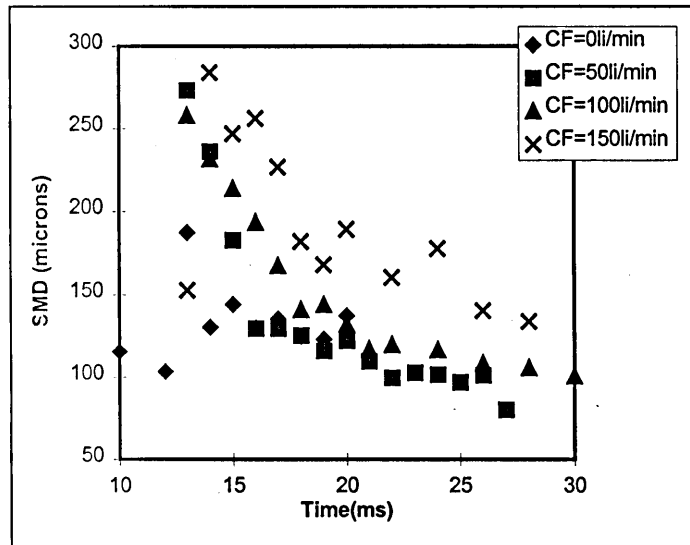


Figure 34 Variation of spray SMD with time after injection

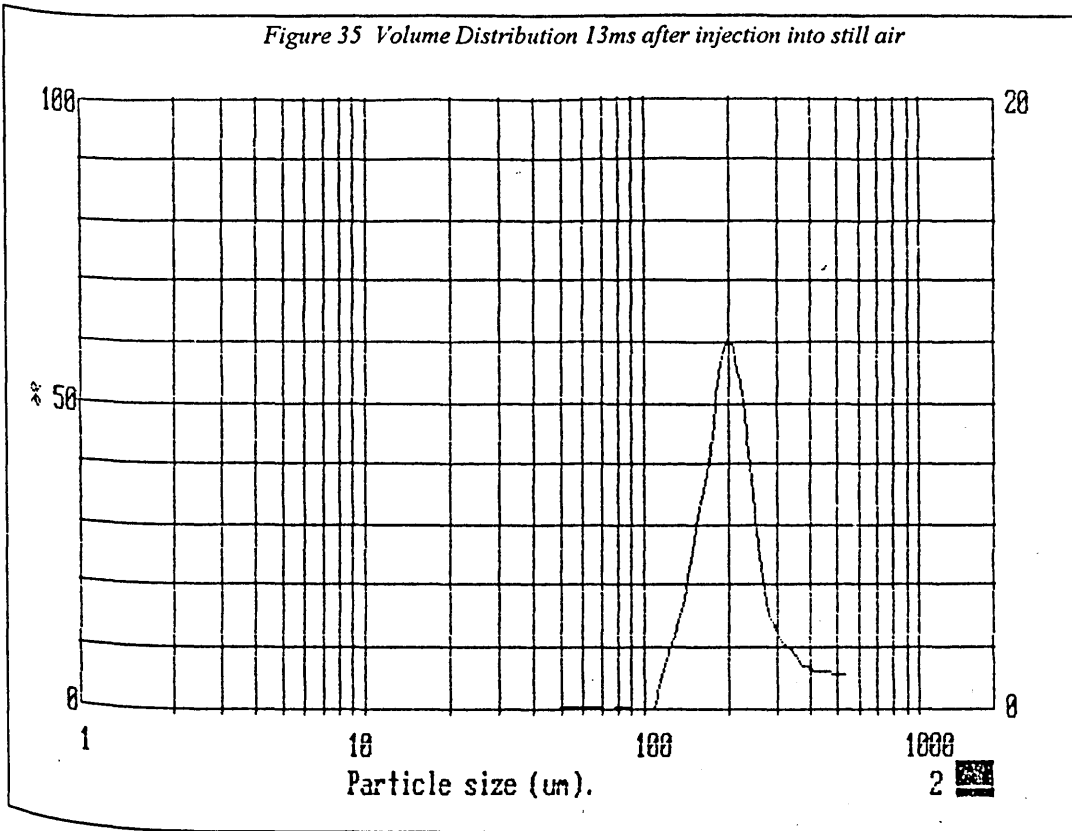
The readings were all taken with the VA height set to 10mm and the radius 40mm.

It can be seen that the trend in all the flow rates is for the SMD to decrease with time after injection. The results that deviate from this trend (the first two data points for zero flow and the first point for CF=150li/min) have very low volume concentrations. This indicates that they are due to a few small droplets sheared from the injector nozzle at the start of injection, prior to the arrival of the main body of the spray.

In general the SMD increases for larger control flows. This indicates that the vortex flow is having no beneficial effect on spray break up. Spray photographs have indicated that the control flow does strip smaller droplets from the spray, but these must all impact upon walls prior to reaching the measurement zone.

For a more detailed analysis of the spray it is possible to examine the frequency distributions of the droplets. Figure 35 and Figure 36 compare the two distributions for the jet passing through quiescent air. It can be seen that two monomodal distributions

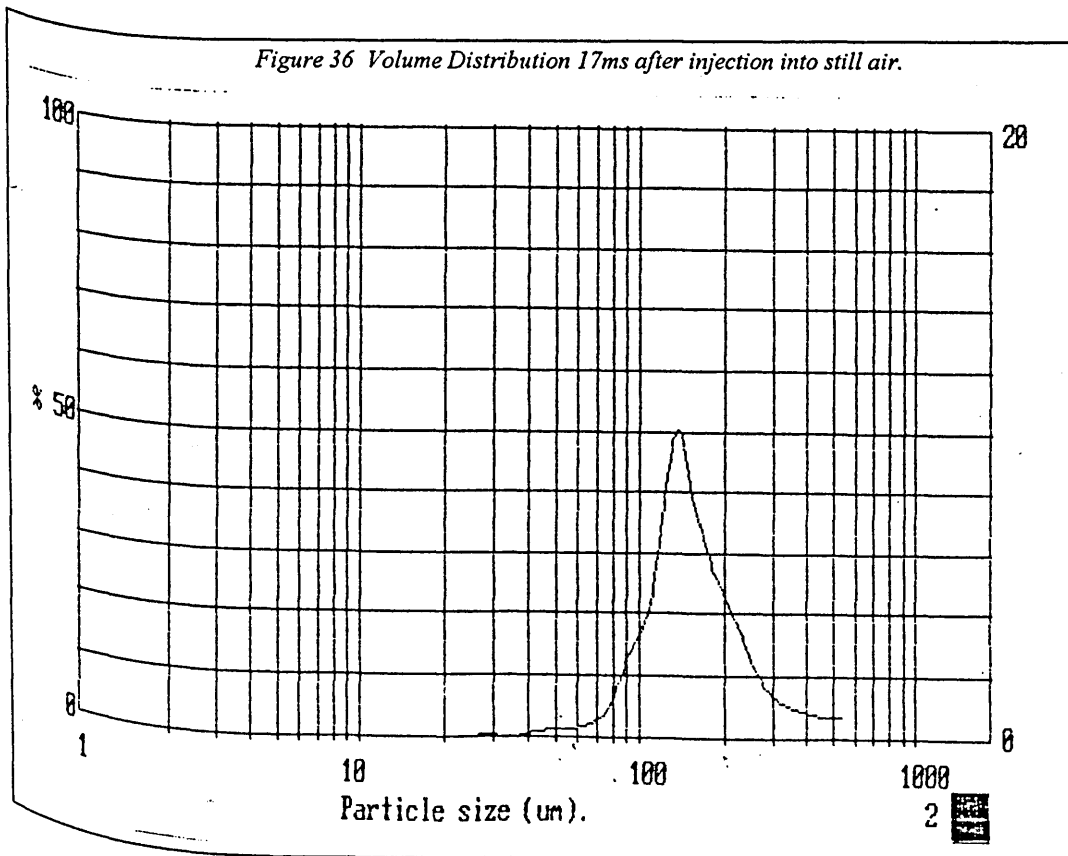
Figure 35 Volume Distribution 13ms after injection into still air

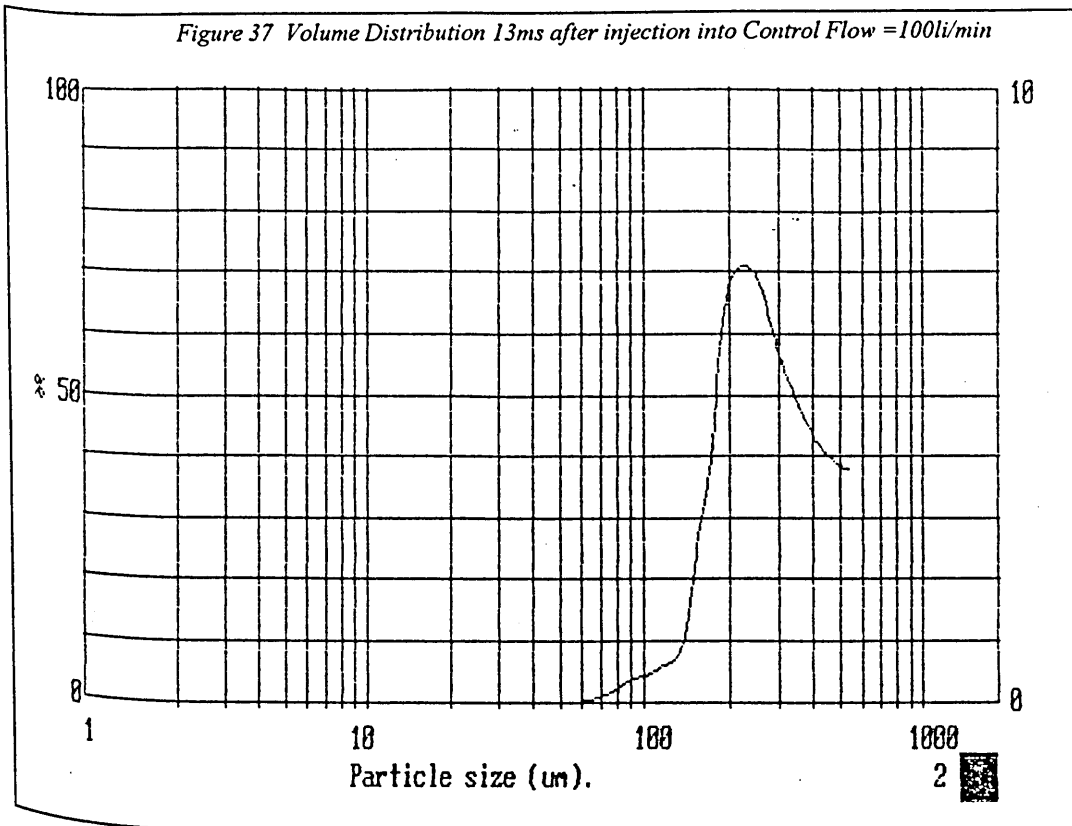


are obtained, the latter peaking at a lower droplet diameter. This is very much as suggested from the photographs and graphs of Sauter mean diameter.

Clearly the introduction of control flow has a significant effect on the frequency

Figure 36 Volume Distribution 17ms after injection into still air.

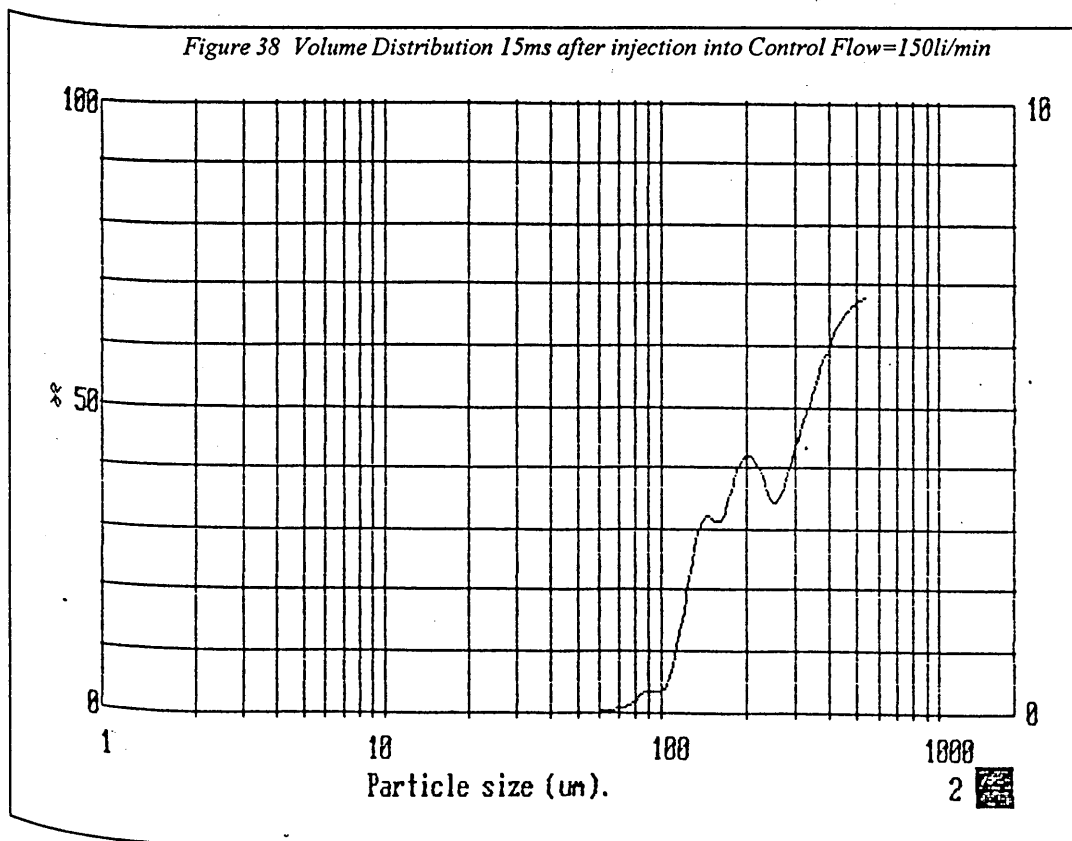




distribution. In Figure 37 there is a group of smaller droplets at around 80  $\mu\text{m}$ , that have been stripped from the spray. More significant than this however is the increased percentage of larger droplets in the spray. This is presumed to be because many of the droplets of around 200  $\mu\text{m}$  size that predominate in the jet without control flow are flung against the walls by the vortex. This centrifuging effect can be observed with all the frequency distributions measured with control flow.

The largest control flow rate at which droplets could be observed in the measurement zone was 150 li/min. Figure 38 shows the volume frequency distributions measured at this flow rate. It can be seen that the peak diameters increase with the control flow and the distribution becomes skewed to the larger diameters. It is believed that this is due not to inferior spray break-up but rather the centrifuging of smaller droplets against the walls reducing their frequency. It can be seen that by the time the control flow reaches 150 li/min this effect is so severe that the very large droplets ( $>300\mu\text{m}$ ) predominate.

A variety of VA configurations were tested to see if the geometry of the vortex chamber influenced the Sauter mean diameter. Figure 39 shows two graphs summarising the SMDs obtained in a variety of set ups. All these readings were taken at  $t=15\text{ms}$  after the start of injection.



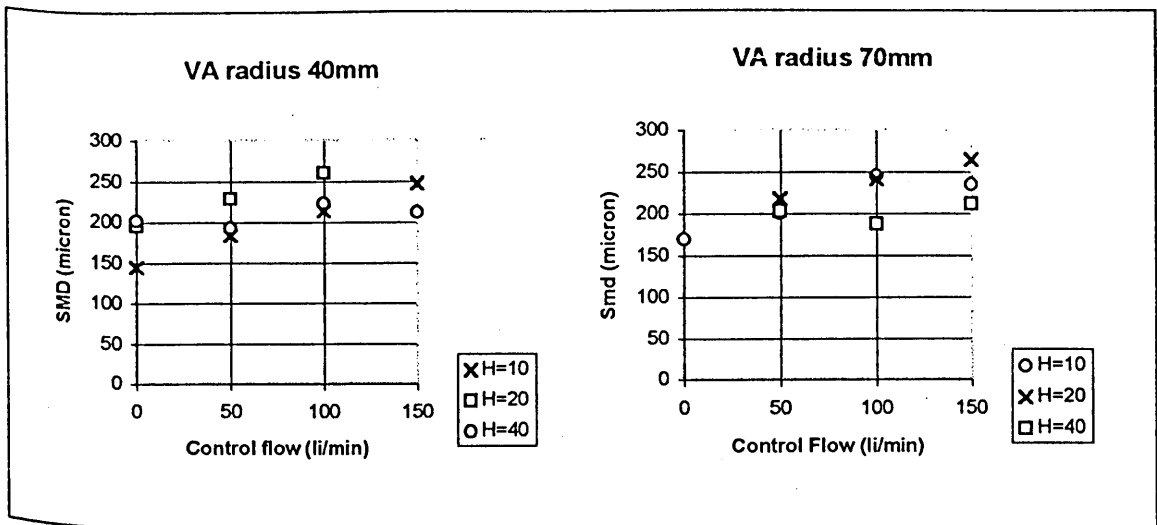
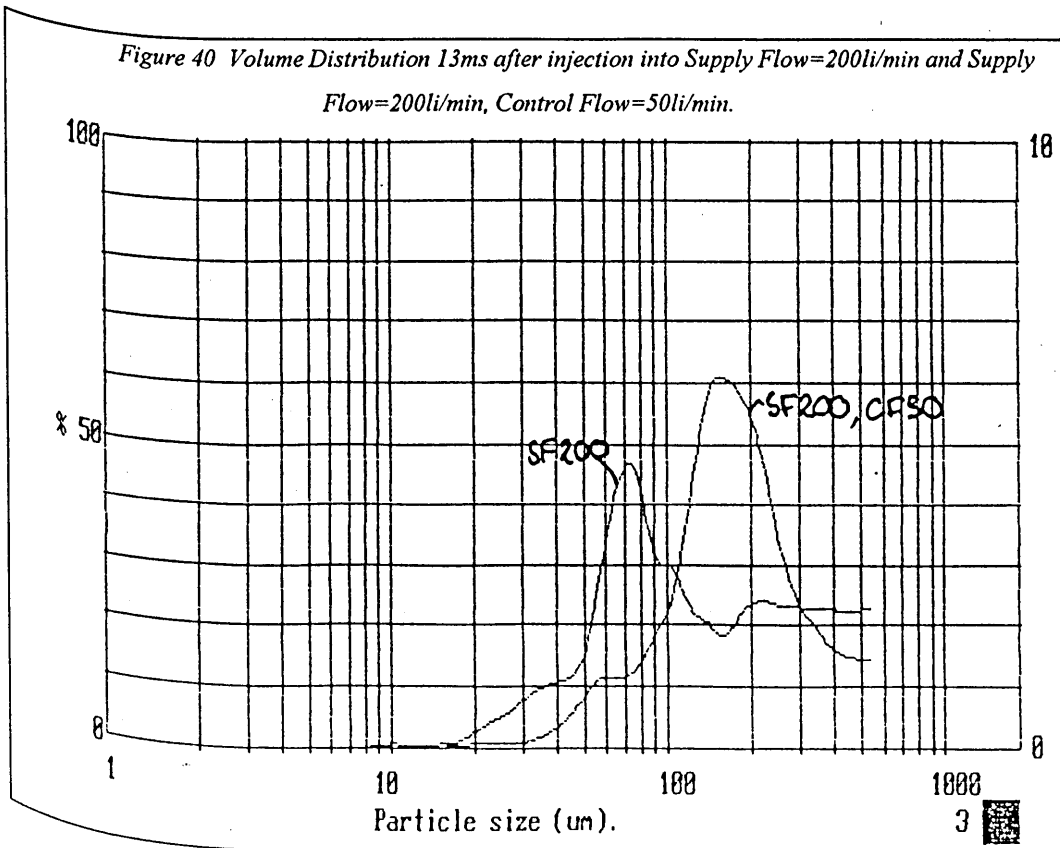


Figure 39 Summary of SMD data

It can be seen that there is no significant difference in the results for the two different radii. Although it appears that there might be some variation in the SMD due to chamber height it is small, and probably due to statistical scatter in view of the small sample size. Thus it would appear that the route to improving the atomising performance of the VA does not lie in altering the internal geometry.

It was clear that the droplets lacked enough forward momentum to resist the centrifuging action of the vortex. It was therefore decided to reduce the vortex intensity

Figure 40 Volume Distribution 13ms after injection into Supply Flow=200li/min and Supply Flow=200li/min, Control Flow=50li/min.



by using mixtures of supply and control flow.

Figure 41 shows SMDs obtained using supply flow only, and mixed supply and control flows. For the supply flow only the SMDs are scattered between 100 and 150 microns. This is significantly better atomisation than that obtained with control flow only. It is unlikely that the supply flow actually produces better atomisation than the much more turbulent control flow, but as there is no tangential velocity component the smaller droplets are not flung against walls. It is also clear that when control flow is introduced the effect is not to improve atomisation but to centrifuge out the smaller droplets.

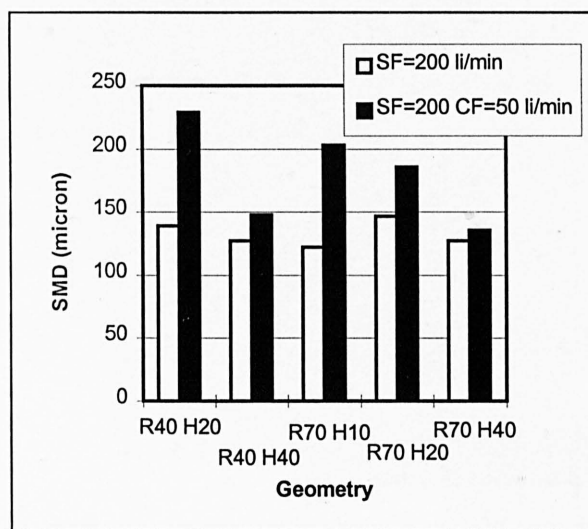


Figure 41 SMD measurements with supply flow through the VA

This effect can be clearly demonstrated by comparison of the frequency distribution of the two cases. Figure 40 shows two sets of measured frequency distributions.

## IX. Discussion of results

The results of this first stage of experiments are disappointing, and the current form of the VA will not improve engine performance. All the results have shown that with any control flow most of the fuel droplets do not reach the measurement zone. They are flung against the walls of the VA chamber, exit nozzle and exit pipe. Only large droplets with their higher momentum reach the measurement zone, and even these are centrifuged at flow rates above about 200li/min.



However the photographs show that the spray is broken up by the vortex flow. If the outlet geometry could be modified to prevent the impact of the droplets in the outlet nozzle then the benefits of better mixture preparation might be obtained.

## CHAPTER 5

### **Designing a VA optimised for atomisation**

*In light of the results from testing on the Variable Geometry Vortex Amplifier a new Vortex Amplifier was designed.*

## I. Criteria for design of new VA

The tests from the VGVA revealed that the VA chamber height was the most important geometric parameter controlling the droplet sizes reaching the measurement zone. This was because the vortex flow caused the spray to disperse rapidly. With a large chamber height the spray was deposited on the walls within the VA. Therefore spray penetration would be best in a chamber that had the lowest possible height compatible with good VA throttling performance.

As the VGVA had indicated that the geometric ratios controlling VA performance had little effect on the droplet sizes produced, it is possible to optimise all these ratios for throttling performance. The outlet diameter of the VGVA was 20mm. This was maintained in the new VA. The chamber height was set as low as possible whilst still retaining the VA outlet as the smallest flow area in the VA. All the other aspects of VA geometry were optimised to give the best VA performance.

The VGVA had also shown that the outlet geometry was significant and had to be designed to prevent droplet impaction. With this in mind three outlet diffusers were designed for the VA. These could be interchanged to establish the best configuration for atomisation. In addition the flow from the VA could be discharged into either of two interchangeable pipes, which were both designed to allow optical access.

## II. Steady flow performance of VA

A paper by King<sup>15</sup> contains a design process with which to optimise the performance of a VA. The VA performance is controlled by eight geometric parameters which are normalised with respect to either the VA throat diameter or the VA throat area. The VA performance can be optimised with respect to either the flow (max TDR) or the pressure (max CPR), or a compromise design that maximises the ratio TDR/CPR.

If used as an intake port throttle a VA would have to regulate the flow rate in an engine, so a high TDR is desirable. However it is hoped a VA can reduce pumping work by reducing the manifold vacuum confronted by the cylinder during intake valve opening. This means a low CPR is also desirable. In view of this it was decided to design a new VA to the compromise geometry. Figure 42 shows the ratios suggested by

the design process for each of the optimum geometries, together with the expected performance of the VA.:-

| Ratio     | Description   | High<br>TDR | High<br>TDR/CP<br>R | Low<br>CPR |
|-----------|---|-------------|---------------------|------------|
| $A_s/A_e$ | Supply area ratio   | >3          | >3                  | >3         |
| $h/d_e$   | Chamber height ratio  | 0.19        | 0.19                | 0.19       |
| $l$       | Length of exit throat<br>(N <sup>o</sup> of exit diameters)   | <1          | £1                  | ³2         |
| $r$       | Blending radius on exit<br>(N <sup>o</sup> of exit diameters) | ³0.25       | ³0.25               | £0.25      |
| AR        | Diffuser area ratio   | 4<AR<9      | 4<AR<9              | 4<AR<9     |
| $A_c/A_t$ | Control jet area ratio  | 14          | 3.5                 | 1.2        |
| $d_o/d_e$ | Chamber diameter ratio  | 2           | 2.5                 | 6          |
| TDR       | Predicted   | 20          | 16                  | 10         |
| CPR       | Predicted   | 2.7         | 1.3                 | 1.1        |
| TDR/CPR   | Predicted   | 7.5         | 12.5                | 9.1        |

Figure 42 Geometric Ratios for best performance of a VA

It can be seen that the control jet area ratio and the chamber diameter ratio are highly significant in determining VA performance.

The new VA was designed to give high TDR/CPR. Only two changes were made from the optimum ratios shown in Figure 42. The exit pipe attached to the VA was not wide enough to allow a diffuser ratio of 4. Also the parallel section at the outlet throat was not included in the design.

Three diffusers were made to fit the VA outlet. They all had the same exit area ratio of 1.96. They were of different lengths (10mm, 20mm and 40mm) and consequently different exit angles. The 10mm long diffuser had a sufficiently large angle to be considered a sharp edged orifice. The two longer diffusers had exit angles of 5° and 11.3°.

The parallel outlet section was omitted from the VA throat after considering the results from the tests on the first VA. These indicated the importance of reducing the residence time of the spray within the VA if droplet impaction was to be minimised. This omission should result in a slight increase in the CPR relative to that predicted by the design algorithm.

Additionally it should be noted that King recommends the inclusion of a pip on the back wall of the VA chamber positioned opposite the outlet. However as this was the intended injector position this feature could not be included. The presence of a pip enhances the turn down ratio of VAs with high values of  $A_e/A_p$ , such as that recommended for the high TDR/CPR geometry. Therefore the new VA should show a slightly lower TDR than that predicted by the design algorithm.

The VA was built according to these design principles. A scale drawing of the VA is included in Figure 44, with the fuel injector in position. Included in this drawing are the three interchangeable outlet diffusers that could be attached to the VA, and the two outlet tubes.

One of the outlet tubes is a large, square section viewing chamber. This was designed to allow easy optical access to the spray from the VA without any risk of droplet deposition. The other is a round section tube which provides a more realistic approximation of the geometry the VA would discharge into in an engine. Figure 43 shows a photograph of the VA and test rig, with the square section outlet tube attached.

Figure 43 Photograph of VA installed in test rig

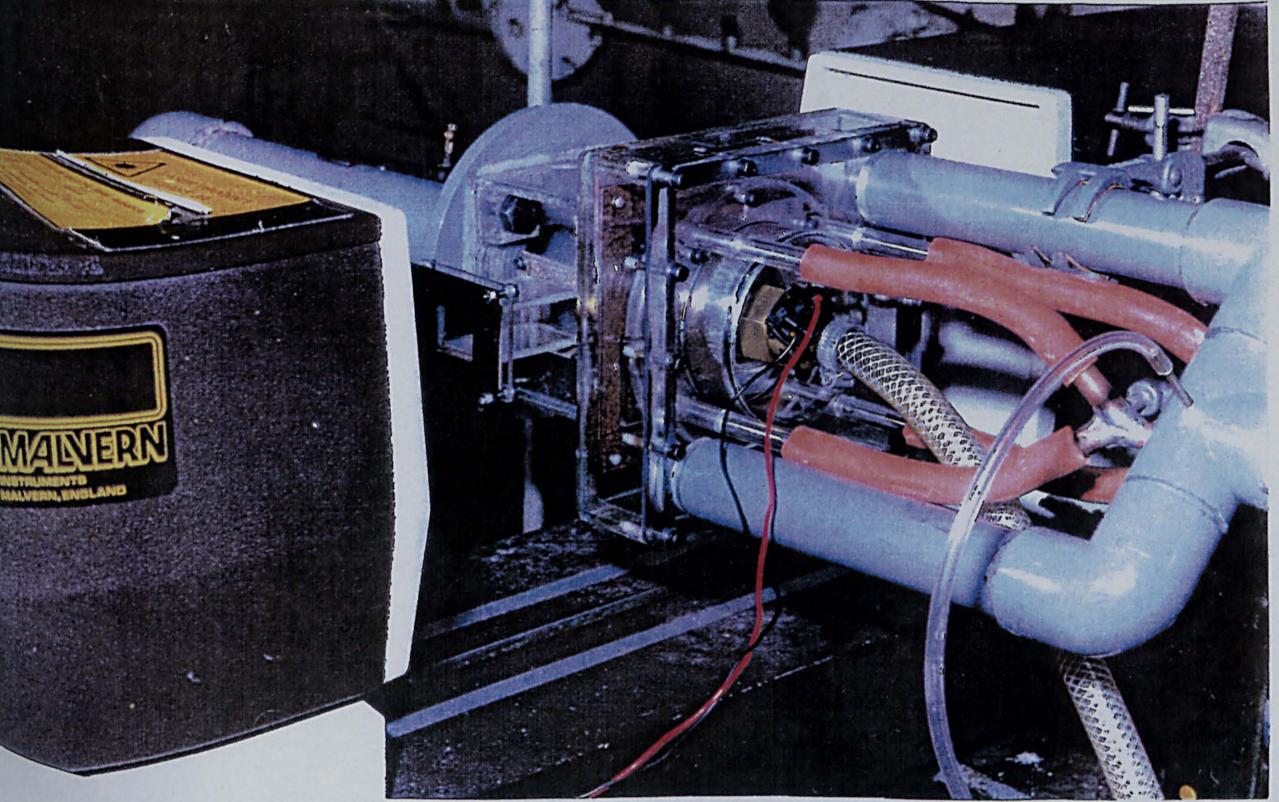
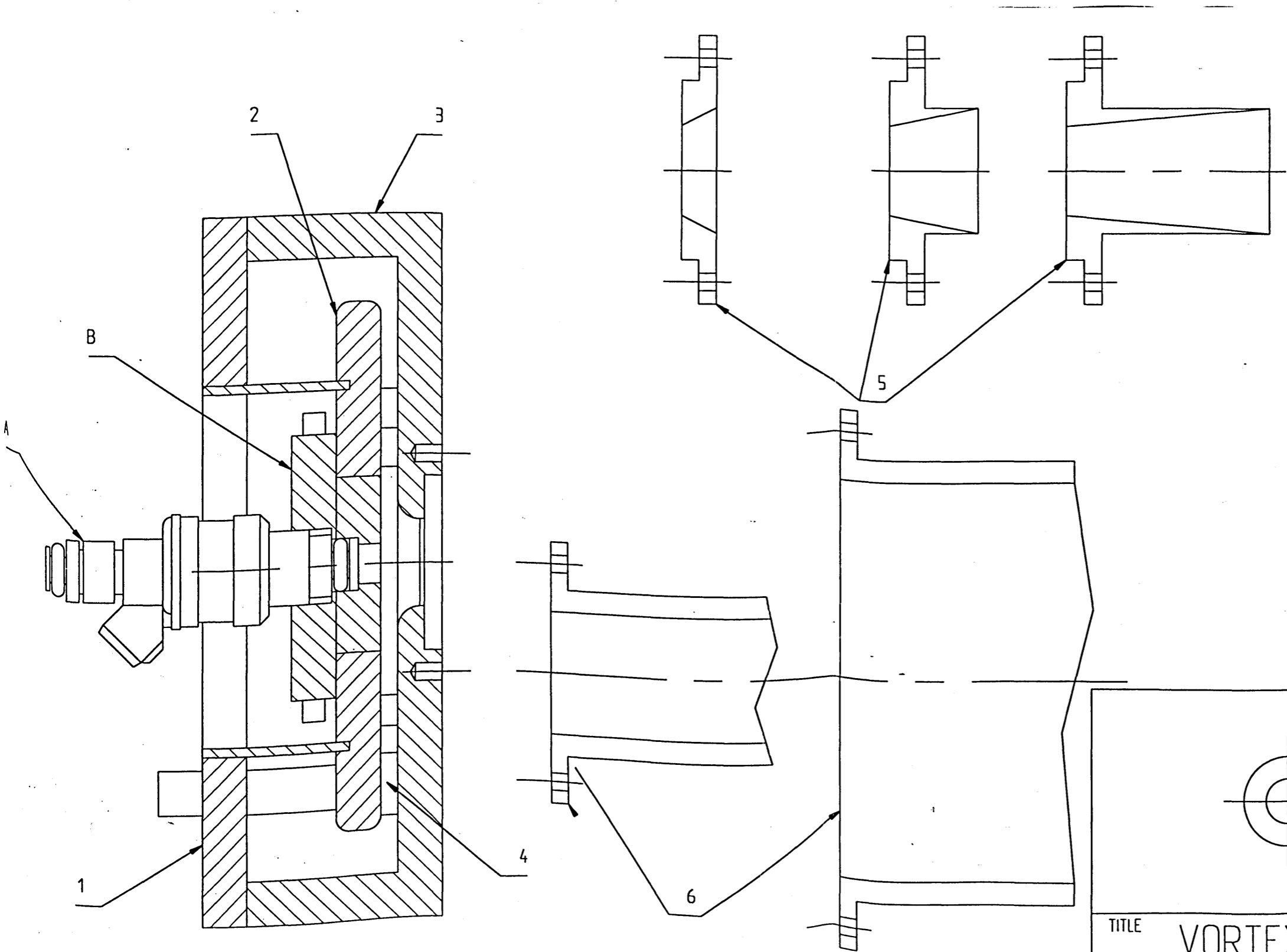
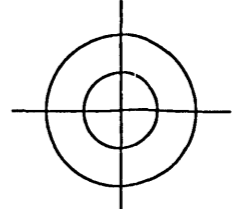
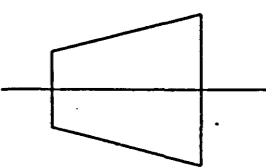


Figure 44 Geometry of VA



| NO | DESCRIPTION              |
|----|--------------------------|
| 1  | VA LID                   |
| 2  | CHAMBER ROOF             |
| 3  | VA BODY                  |
| 4  | CONTROL BLOCK            |
| 5  | OUTLET NOZZLES           |
| 6  | OUTLET PIPES             |
| 7  | DESCRIPTION              |
| 8  | DESCRIPTION              |
| A  | FUEL INJECTOR            |
| B  | INJECTOR OFFSET ADJUSTER |

TITLE VORTEX AMPLIFIER (1 of 7)

SCALE 1:1

DATE 25/7/95

After the VA had been constructed it was incorporated into the existing test rig and its steady flow operating characteristics were tested. Each of the outlet nozzles was tested with the VA exhausting to atmosphere. As expected the best VA performance is obtained when the VA is fitted with the longest outlet diffuser. The normalised steady flow characteristics for this set-up are compared with the best results from the VGVA (VA Radius=50mm, VA height=10mm) in Figure 45.

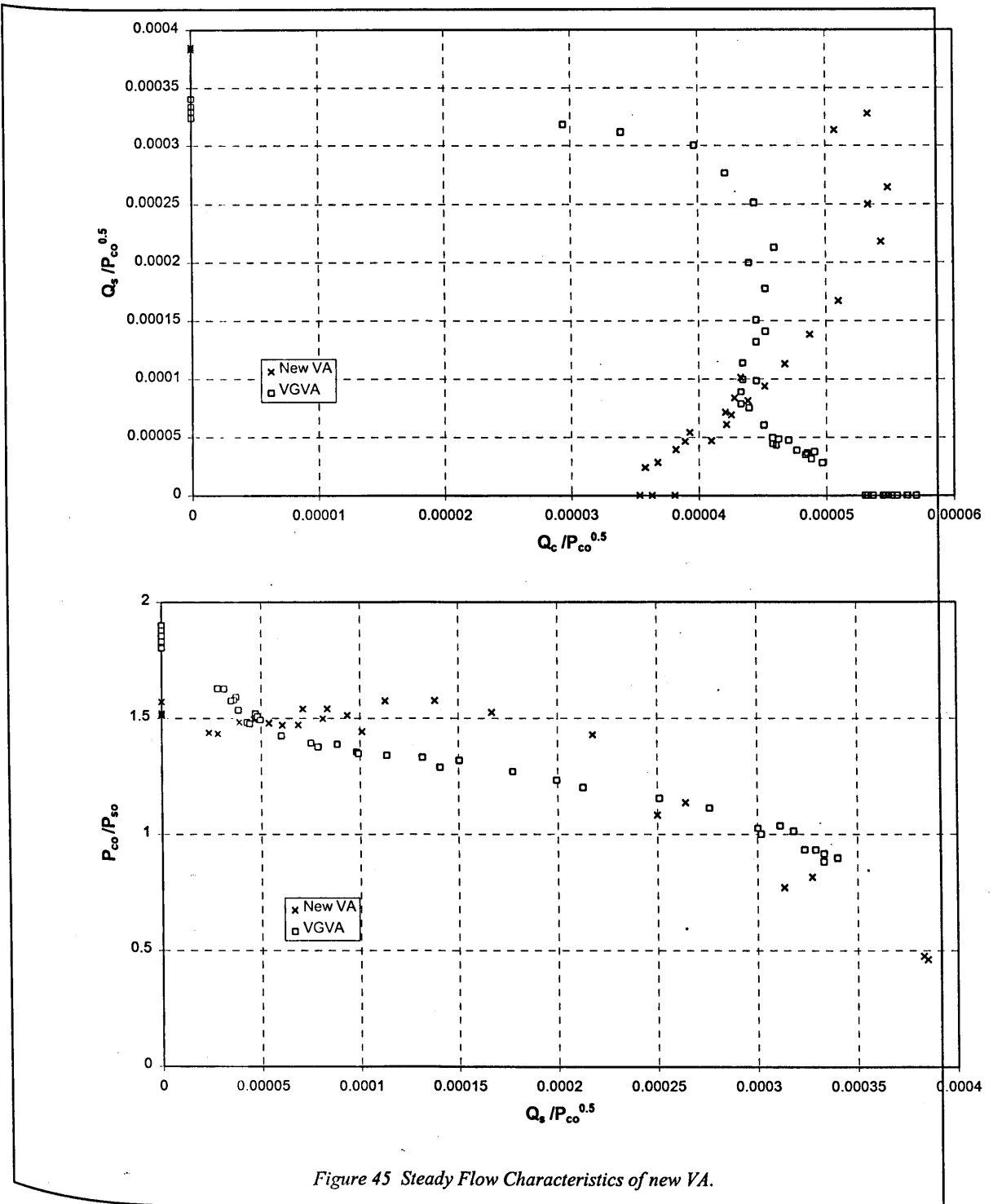


Figure 45 Steady Flow Characteristics of new VA.



Comparing the characteristics of the new VA with those from the VGVA reveals substantial differences. The new VA is much more bistable. The improved design of the flow path for supply flow means that for a given  $P_{SO}$  the new VA achieves a higher flow rate. This can be seen by the higher maximum value of normalised supply flow in the first graph. As the control flow increases, the better supply flow path and smaller control port area mean turndown starts more slowly in the new VA. This is illustrated by the higher normalised control flow for a given normalised supply flow in the top half of the first graph. However, as the vortex becomes established, turndown then takes place much more rapidly. Consequently less control flow is required to achieve cut off. This means there is a significant improvement in CPR at the vortex state.

From these results the TDR and CPR for the new VA can be calculated to be 8.7 and 1.5 respectively. This is an improvement upon the VGVA values of 4.3 and 1.85. However they differ from the values predicted by King (TDR 16, CPR 1.3, see Figure 45) as the TDR is much lower than predicted and the CPR is higher.

The higher CPR is due to omitting the parallel outlet length in the design. This affects the performance of the VA at high swirl.

The TDR is considerably lower than the value of 16 predicted in the design algorithm by King. It was decided to investigate this anomaly further.

It can be seen in Figure 42 that the geometry of the new VA can be modified so that it is very close to that of the optimum geometry for high TDR. This can be achieved by partially blocking the control ports. This was done to increase  $A_c/A_t$  to 14, and the steady flow characteristics were measured.

With the control ports partially blocked to approximate the high TDR design, the VA was found to give a TDR of 20.9 and a CPR of 2.8. For this design the TDR and CPR are both very close to the predicted values of 20 and 2.7. This confirms the accuracy of the design technique.

The low TDR observed on the VA compared to that predicted for the high TDR/CPR geometry is probably due to some instability that affects the low swirl end of the characteristic. The most likely cause is Transport Delay surge which is described in **Chapter 2**, Section V. This would have the effect of reducing the flow for a given value of  $P_{SO}$ . Clearly if transport delay surge was present with supply flow only in the VA, this would drastically reduce the measured value of TDR.

The two VA geometries tested differ only in the area of the control ports. When there is no flow through the control ports the geometry of the high TDR and high TDR/CPR VA is identical. Thus the value of normalised supply flow,  $Q_s/(P_{SO})^{0.5}$ , should be the same for both VAs when only supply flow enters the VA. This is not the case, indicating the presence of VA instability caused by transient flow through the control ports. The VA was also tested with pure supply flow with the control ports completely blocked off. The same value of normalised supply flow was obtained as with the high TDR geometry.

The value of  $Q_s/(P_{SO})^{0.5}$  measured on the high TDR geometry VA can be used to calculate the TDR that would have been recorded with the compromise geometry VA if the instability had not been present. This gives a value of 13, which is acceptably close to the predicted value. This confirms that the shortfall in TDR is caused by the interaction of the VA with the rig. The VA design technique is not compromised.

For droplet sizing experiments the flow regime of most interest is the vortex state. It is not expected that the instability in the low swirl region of the VA characteristic will significantly affect the results. Even under supply flow conditions it seems unlikely that the amount of swirl imparted to the flow by the instability will be particularly significant.

Data from a thesis by King<sup>17</sup> gives the steady flow characteristics for a VA with geometry optimised to give low CPR. It was decided to compare the results from the high TDR and high TDR/CPR geometries tested in this project with the results measured by King. As these three VAs are different geometrically it is necessary to choose a characteristic length to include in the dimensionless ratios for a comparison of the data. If the choice of characteristic length (which is justified below) is :

$$\sqrt[4]{d_e^2 A_T}$$

(where  $d_e$  is the outlet throat diameter and  $A_T$  the area of the tangential inlet) then the data from the three VAs can be plotted as in Figure 46.

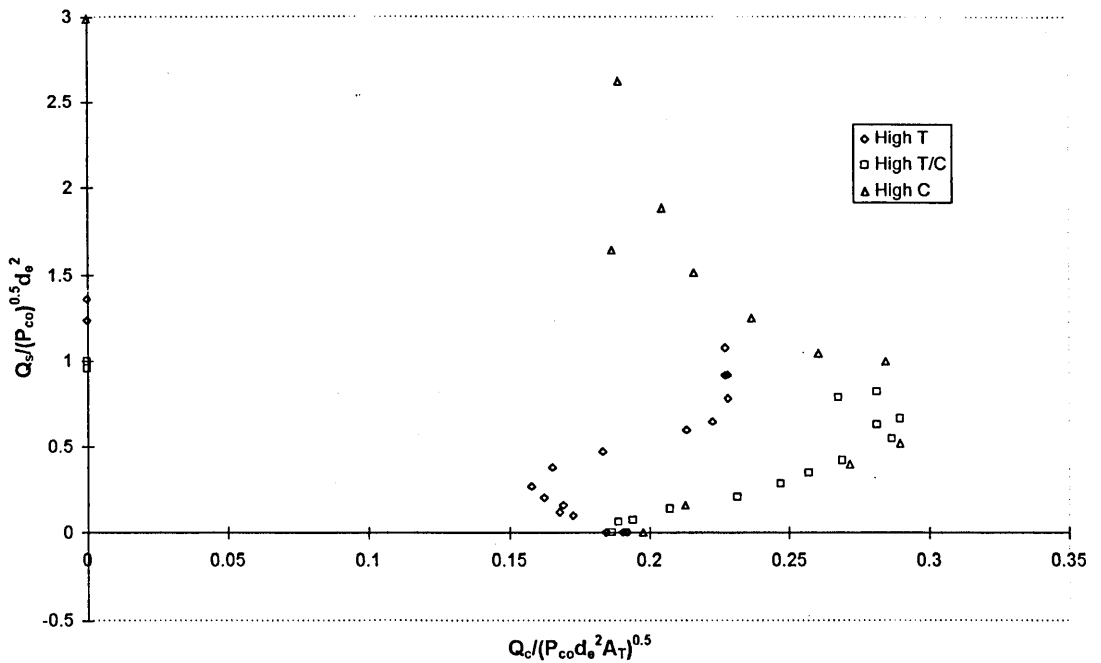


Figure 46 Data Plotted from three different VAs using dimensionless ratios.

The data for the control flow only condition collapses to one point for all three geometries. Comparison with earlier results show that  $Q_c / (P_{co} d_e^2 A_T)^{0.5}$  is higher at cut off for all the geometries which were tested with the VGVA. The configuration from which the steady flow characteristic in Figure 45 is taken (VA Radius=50mm, VA height=10mm) had a value of 0.31 for  $Q_c / (P_{co} d_e^2 A_T)^{0.5}$ . It appears that optimising the VA geometry involves minimising the value of  $Q_c / (P_{co} d_e^2 A_T)^{0.5}$  at cut off.

The choice of dimensionless length was based on consideration of the momentum of the air flow entering the VA. The momentum of the control flow entering the VA is proportional to the control flow rate divided by the area of the control ports ( $Q_c^2 / A_T$ ). It can be seen that the square root of this momentum is incorporated in the dimensionless control flow.

Clearly the design process sizes the control ports to optimise the momentum of the control flow required to achieve cut off. This means that for a given cut off control flow it achieves the lowest  $P_{CO}$  (and hence CPR) possible.

Figure 46 shows that the dimensionless control flow through the VA at cut off is the same for all optimised geometry VAs. This means that the cut off flow data from the low CPR geometry VA can be scaled to represent the flow within any optimised VA. Extensive flow field data was gathered by King for the low CPR geometry VA

using hot wire anemometry. The equivalence of the optimised geometry VAs allows the velocity data measured by King to be used to predict and explain observations on the VA used in this project. The next two chapters describe models of droplet flow path and droplet breakup based on this hot wire data.

## CHAPTER 6

### **Modelling droplet motion**

*To better understand the processes occurring within the Vortex Amplifier a model was developed to describe the motion of droplets within the throat.*

## I. Introduction

To understand the experimentally observed droplet behaviour it is important to discern how the droplets and the air flow interact within the VA. Unfortunately it is extremely difficult to show this experimentally. This is because the small size of the chamber makes optical access difficult and the perspex walls are quite reflective, so that obtaining good quality photographs using a camera flash is very difficult. Little can be learned from observation with the naked eye, as the injection pulse lasts for just 10ms and events within the VA are very rapid. In the light of these considerations it was deemed necessary to undertake some numerical analysis.

One option would have been to model both the air flow and droplet motion numerically. This would have had the advantage of flexibility in defining the VA geometry, and also allowed comparison between many different flows and geometries. However highly swirling flows such as those encountered in the VA are notoriously difficult to model. The large velocity gradients mean that the 'false diffusion' arising in the numerical solution is significant, and to reduce its magnitude a very fine mesh is required. Another problem is that the boundary condition at the exit from the VA cannot be specified as it is a region of recirculating flow. To overcome this the VA must be modelled with a large downstream plenum attached, with the boundary condition specified at the exit from the plenum, where the pressure will be uniform. This further increases the number of nodes required to solve the problem. The difficulties of modelling the VA airflow with a CFD package were therefore considered to rule this out as a practical option for providing data on the droplet behaviour within the VA.

Fortunately the PhD thesis by King<sup>49</sup> contains detailed data on the flow field within a VA, obtained by measurements with a hot wire probe. It was decided to use this data to describe the air flow in the VA. The motion of the droplets within this experimentally determined flow field could then be computed. Although this restricted the VA geometry and flow conditions that could be modelled it was felt that the simplicity of this approach offered significant advantages.

## II. VA data

The PhD thesis by King<sup>49</sup> contains data on the mean and fluctuating velocity in a VA. The VA used was a low CPR design. It was a large scale VA with a throat diameter of 3.2", a chamber diameter of 9.59" and chamber height of 0.7". To allow visibility it was constructed from perspex. The VA design included a straight section at the throat and an outlet diffuser.

The velocity data was gathered with a six orientation, single wire, hot wire probe that was developed for the purpose. All three velocity components, both mean and fluctuating, were measured at 318 stations in the flow, at five different flow conditions.

The flow and pressures through the VA were measured for a constant supply to outlet pressure drop of 4.5 i.w.g. Five significant points on this characteristic were chosen for collection of velocity data. The steady flow characteristic (which is the same as that plotted in Chapter 5, Figure 46 in non dimensional form) is shown in Figure 47. The characteristic featured a discontinuous jump. This is shown on the graph by omitting the line joining the two measurements either side of the discontinuity.

The flow conditions where hot wire data was gathered are shown as solid points. They are supply flow only, three points of mixed supply and control flow and control flow only. Of the mixed flow points, one was just above the discontinuity, one just below, and one was in a region of low frequency oscillation.

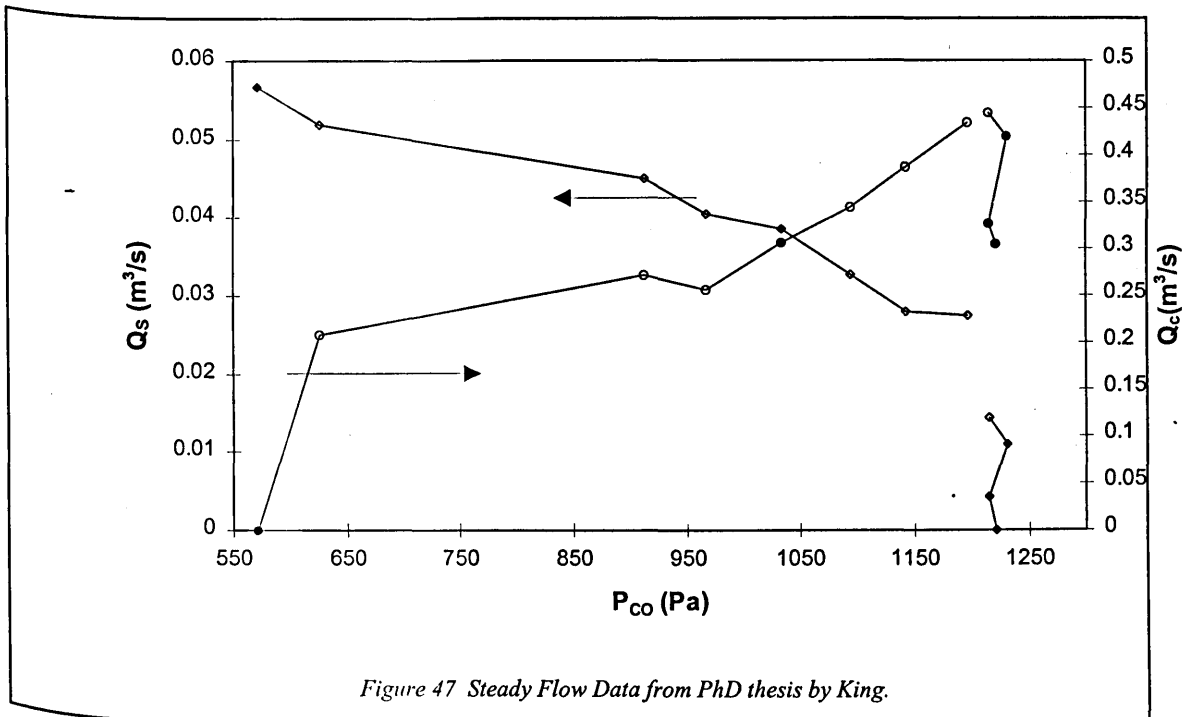


Figure 47 Steady Flow Data from PhD thesis by King.

The measurement of velocities in rotating flows by intrusive methods is prone to inaccuracy, because the structure of rotational flows is liable to be affected by probes. To indicate the amount of interference caused, the static pressure readings were monitored as the hot wire probe was inserted into the flow and traversed across it. Variations in static pressure readings amounted to no more than 2.5%, which was considered to indicate minimal interference. Further evidence of this was provided by the close agreement between readings taken in the VA outlet whether the probe was inserted from the chamber back wall or the outlet wall. The probe stem had a diameter of 2 mm, which was of the same order as the small scale turbulence in the flow. This meant that the wake created by the probe would be of the same order as the dissipative eddies. It was suggested that this accounted for the probe not significantly affecting the flow field.

The mean velocity data was presented as three contour plots for each point at which data was recorded. These showed radial, axial and tangential velocity components. The plots are reproduced in Chapter 2, Figure 9.

The data for the fluctuating velocity components was also recorded. Two types of fluctuation are present in the flow. The first is caused by the turbulent eddies in the flow. The second is flow field oscillations caused by fluctuations in flow and pressure at the inlets and outlet of the VA. The averaging time for the mean velocities was large compared to the time for both sorts of fluctuation. This meant that the fluctuating velocity measurements included both turbulent eddies and oscillations in the flow through the VA.

The fluctuating data was also presented as contour plots. The parameters plotted were 'the relative intensity of the total fluctuating velocity component' (FV), and 'the relative intensity of the fluctuating component of tangential velocity' (RI of  $V_T$ ). These are defined as:-

$$FV = \frac{\sqrt{\tilde{V}_T^2 + \tilde{V}_R^2 + \tilde{V}_Z^2}}{V_e} \times 100\%$$

and

$$RIofV_T = \sqrt{\frac{\tilde{V}_T^2}{V_e^2}}$$



Where  $V_e$  is the mean axial velocity at the exit throat, i.e.:

$$V_e = \frac{Q_s + Q_c}{A_e}$$

It can be seen that the FV is the square root of the relative kinetic energy of the fluctuations. The square root was used to compress the range of the parameter so it could be usefully plotted.

The data for mean velocity was used in the computer program designed to predict the droplet behaviour. The program required the air velocity data to be entered at discrete positions. The VA that was to be modelled was much smaller than the large scale one used for collecting velocity data. Therefore the data had to be tabulated and scaled before it could be used in the computer model.

A VA of practical dimensions for use within an engine has a throat diameter of 20 mm, so the velocities had to be scaled to a VA of this size. The dimensionless ratios governing flow within a VA are given by Boucher and Kitsios<sup>19</sup> as:

$$\frac{(\rho p_{co})^{1/2} l}{\mu}, \frac{Q_c}{l^2 (p_{co} / \rho)^{1/2}}, \frac{Q_s}{l^2 (p_{co} / \rho)^{1/2}}, \frac{p_{cs}}{p_{co}}$$

For the flow in two different VAs to be equivalent all these dimensionless ratios must be equal. Setting them equal for the two cases and rearranging leads to the equality:

$$\frac{Q_{c1}}{Q_{c2}} = \frac{l_1}{l_2}$$

- In the vortex state the flowrate  $Q_c$  is equal to the product of the throat area and the average exit velocity. It was assumed that all the velocities in the flow scaled by the same factor as the average velocity. Thus

$$u_1 = u_2 \left( \frac{l_1}{l_2} \cdot \left( \frac{d_{e2}}{d_{e1}} \right)^2 \right)$$

Equation 1

It was demonstrated in **Chapter 5** that an appropriate choice of characteristic length was

$$l = \sqrt[4]{d_e^2 A_T}$$

If this characteristic length is calculated for both the VA in this project and that used by King, then substitution in Equation 1 gives the factor required to scale velocities between the two. This means the velocities from the larger VA have to be scaled up by a factor of 3.13 to simulate the smaller chamber.

In the pure control flow condition for the large scale VA,  $Q_C = 2190$  li/min and  $P_{CO} = 4.8$  inches of water or about 1200Pa. These values can be scaled using the dimensionless ratios to find that for a VA outlet of 20 mm diameter the equivalent values will be  $Q_C = 417$ li/min and  $P_{CO} = 0.33$ ba. The measured pressure drop at 400li/min on the VA described in is 0.38ba. Thus the scaled hot wire probe data can be considered to be a reasonable approximation to the VA used in this project.

It should be noted that the scaling gave peak tangential velocities of 120m/s ( $Ma \approx 0.3$ ). This means that the incompressible flow assumption made when equating the dimensionless ratios that contain a density term is violated. However as these peak velocities are very localised it seems unlikely that this inaccuracy will significantly affect the results.

It has already been assumed that the velocity at any point within the VA scaled with the average outlet throat velocity. This means that the velocity data could be divided by the flow through the VA, to give the velocity field corresponding to a flowrate of 1 li/min through the VA. This could then be scaled to any flowrate of interest to give the velocity of the air in the VA.

The velocities for a VA with a 20 mm diameter exit were calculated for the control flow data. They were entered in three text files that could be loaded by the FORTRAN programme which calculated the droplet motion. These contained the tangential, radial and axial velocities on a plane in the VA outlet, at discrete points. The spacing between grid points was 1.55mm. The velocity was given a value of zero at grid points outside the VA walls. The flow could be described by the velocities in one plane as it is angularly symmetrical in the region of the outlet. The geometry of the VA exit and the grid of points where velocity is tabulated are shown in Figure 48.

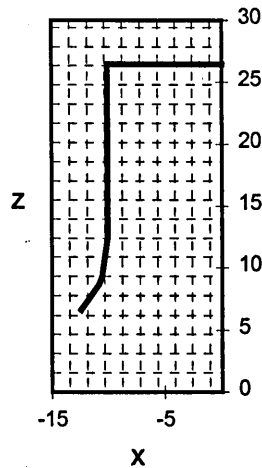


Figure 48 VA geometry and grid of air velocity

This outlet geometry is not exactly the same as that in the VA used in droplet sizing experiments. This is because of the parallel section at the outlet which is not included in the new VA. The actual diffusers used in the experimental work are compared with the modelled geometry in Figure 49.

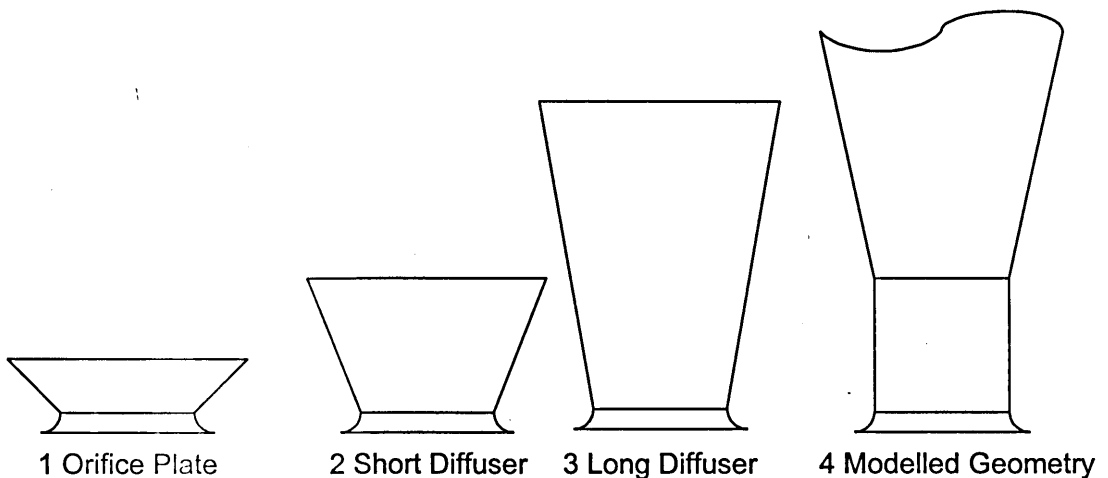


Figure 49 Outlets for the vortex amplifier

The new VA can be expected to behave slightly differently than predicted by this model. The parallel outlet section increases the length of time the droplets spend in the high swirl outlet section. Droplets which impact with the walls of the parallel throat in the model should be carried through either of the first two outlets. However they would most probably impact in the long diffuser.

### III. Droplet motion in the VA

The equation describing the motion of a drop in an air stream is (from Heywood<sup>50</sup>):-

$$\left(\frac{1}{6}\pi D_d^3 \rho_f\right) \bar{a} = m_d \bar{g} - \frac{1}{2}(\bar{v}_d - \bar{v}_g) |\bar{v}_d - \bar{v}_g| \rho_g C_D \frac{\pi D_d^2}{4}$$

Where  $C_D$  is a strong function of Reynolds number:-

$$C_D = 27 \text{Re}^{-0.84}$$

$$\text{Re} = (\rho_g D_d |\bar{v}_d - \bar{v}_g| / \mu_g)$$

As the droplets being modelled were in the sub 200 $\mu\text{m}$  size range it was decided to neglect the gravitational term for the sake of simplicity. It can be seen that the gas and liquid properties required to solve the equation are liquid density, air density and air viscosity. The values input to the programme were:

$$\rho_f = 684 \text{kg/m}^3$$

$$\rho_g = 1.0 \text{kg/m}^3$$

$$\mu_g = 1.85 \times 10^{-5} \text{Pa.s}$$

With this input data the droplet motion could be described in three dimensions by a set of six differential equations. Three of these describe the droplet co-ordinates and three describe the velocities in the x, y and z directions. The droplet position was described by a set of Cartesian co-ordinates. These have their origin at the centre of the VA back wall (as shown in Figure 48), with Z being the axial direction. Thus the general form of the equations describing droplet position is:-

$$\frac{dx}{dt} = v_x$$

and that for the equations describing velocity is:-

$$\frac{dv_x}{dt} = a_x = -\frac{3}{4}(v_{dx} - v_{gx}) |v_d - v_g| \rho_g C_D / D_d \rho_f$$

where

$$|v_d - v_g| = \sqrt{(v_{dx} - v_{gx})^2 + (v_{dy} - v_{gy})^2 + (v_{dz} - v_{gz})^2}$$

A set of equations of this form can be solved over a specified time period by a variety of numerical methods, notably Runge-Kutta and various predictor-corrector methods. The NAG FORTRAN library contains sub routines to perform either an Adams-Bashforth predictor-corrector method or a fourth order Runge Kutta scheme. Either sub routine could be called from the FORTRAN program with minor changes and when they were compared both schemes agreed to three decimal places. As runtime for both schemes was only a few seconds on a 486 specification PC then it was arbitrarily decided to use the predictor-corrector method to obtain the following results.

A flowchart describing the programme is shown in Figure 50.

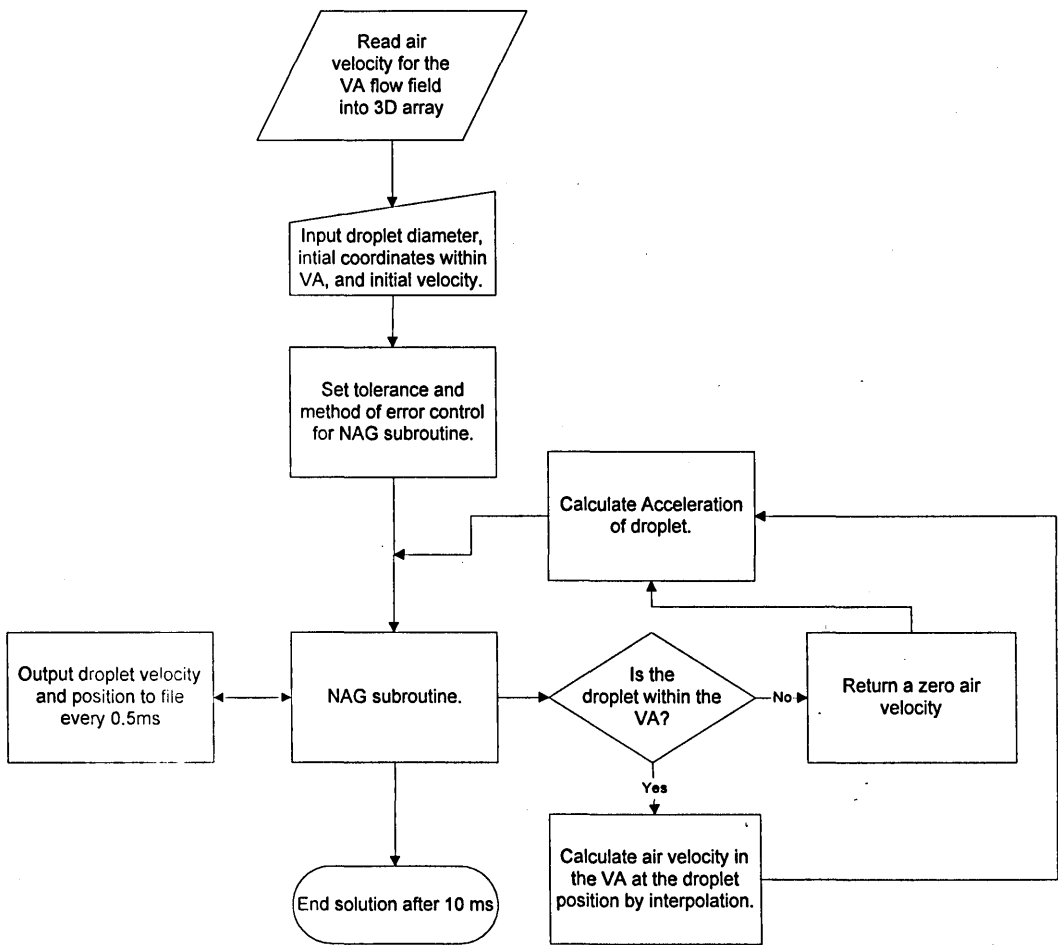


Figure 50 Flowchart describing program to solve motion of a droplet within an experimentally determined VA flow field.

## IV. Results and Discussion

In the experimental work the jet from the injector was found to have a velocity of around 10m/s and a range of droplet sizes from around 50 $\mu$ m to just under 200 $\mu$ m. After the programme had been thoroughly tested it was decided to simulate the behaviour of drops in this size range when they were injected into the VA outlet. The simulation was run for a variety of air flow rates. The results are presented as graphs of droplet position in the x-z and x-y planes.

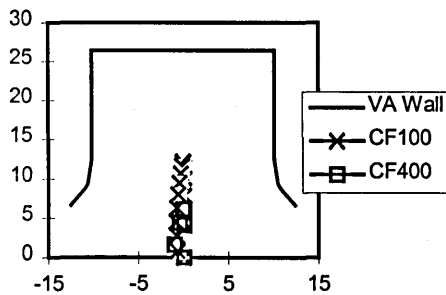


Figure 51 X-Z motion with droplet diameter 50 $\mu$ m

It can be clearly seen in Figure 51 that a droplet of 50 $\mu$ m diameter injected into the reverse flow core of the control flow is flung back against the rear wall of the chamber. This occurs even when the flowrate is as low as 100 li/min. It should be borne in mind that the penetration of a spray is always greater than that for a single droplet, as the airflow is affected by the momentum of the liquid. Therefore some small droplets could pass through the VA, especially if the shorter outlets are fitted. It seems likely that some small droplets will always be thrown against the walls with control flow only.

The greater momentum of larger droplets means they have greater penetration when injected into the VA. The results obtained from simulating a 150 $\mu$ m droplet are shown in Figure 52.

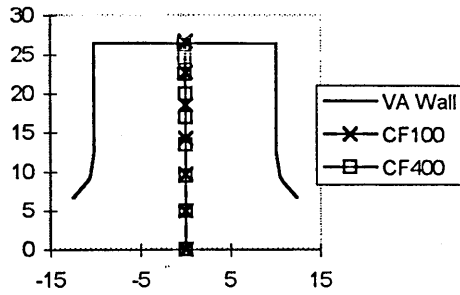


Figure 52 X-Z motion with droplet diameter 150µm

It can be seen that a 150µm droplet passes through the VA with very limited effect from the flow. This is consistent with the measurements from the VGVA, where droplets of this size and above were observed to pass through the vortex without being flung against the walls.

To see whether it was possible to make more small droplets pass through the VA outlet without impacting, it was decided to move the point of injection away from the centre of the VA roof. It was reasoned that injection into the reverse flow core led to large drag and rapid deceleration of the drop. Thus the drop was injected at the stagnation point between the reverse flow core and the downstream flow.

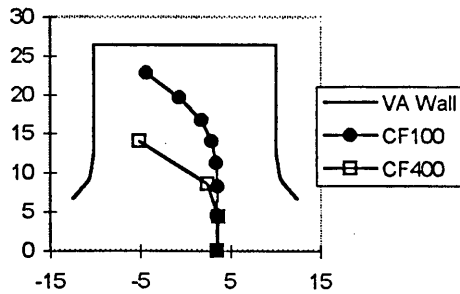


Figure 53 X-Z motion with droplet diameter 50µm, off centre injection

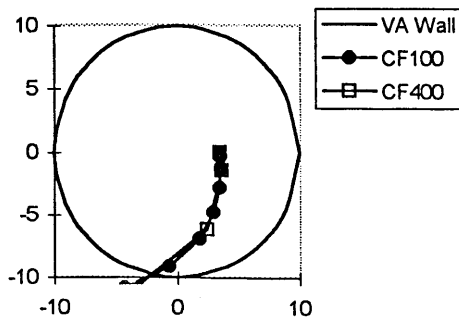


Figure 54 X-Y motion with Droplet diameter 50µm, off centre injection.

It can be seen that this strategy has indifferent success. Although the droplet penetration is increased, the droplet still impacts with the wall. Also it should be noted that in a real turbulent flow the position of the recirculating flow would not be fixed, and so it would be impossible to inject fuel at the exact edge.

The FORTRAN model is supported by the experimental findings of the earlier work. It confirms the problem of droplets being flung against the VA walls by the high tangential velocity. Although the reduction in VA height will reduce the effect of this problem, the simulation indicates that it will not eliminate it.

#### IV.i Limitations of modelling

Although the findings of this modelling are broadly supported by experimental observations of extensive droplet deposition, there are a number of considerable limitations to the technique. Consequently care should be taken in interpreting the results.

A significant limitation of the technique is that it considers the movement of an individual droplet through a time invariant flow field. Obviously significant deviations from real spray behaviour, where thousands of droplets traverse a turbulent flow, are to be expected. Due to the statistical fluctuations of a turbulent flow, some droplets that the model will predict to impact will be observed to pass through the VA.

Another limitation of modelling a single drop is that no account is taken of the exchange of momentum between the spray and the airflow. It is well known that the penetration of a spray of droplets is significantly greater than that of an individual droplet. This is due to entrainment of the surrounding air by the spray. This means that the results of this model will give pessimistic estimates of spray deposition. Again it was felt that the added complexity of modelling this effect would not significantly improve the usefulness of the model output.

Finally the model takes no account of droplet breakup by the air flow. Clearly this is an important process within the VA. However ignoring this effect does not render the results of the model worthless. Due to the statistical nature of turbulence not all the droplets in a spray will be disrupted. Droplets of 50 $\mu$ m diameter have been



observed to pass through the VA at control flow rates of 400 li/min. Thus the modelling the flow path of such a droplet at this condition remains a useful exercise.

Despite these considerable limitations the model can accomplish the intended purpose of indicating the severity of spray deposition. It also provides information on the effectiveness of tactics that might be used to reduce it. It was felt that the added complexity of a more realistic model would not significantly enhance this ability.

## CHAPTER 7

### **Modelling droplet breakup**

*A literature review of models for droplet breakup was conducted and one model was adapted to describe the droplets within the Vortex Amplifier.*

## I. Droplet break-up in turbulent flows

The initial model of the droplet motion within the VA is described in **Chapter 6**. It computes the droplet trajectories by treating them as discrete spheres. Whilst this provides valuable support to the observation that droplets impacting on the walls is a significant problem, it would also be useful to model droplet break-up. To this end a literature survey was conducted to determine the significant factors affecting droplet break-up.

## II. Weber number criteria

The break-up of a droplet is controlled by the balance between the surface tension force resisting break up and the disruptive forces. The stabilising surface tension forces are proportional to the product of surface tension and droplet size ( $Sd$ ). The disruptive forces are usually due to inertial effects arising from the relative gas and liquid velocities. The dimensionless group comparing these forces, the Weber number, is therefore defined as:

$$We = \frac{\rho_g \Delta u^2 d}{\sigma}$$

Equation 2

When the disruptive forces exceed the stabilising forces the droplet will break up. Thus the droplet will be liable to break up when its Weber number is above a certain critical value. For an inviscid droplet with a steady laminar flow around it the critical Weber number is 13. However the viscosity of the liquid in a droplet also resists droplet deformation. This means that the critical Weber number is dependent upon the viscosity or Ohnesorge number,  $Z$ , defined as:

$$Z = \frac{\mu_L}{(\rho_L d \sigma)^{1/2}}$$

Equation 3

This number relates the relative importance of the viscous and surface tension forces in the liquid. The critical Weber number increases with the viscosity number.

In real sprays application of the critical Weber number is complicated. This is because the relative velocity term in the Weber number depends upon the turbulence characteristics of the surrounding gas flow. Droplet size also depends upon droplet residence time within the high velocity gas.

### III. Turbulent flow

Turbulent flow arises when the main flow is unstable. Disturbances are amplified so that they produce primary eddies which are of the same scale as the main flow. These primary eddies are also unstable and so break down into smaller eddies. This continues until the oscillations reach the scale of the smallest eddies in the flow. This effect is known as an eddy cascade. Nearly all the energy dissipation takes place in the smallest eddies, as they have a Reynolds number of around 1 and so are damped by viscous forces.

If the size of the primary eddies is much larger than the energy dissipating eddies clearly a wide range of intermediate eddies exist. These transfer energy from the largest to the smallest eddies. This energy transfer can occur in any direction and so the directional information of the large eddies is gradually lost. This fact led Kolmogoroff to conclude that all eddies that are much smaller than the primary ones are independent of them statistically. Thus the only information passed to the smaller eddies is the amount of kinetic energy they receive. According to this theory of local isotropy, the statistical properties of any small scale oscillation should only be determined by  $\epsilon$ , the local energy dissipation rate per unit mass of fluid.

Isotropic turbulence occurs when the root mean square values of the fluctuating velocities are equal, i.e.:  $\overline{u^2} = \overline{v^2} = \overline{w^2}$ . This is not the case in most real flows, but Kolmogoroff used his conclusions to enable him to assume isotropy if the volume of fluid considered is small compared to the primary eddies. So although primary eddies are clearly not isotropic in most flows, isotropy can be assumed in small areas of the flow. Isotropic turbulence is much simpler to analyse than non-isotropic turbulence, so the theory of local isotropy allows useful predictions to be made about turbulent flow. The two requirements for the theory of local isotropy to hold are a high Reynolds number and for the scale of the main flow to be very much greater than the turbulent microscale.

The following discussion considers the implications of local isotropy upon analysing turbulent flow. Similar conclusions can be found in several standard texts<sup>51</sup>.

The energy dissipating eddies have a scale of  $\eta$ , known as the turbulent microscale. It is the scale of eddies with a Reynolds number of one. Dimensional analysis allows some simple relations between  $\mathbf{E}$ , the kinematic viscosity  $\nu$  and the flow velocities. The turbulent microscale is:

$$\eta = \nu^{3/4} \epsilon^{-1/4}$$

Equation 4

The mean-square relative velocity between two points in the flow can also be found using the theory of local isotropy. If  $r$  is the distance between the two points and  $r$  is small compared to the scale of the main flow, then:

$$\overline{u^2(r)} = C_1 \epsilon^{2/3} r^{2/3}$$

Equation 5

This relationship holds as long as the separation of the two points is considerably bigger than the turbulent microscale. If  $r$  is smaller than  $\eta$  then the energy dissipation affects the relative velocity so that:

$$\overline{u^2(r)} = C_2 \frac{\epsilon}{\nu} r^2$$

Equation 6

The universal constants  $C_1$  and  $C_2$  must be determined from measurement.

If the turbulent air flow around a droplet is to be modelled with the theory of local isotropy then the droplet must be much smaller than the scale of the primary eddies, and the Reynolds number must imply highly turbulent flow. In a vortex amplifier with a 20mm throat diameter, a control flow of 400 li/min implies an average axial velocity of 22.2 m/s at the throat. This gives a Reynolds number of 22900, meaning the flow is highly turbulent.

The rate of energy dissipation in the VA is the product of the mass flow rate and the energy loss per unit mass:

$$\text{Energy dissipation rate} = \dot{m} \left( \frac{p_{\text{inlet}} - p_{\text{outlet}}}{\rho} + \frac{u_{\text{inlet}}^2 - u_{\text{outlet}}^2}{2} \right)$$

Equation 7

The pressure drop across the VA for a control flow of 400 li/min is 33000 Pa. The average inlet and outlet velocities can be found from the flow areas. When these values are substituted into Equation 7, the value of energy dissipation rate for this flow condition is found to be 240 Watts. This can be divided by the mass of air in the VA to find the value of energy dissipation rate per unit mass. As the volume of the VA is roughly  $1.5 \times 10^{-5} \text{ m}^3$  this value is 15870 kW/kg. This means Equation 4 gives the average turbulent microscale as  $4.5 \mu\text{m}$ . However the value of  $\epsilon$  will vary throughout the VA, so the turbulent microscale will vary considerably.

### III.i The breakup of drops smaller than the turbulent microscale

The theory of local isotropy shows that the velocity distribution around a droplet will depend upon its size relative to the turbulent microscale. This can be seen by the difference in Equation 5 and Equation 6. The correct equation to use to find the mean square relative velocity across a droplet depends on its size relative to the turbulent microscale. Kolmogoroff<sup>52</sup> used the result for relative velocity in Equation 6 to find the disruptive inertial stress,  $\rho u^2$ , on a droplet smaller than the turbulent microscale. He compared this with the stabilising surface tension stress to find the largest droplet that could survive without breakup. The resulting stress balance gave:

$$d_{\text{max}} \propto \left( \frac{\sigma v}{\rho_c \epsilon} \right)^{1/3}$$

Equation 8

However this equation has been strongly criticised by Shinnar<sup>53</sup>, amongst others, as below the turbulent microscale disruptive forces will be viscous not inertial. The analysis by Taylor<sup>54</sup> for a droplet being stretched into a cylinder by two dimensional, viscous flow gives:-

$$d_{\max} = \frac{2\sigma(\mu_d + \mu_l)}{\alpha\mu_l\left(\frac{19}{4}\mu_d + 4\mu_l\right)}$$

Equation 9

This equation has been adapted by several researchers but there is uncertainty about what to use for  $\alpha$ , the principal positive strain rate in a real, three dimensional, turbulent flow. However most droplets in the spray injected into the VA will be considerably larger than the turbulent microscale of the airflow. This means that Equation 9 would be inappropriate to describe the droplet breakup in the VA.

### III.ii The break up of drops larger than the turbulent microscale

If the droplet size is greater than the turbulent microscale then the main disruptive forces are inertial. These forces arise due to changes in eddy velocity over the length of the droplet. The velocity changes are described in Equation 5, and can be used to find the disruptive force on the droplet. Kolmogoroff<sup>1</sup> and Hinze<sup>55</sup> equated these with the stabilising surface tension force and so deduced the maximum stable droplet size described in Equation 10.

$$d_{\max} \propto \sigma^{0.6} \varepsilon^{-0.4} \rho^{-0.6}$$

Equation 10

When Equation 10 is written in terms of critical Weber number it becomes:

$$d_{\max} = C_1 We^{0.6} \sigma^{0.6} \varepsilon^{-0.4} \rho^{-0.6}$$

Equation 11

This equation has been widely utilised by chemical engineers, particularly for scaling experimental results for liquid-liquid emulsions in stirring tanks. It has also been successfully applied for bubbles in a liquid. However Kocamustafaogullari<sup>56</sup> suggests that the equation may not be applicable to liquid drops in gas flow. Empirical equations fitted to experimental data show  $d_{\max}$  to be strongly dependent on the liquid to gas density ratio<sup>57</sup>. He suggests that the entrainment of liquid drops by gas eddies cannot be complete. This means that in relation to the small scale eddies the droplet acts as a

motionless solid body. Therefore the droplet break-up is strongly influenced by local relative velocity. The limiting local relative velocity at which a fluid will flow around a particle suspended in it,  $u_{r \max}$ , is given by Levich<sup>58</sup> as:-

$$u_{r \max} = C_3 \left[ \varepsilon d_{\max} (\rho_L / \rho_g) \right]^{1/3} (|\Delta\rho| / \rho_L)^{1/2}$$

Equation 12

From Equation 5 and Equation 12 it can be seen that when the density of the dispersed phase is higher than that of the continuous phase:

$$\frac{u_{r \max}}{(u^2)^{1/2}} \approx \left( \frac{\rho_L}{\rho_g} \right)^{1/3}$$

Equation 13

This shows that the velocity of the flow over the surface of the droplet is considerably larger than the velocity difference across the droplet due to turbulent fluctuations. As the liquid density is much greater than that of the gas, when  $u_{r \max}$  is used to define the disruptive inertial force on the droplet, the maximum droplet diameter simplifies to:

$$d_{\max} = \left( \sigma We_{cr} / C_3 \rho_g \right)^{3/5} (\rho_g / \rho_f)^{2/5} \varepsilon^{-2/5}$$

Equation 14

where  $C_3$  is a proportionality coefficient from Equation 12, and should be of the order of 1. Kocamustafaogullari<sup>56</sup> correlated this equation with experimental data<sup>59</sup> for a simple flow field where  $\varepsilon$  can be determined. He found  $We_{cr} / C_3 = 12.2$ . This gave acceptable correlation with the results of other experiments<sup>60,61</sup>, although further experiments would be desirable to fully validate the value of  $We_{cr}$ .

The idea of droplet break-up at a critical Weber number has been questioned by Clark<sup>62</sup>. He points out that although the static deformation of a droplet is a function of Reynolds number, in a turbulent flow the duration of the applied inertial forces is short. He develops a model of drop deformation, analogous to a spring mass damper system, to find the natural oscillation frequency of a droplet. Under the action of an impulse



force he found that the maximum stable droplet diameter was a function of all the variables in the problem, namely drop diameter, internal and external phase viscosity and densities, surface tension and the magnitude and duration of the impulse force. He suggests that the static deflection is only applicable if the duration of the disturbing force is much greater than the deformation time of the drop. Otherwise dimensionless deformation should correlate data better than Weber number. His experiments<sup>63</sup> provide reasonable, but inconclusive, support for this suggestion. However his model suffers from the drawback that its application requires detailed statistical knowledge of the turbulence in order to determine the disturbing forces. The simplicity of Equation 14 is to be preferred for modelling droplet break-up in the inertial range. However there remains the difficulty of estimating  $\epsilon$  in the flow in the VA, and some uncertainty as to the accuracy of the value of  $We_{cr}$ .

#### IV. Modelling turbulent flows

It is planned to use the extensive flow field data measured by King to model the breakup of droplets in the vortex amplifier. It will again be scaled from his large 3.2" throat diameter VA to a 20mm throat diameter VA which is similar to the one used in experiments.

To estimate the maximum droplet diameter in the VA using Equation 14 it is necessary to estimate  $\epsilon$ , the local energy dissipation rate, throughout the flow. The crudest way to do this is to find the average value of  $\epsilon$  within the VA. This is a very rough technique as the value of  $\epsilon$  will vary considerably between the highly turbulent flow in the VA throat and the flow at the diffuser outlet. However it does provide a simple estimate for the value of  $\epsilon$ .

The static pressure drop across the VA provides the driving energy for turbulent dissipation. For the control flow state, the data from King shows that the static pressure drop is 1.12 kPa. This scales to 33 kPa for a VA with a 20 mm throat. Table 1 shows how an average value for  $\epsilon$  can be calculated and used to estimate the maximum droplet size. The value used for the surface tension of n-heptane is  $0.02 \text{ N/m}$ <sup>64</sup>. Clearly as most of the energy dissipation occurs in the VA throat the local values of  $\epsilon$  will be higher, giving smaller drop sizes.

| Parameter                                    | Source                               | Value in modelled VA                    |
|--|--------------------------------------|---|
| Pressure Drop, $\Delta P$                    | Scaled from Kings VA                 | 33000 Pa                                |
| VA volume, Vol.                              | Scaled from Kings VA                 | $3.44 \times 10^{-4} \text{ m}^3$       |
| Control flow rate, $Q_C$                     | Scaled from Kings VA                 | $7 \times 10^{-3} \text{ m}^3/\text{s}$ |
| Specific energy dissipation rate, $\epsilon$ | $(\Delta P \times Q_C) / \text{Vol}$ | 667 kW/kg                               |
| $d_{\max}$                                   | Equation 14                          | 148 $\mu\text{m}$                       |

Table 1 Calculating maximum stable drop size from average energy dissipation rate

King measured the pressure drop across just the exit throat, by placing static pressure tappings in the VA body. He found a pressure drop of 0.656 kPa. This scales to a pressure drop of 18.3 kPa for a 20 mm throat. As the volume of the throat is around  $1.02 \times 10^{-5} \text{ m}^3$ , the local average value of energy dissipation rate is 12500 kW/s. As there is quite considerable acceleration through the throat some of this energy dissipation will be due to the increased kinetic energy of the flow. However if this value is taken as a rough estimate of  $\epsilon$ , then Equation 14 estimates  $d_{\max}$  as 46  $\mu\text{m}$ . Bearing in mind that this is a maximum droplet size the potential of the VA outlet flow to produce fine sprays is supported.

The values of energy dissipation rate scaled from the experimental data on the VA used by King will be lower than those found for the VA used in the current project. This is because the VA used by King contained a parallel outlet throat. This significantly increases the volume of the VA. Thus the VA used in the current project can be expected to produce smaller maximum droplet sizes as local values of  $\epsilon$  are higher. To calculate the magnitude of this effect Equation 14 was used to evaluate droplet size for the energy dissipation rate across the experimental VA calculated on page 108 (15870 kW/kg). This predicted  $d_{\max}$  as 42  $\mu\text{m}$ . Obviously the inclusion of the outlet throat does not significantly effect predicted droplet sizes.

To obtain a clearer idea of the distribution of the energy dissipation in the VA outlet more detailed study of the flow is required. For this some simple analysis of turbulent flow is required. The Navier Stokes equations governing the velocity of an incompressible fluid are, in tensor notation:-

$$\frac{\partial \tilde{u}_i}{\partial t} + \tilde{u}_j \frac{\partial \tilde{u}_i}{\partial x_j} = -\frac{1}{\rho} \frac{\partial \tilde{p}}{\partial x_i} + \nu \frac{\partial^2 \tilde{u}_i}{\partial x_j \partial x_j}$$

Equation 15

The velocity of the fluid can be broken down into a time averaged mean and a fluctuating component:-

$$\tilde{u}_i = U_i + u_i$$

Equation 16

If this is done the equation governing the mean kinetic energy of the turbulent velocity fluctuations can be obtained through manipulation of the Navier Stokes equations:-

$$U_j \frac{\partial}{\partial x_j} \left( \frac{1}{2} \overline{u_i u_i} \right) = -\frac{\partial}{\partial x_j} \left( \frac{1}{\rho} \overline{u_j p} + \frac{1}{2} \overline{u_i u_i u_j} - 2 \overline{\nu u_i s_{ij}} \right) - \overline{u_i u_j} S_{ij} - 2 \overline{\nu s_{ij} s_{ij}}$$

Equation 17

Where  $S_{ij}$  and  $s_{ij}$  are the mean and fluctuating rates of strain defined as:-

$$S_{ij} \equiv \frac{1}{2} \left( \frac{\partial U_i}{\partial x_j} + \frac{\partial U_j}{\partial x_i} \right)$$

$$s_{ij} \equiv \frac{1}{2} \left( \frac{\partial u_i}{\partial x_j} + \frac{\partial u_j}{\partial x_i} \right)$$

Equation 18

The left hand side of Equation 17 is the rate of change of the mean kinetic energy of the turbulent velocity fluctuations. The right hand side of the equation shows this to be due to pressure gradient work, transport by turbulent velocity fluctuations, transport by viscous stresses and two kinds of deformation work. The first of the deformation work terms is the turbulence production by the Reynolds stresses, which represents the exchange of kinetic energy between the mean flow and the turbulence. The second deformation work is the loss of turbulence energy to viscous forces. At high Reynolds number where dissipation processes are isotropic this second term is equivalent to the energy dissipation rate  $\epsilon$ .

Unfortunately Equation 17 cannot be used to estimate  $\epsilon$ . The terms in  $s_{ij}$  cannot be estimated from the available experimental data. Also to estimate mean values of the

products of fluctuating velocity components, would require an estimate of the correlation between them. Due to the closure problem of Equation 17 it is not used in CFD models and instead a modelled turbulent kinetic energy equation has been developed. The assumptions required to derive this equation are:

- Assume gradient diffusion of kinetic energy to replace the transport terms
- Neglect pressure gradient work
- Replace Reynolds stresses by eddy viscosity equation  $P_k$

This gives the modelled turbulent equation as:-

$$\rho \frac{\partial}{\partial x_j} \left( \frac{1}{2} \overline{u_i u_i} \right) = \frac{\partial}{\partial x_i} \left( \frac{\mu_t}{\sigma_k} \frac{\partial \overline{u_i u_i}}{\partial x_i} \right) + P_k - \rho \epsilon$$

$$P_k = \mu_t \left\{ 2 \left( \frac{\partial U_i}{\partial x_i} \frac{\partial U_i}{\partial x_i} \right) + \left( \frac{\partial U_i}{\partial x_j} \right)^2 \right\}$$

Equation 19

The value  $\sigma_k$  is a turbulent Prandtl number and is usually assumed to be one. All the terms in the modelled kinetic energy equation can be found from the data in Kings thesis. The gradients of mean velocity can be found by interpolating between the tabulated values of mean velocities. The data for the kinetic energy of the fluctuations is presented as contour plots relative to the outlet velocity. Assuming that this distribution will remain the same when scaled to the smaller VA, these values can be tabulated and used in the same way to determine the  $u_i u_i$  terms.

Thus, to give a clearer picture of the distribution of epsilon, these terms were derived from Kings data. The only problem that remained was choosing an appropriate value for the turbulent viscosity. The equation usually used to determine  $\mu_t$  with the modelled KE equation is:-

$$\mu_t = C_\mu \rho \frac{k^2}{\epsilon}$$

Equation 20

where  $C_\mu$  is a turbulent constant with a value of 0.09. A FORTRAN programme was written to solve the modelled KE equation and thus estimate  $\epsilon$ . The tabulated data from Kings thesis was scaled to the VA of 20 mm throat diameter and was then read in

by the programme. It then used the average value of  $\epsilon$  estimated earlier (12500 kW/s) in Equation 20 to give an initial value of  $\mu_t$ . This was then used to estimate a new value of  $\epsilon$ . This continued until the value of  $\mu_t$  converged.

The results from these iterations are shown in a contour plot (Figure 55). This shows a number of interesting points. As might be expected it shows that the area of highest epsilon values is in the area of high tangential velocities, and that the potential for droplet shatter in the recirculating flow around the centre line is relatively small. It also shows that the flow in the VA outlet is capable of producing small values of  $d_{max}$ . As the previous model of droplet motion has shown that most droplets in the flow will be spun out into the areas of high tangential velocity, it seems to indicate that if droplet impaction onto the walls can be avoided, then the VA will produce a fine spray.

It is worth bearing in mind that the results from this section of work indicate trends only. A number of assumptions have been made that will affect the accuracy of the results. The numerical constants in the equations used to find  $E$  and  $d_{max}$  have all been assumed, based on accepted values. The assumptions involved in deriving the modelled KE equation are likely to lead to significant inaccuracies, as it is known that the  $k-\epsilon$  CFD approach is weak in predicting flows with high velocity gradients and curved streamlines. Also in addition to any experimental errors in Kings data, there is the possibility of it not accurately representing the 20 mm throat VA. This is particularly pertinent for the scaling of the data for relative intensity of the fluctuating velocity. To achieve the scaling it was assumed that the intensity of the fluctuations was the same relative to average outlet velocity for both VA s. Whilst it seems reasonable that the distribution should be the same in both VAs the magnitude of fluctuation relative to the outlet velocity may very well vary. This is particularly the case if rotational fluctuations are significant, as seems likely in these flow conditions.

Given the assumptions that have had to be made in order to obtain a numerical prediction of droplet size, it is clear that the plot of predicted maximum droplet size is best used only as a guide, rather than absolute values. However the work is valuable in improving the understanding of the experimentally observed results.

## Maximum stable drop size in VA

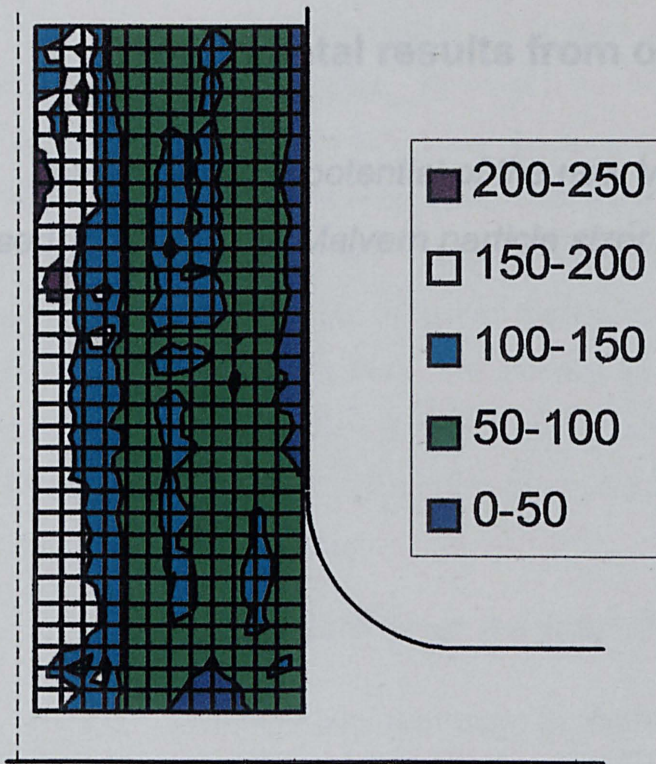


Figure 55 Maximum stable drop size ( $\mu\text{m}$ ) in outlet flow from the VA at control flow = 400 li/min

## CHAPTER 8

### Experimental results from optimised VA

*The atomisation potential of the new Vortex Amplifier was assessed, both with the Malvern particle sizer and photographically.*

## Overview

The two preceding chapters presented numerical simulations of droplet behaviour within the new VA. These indicated that there was a strong potential for it to produce very fine sprays. They also suggest that droplets impacting on the VA diffuser walls may still cause serious problems. However it was hoped that the greatly reduced chamber height of the new VA would allow the spray to penetrate beyond the VA diffuser without significant quantities impacting upon the walls.

Once again the spray was measured with the Malvern particle sizer. Photographs of the spray were taken to confirm the Malvern particle sizer readings and provide an indication of the flow pattern. The potential for good atomisation is greatest when there is pure control flow through the VA, and so most of the tests concentrate on this condition. The tests examine the effect of varying the flow rate and changing different aspects of the VA geometry.

## **I. Malvern Particle Sizer measurements on new VA**

### **I.i Droplet sizes produced by the VA with control flow**

The Malvern particle sizer is the primary method of evaluating the spray atomisation. The SMD values presented throughout this chapter were obtained using it. The method of data gathering was the same as that described in **Chapter 3** for the previous spray measurements with the VGVA. Thus each plotted data point is an average of twenty sweeps of the detector, so represents data from twenty different firings of the injector. The firing of the injector is synchronised with the Malvern detector sweep by a data acquisition board producing a triggering pulse.

As described in **Chapter 5** the new VA was designed so that the diffuser and the downstream geometry could both be varied. In the first series of spray measurements the VA was fitted with the orifice plate diffuser, and the large volume viewing box was attached to the outlet.

This is an impractical geometry for use in an engine. The orifice plate gives comparatively poor VA performance. In addition a large volume would introduce severe transient control problems in an engine. However this arrangement allows the spray produced by the vortex flow to be easily observed. This allows confirmation of



the atomising potential of the VA, and provides a baseline to indicate how well more practical outlet geometry would perform.

The measurement zone where the laser beam from the Malvern particle sizer intersected the spray was 60mm downstream of the VA backwall. Visual observation of the VA and viewing chamber confirm that very little fuel is deposited against the walls prior to the measurement zone.

Tests indicate that the main body of the spray passes through the measurement zone the period between 12 and 16 milliseconds after injection. To allow easy comparison between sprays produced at different control flow rates it was decided to use the SMD measurement 14ms after injection as typical of the spray,. Spray measurements were conducted over a wide range of control flow rates, and the SMDs of the sprays at 14ms after injection are presented in Figure 56.

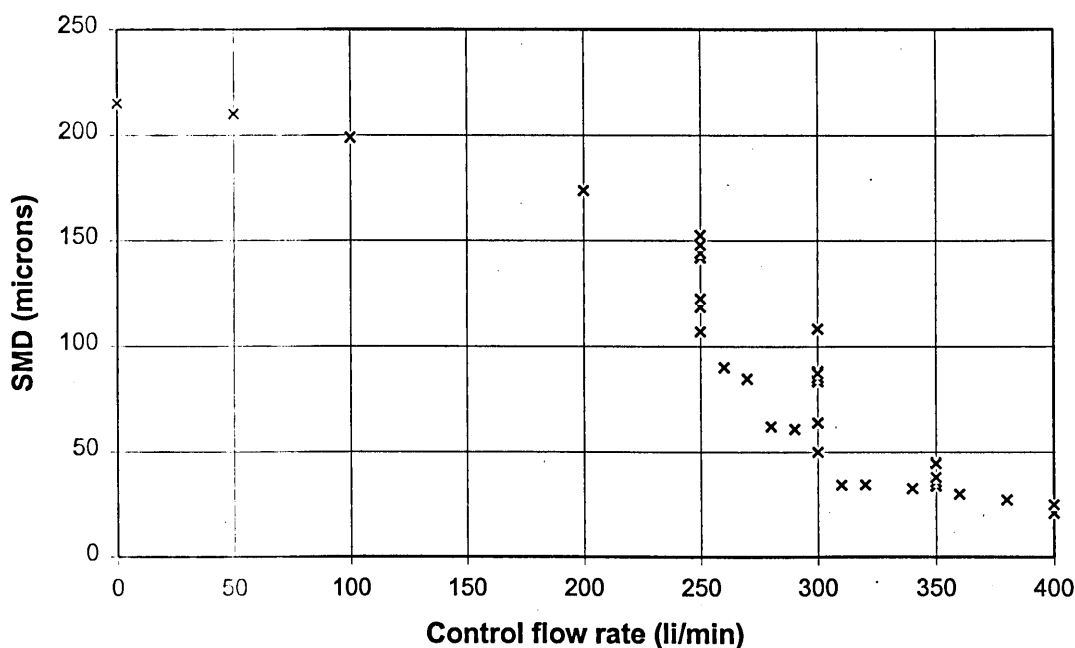


Figure 56 Measured SMDs with control flow through the VA

It can be seen in Figure 56 that the VA is an effective atomiser. It reduces the SMD of the spray from 215 $\mu$ m with no flow to 25 $\mu$ m when the control flow is 400 li/min. Excellent atomisation is achieved at all flows above 300 li/min.

Another feature of the results is the large scatter in the measured SMD at flowrates between 200 and 300 li/min. In this region the SMD measured could vary across a 60  $\mu$ m range. However outside this range the scatter of the measurements was

much lower. For instance at 350 li/min all the measurement lie within a 10  $\mu\text{m}$  range, and at 400 li/min the range is less than 5 $\mu\text{m}$ .

The pressure drop across the VA is 0.385ba at 400 li/min. At this pressure drop air shrouded injectors produce a spray with an SMD of roughly 40 $\mu\text{m}$ , and require a pressure drop of around 0.6 bar to achieve a spray SMD of 25 $\mu\text{m}$ <sup>7</sup>. This seems to indicate that the VA could achieve good spray atomisation over a much wider range of engine conditions than an air shrouded injector.

### **I.ii Effect of varying the VA outlet diffuser**

In any practical application the VA would be fitted with a diffuser on its outlet rather than just an orifice plate. This is to reduce the supply flow pressure drop, which in an engine application would increase the volumetric efficiency. The VA in the test rig was designed so that two different diffusers, as well as the orifice plate, could be attached to the outlet. These both have the same area ratio of approximately 3.6:1, and were 20mm and 46mm long.

Attaching these to the VA could effect the spray arriving at the measurement zone in two ways. The attachment of a diffuser will change the pattern of airflow at the VA exit where atomisation takes place, which could alter the spray SMD. Also the spray may be deposited against the diffuser walls. The numerical simulation has shown that the latter will tend to affect mainly the smaller droplets, causing the measured SMD to rise.

The spray SMDs were measured with each outlet attached. The viewing chamber was still used, attached to the VA outlet, to allow easy optical access, and the diffusers discharge into this. Spray SMDs were measured with the Malvern particle sizer. Photographs were taken to support these measurements. The measurements were again taken 14ms after injection with the measurement zone in the same position as in the first set of tests.

The SMDs of sprays measured with different outlet diffusers are shown in Figure 57.

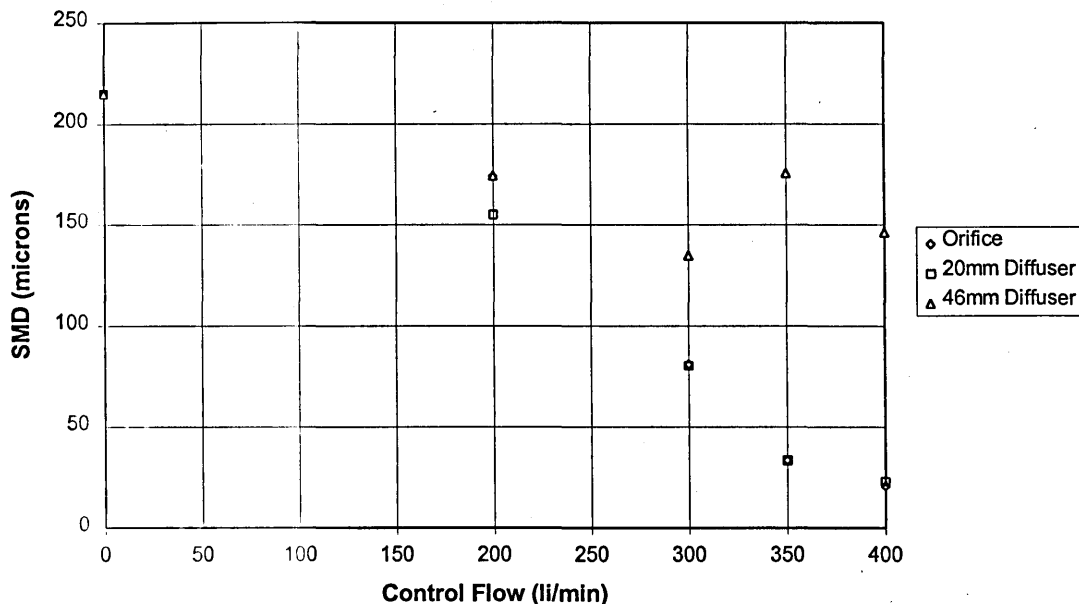


Figure 57 Measured SMDs with different outlet diffusers.

It is clear that at control flows below 200 li/min the VA outlet has a minimal effect on the SMD measured by the Malvern particle sizer. The difference in the SMD values observed at this flow rate are within the range of experimental scatter found in earlier tests. However at higher flow rates the longer diffuser clearly affects the spray. Both the orifice and shorter diffuser outlet both show a considerable reduction in SMD as control flow increases. In contrast the large diffuser fails to reduce the droplet diameter below  $130\mu\text{m}$ , and so would produce very poor air to fuel mixing.

It would appear that the smaller droplets in the spray are being deposited on the diffuser walls, so that the measured SMD of the spray increases. The shorter diffuser performs as well as the orifice plate, with the data points being practically identical, and it would appear that the spray passes through it without significant deposition of fuel on the walls.

### 1.iii Effect of varying injector position

The numerical simulation of droplet breakup within the VA had shown that the most turbulent flow lay off the central axis of the VA. It was therefore possible that atomisation might be improved by injecting the spray off centre so that more of the fuel would pass through this highly turbulent region.

In addition the simulation on droplet motion in the VA had shown that droplets injected into this region penetrated further into the VA. This is because of the core of reversed flow at the centre of the VA outlet. Thus it was felt that offsetting the injector may reduce droplet deposition.

The injector was moved so that its axis was offset from that of the VA chamber by 5mm. The orifice plate was attached to the VA outlet and the flow exited into the viewing chamber. The SMD measurements obtained are compared in Figure 58 with those already obtained for a centrally positioned injector in the same conditions.

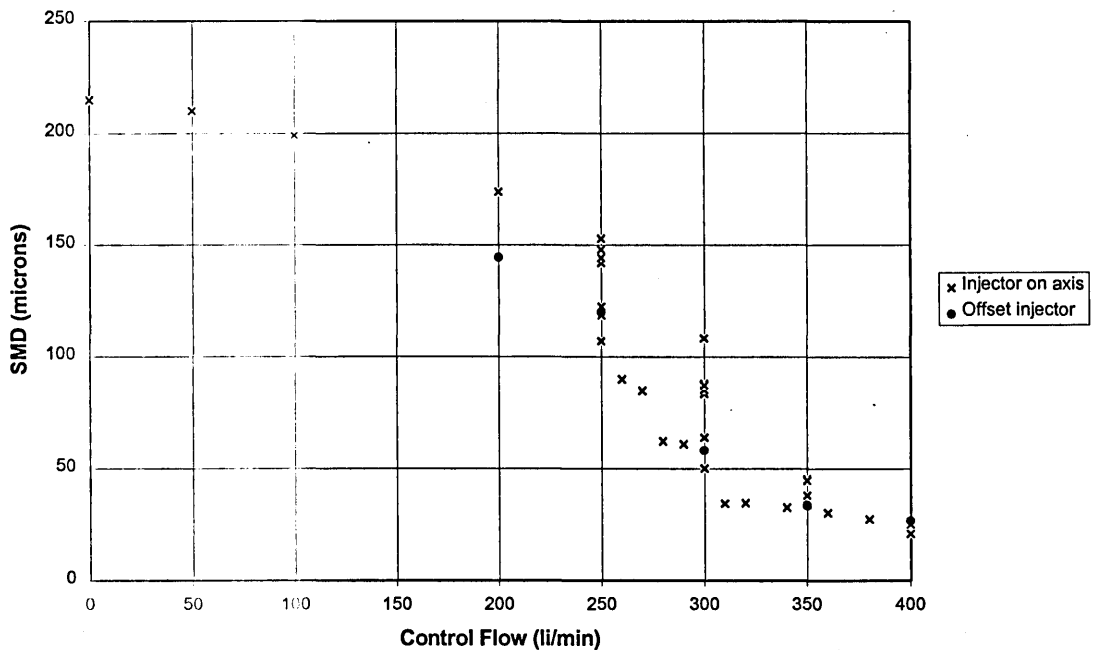


Figure 58 Comparison of results for axial and offset injector positions

The results appear to indicate that there is an advantage in having the injector offset at lower flow rates. This is because the SMD of the spray produced with the injector offset is always at the lower end of the range of SMDs observed with the centrally placed injector. Thus although the best performance for the centrally placed injector is as good as that with the offset injector, the offset injector achieves this performance repeatably.

The higher values in the range of SMDs observed with the centrally placed injector are caused by the bulk of the spray not passing through the most turbulent part of the flow. At the higher flow rates the swirl is sufficient to ensure that the spray is

centrifuged into the most turbulent region wherever the injector is placed. This means there is less scatter at the high control flow end of the graph, and the measurements from the centrally positioned and offset injectors are the same.

#### **I.iv Results with supply flow and mixed control and supply flow through the VA**

The preceding tests have established that the VA can atomise the spray effectively at high control flow rates. To see how effective the atomisation is across the rest of the VA flow regime tests were conducted with supply flow and mixed supply and control flow. The proportions of supply flow and control flow into the VA were varied with the control valves fitted in the rig. Spray measurements were taken in the same way as for the previous tests.

##### ***I.iva Test with pure supply flow***

Spray measurement were taken with only supply flow passing through the VA at the same levels of flow that had been used in the experiments with control flow. The orifice plate was attached to the outlet of the VA and the spray discharged into the viewing chamber. The position and timing of the measurements were kept the same as the previous tests.

The results from these tests are shown in Figure 59. For comparison the SMDs measured previously with control flow through the VA are also shown on the graph. Unsurprisingly the supply flow produces considerably larger droplet sizes. This confirms that the excellent atomisation produced by the VA is largely due to the very turbulent nature of the vortex flow.

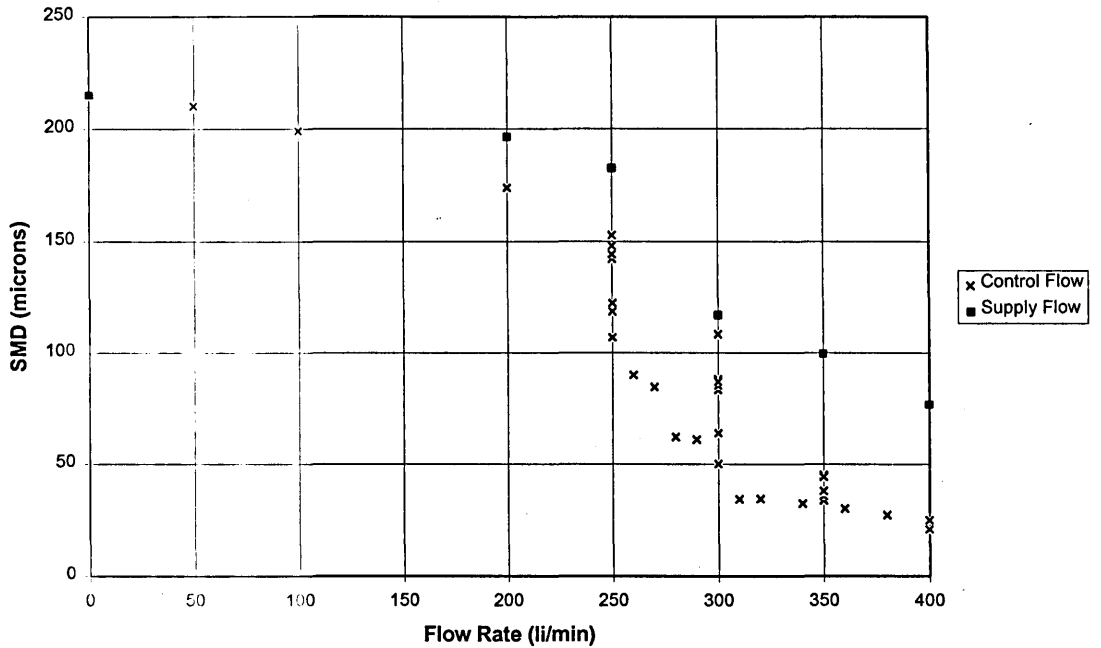


Figure 59 Comparison of measured SMD for supply and control flow

#### *1.ivb Test with mixed supply flow and control flow*

Tests were also conducted with mixed mode flows. These were conducted in the same way as the pure supply flow tests, but control flow was introduced. The flow through the VA was kept constant at 400 li/min and the relative proportions of control and supply flow were varied.

The results from these tests are shown in Figure 60. As expected the best atomisation is achieved with pure control flow, and atomisation remains good until the supply flow increases beyond 3/5ths of the total flow.

A surprising feature of the results is that with mixed flow at low control flow rates the atomisation is worse than that achieved by the pure supply flow. The explanation for this can be found in the velocity distribution within the VA. The introduction of control flow causes the axial velocity at the centre of the VA outlet to fall. This is because the tangential momentum imparted by the control flow causes the axial velocity distribution across the outlet to peak close to the walls and be lower in the centre. As the injector was centrally positioned in these tests this means that as control flow is increased the fuel is injected into lower velocity air flow. This means that the relative velocity between the spray and the airflow, which provides the disruptive force to shatter the spray, is reduced. This leads to the observed rise in droplet size until the

vortex becomes sufficiently turbulent to shatter the spray and distribute it throughout the outlet flow.

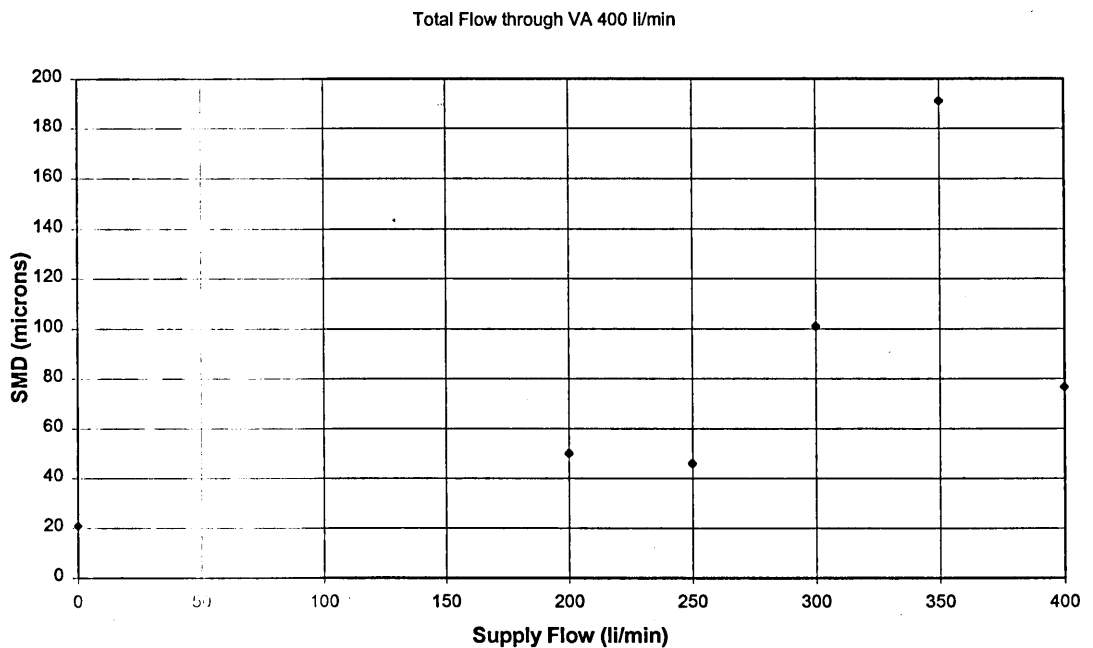


Figure 60 Measured SMDs for mixed mode flow through the VA

#### I.v Effect of varying pipework downstream of the VA

The large viewing chamber attached to the VA outlet in all the experiments above would have deleterious effects on engine control if it were actually fitted in an intake system. This is due to the time lag it would introduce. In practice there is only a short port between the injector and the cylinder in a multi point injection engine. It was therefore necessary to observe the spray from the VA passing through such a short port, to assess how it affected the atomisation. Again there was the possibility of spray being flung against the walls, particularly in light of the modelling results and the experiments in section ii which indicated this happened in the longer diffuser.

A tubular outlet was attached to the outlet of the VA in place of the viewing chamber. This had an internal diameter of 28mm. Windows were attached to allow access for the laser beam at the measurement position which was again 60mm from the VA backwall. The spray was measured in the tube, with either the orifice plate or the smaller diffuser attached to the VA outlet. The VA was supplied with control flow

only. Spray measurements were recorded with the Malvern particle sizer across a range of flow rates.

The results from this testing are plotted in Figure 61. The measurements that were taken earlier with the spray discharged into the viewing chamber are included for comparison.

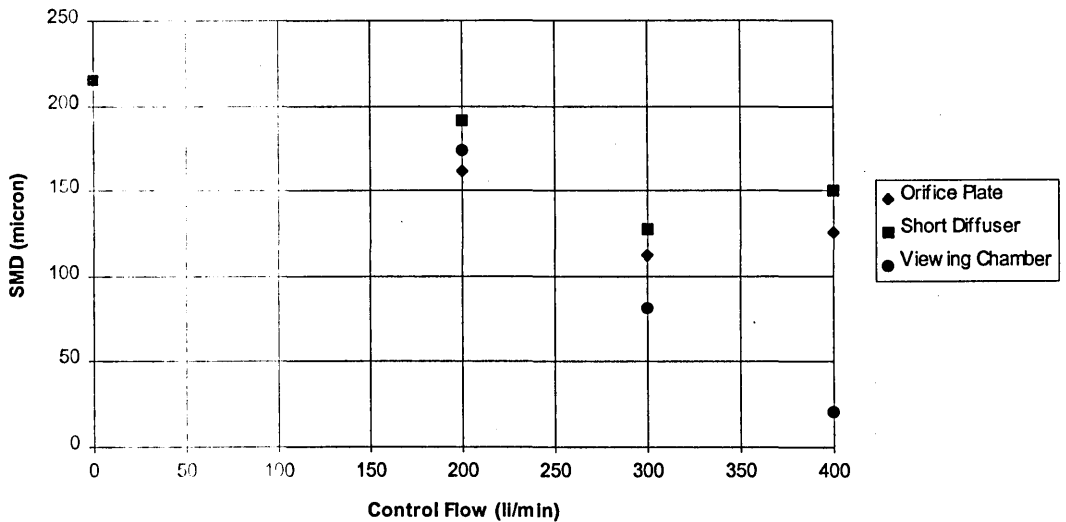


Figure 61 SMD measurements with a tube outlet attached to the VA (viewing chamber results included for comparison).

Again it can be seen that the tube has little effect up to flows of 200l/min. As the flow increases beyond this the SMD is larger than that attained in the viewing chamber. These results are similar to those measured with the long diffuser attached, which appear in Figure 57. Again this can be attributed to the smaller droplets being flung against the walls.

The measurements of SMD with the tube outlet attached indicate that in an engine little fuel would travel down the intake port from the VA to the cylinder without being deposited on the walls. Further testing was undertaken to confirm this. Two different tube lengths were attached to the VA outlet. The flow from these then passed into the viewing chamber, where any fuel carried in the airstream could be measured. The first of these was 100mm long, the second 50mm.

The results from these tests confirmed the severity of the spray deposition. With the longer (100mm) tube no droplets emerged into the measurement zone (160mm from the VA backwall) if the control flow was increased above 100 li/min. With the 50mm



tube droplets were observed at flows up to 200 li/min. Again at higher control flow rates no droplets were carried through the tube. Clearly at the higher flowrates all the spray is deposited against the tube walls.

## II. Photographs of sprays from the new VA

Photographs of the spray produced by the VA were taken to provide further data on spray formation within the VA. These confirmed the validity of the Malvern particle sizer measurements. The photographs of the spray were taken in the large viewing box attached to the VA outlet over a range of control flows.

The spray was illuminated with a normal camera flash. To improve the resolution of the photograph only a thin sheet of the spray parallel to the plane of the camera lens was illuminated. This was achieved by directing the camera flash through a narrow slit so that it lit a sheet of spray in the focal plane of the camera. Due to the high speed of the spray the photographs are not perfectly focused, but they still provide valuable indications of the spray behaviour.

The photographs are presented on figures showing their position relative to the vortex chamber, injector and measurement zone. They are twice actual size.

Two photographs are compared in Figure 62 and Figure 63. The first shows the spray with a low control flow through the VA, the other a high control flow rate. With the low flow rate it can be seen that the spray in the measurement zone contains large droplets and is concentrated in a narrow cone. In contrast in the second photograph very few individual droplets are visible, and most of the spray appears as a fine mist. This is consistent with the very low SMD recorded at this flow rate. Also the spray is not resident in the centre of the viewing chamber, but has been moved out to the sides by the spinning flow. At the top of the photograph it can be seen that the spray from the injector penetrates into the viewing chamber, but is rapidly dispersed by the turbulent flow through the outlet.

Figure 64 and Figure 65 show photographs with outlet diffusers attached. In both photographs the flow through the VA is 400 li/min and is all control flow. The first photograph shows the shorter diffuser. It can be seen that the spray is similar to that with the orifice plate at high control flow in that most of the spray appears as a fine mist of droplets. A few large drops, which appear to have been re-entrained from the

diffuser wall are present. The spray has not been flung as far out to the side as was the case with the spray from the orifice plate, since the diffuser obviously allows for a more gradual expansion of the airflow into the viewing chamber. However most of the fine droplets are at the edge of the flow from the diffuser.

In the photograph of the long diffuser only a few large droplets can be seen exiting the left hand edge of the diffuser. This agrees with the Malvern particle sizer measurements which indicate that most of the spray is deposited in the diffuser.

### III. Discussion

This chapter has presented a considerable amount of experimental data measuring the atomisation potential of the VA. The effect of control flow rate upon the SMD of sprays produced in the VA has been investigated. Some measurements have been made of the influence of the relative proportions of control and supply flow upon the droplet size. This would clearly be important in an engine application where the VA would to operate throughout the entire range of flows, from pure control at idle, to pure supply at wide open throttle. Further testing has considered the effect of a number of different outlet geometries on the effectiveness of the atomisation.

#### III.i Accuracy of results

The quantitative measurements of droplet size were obtained with a Malvern particle sizer. This is a very accurate instrument. However there is still a level of uncertainty in the results. This is mainly attributable to the measurement of a volatile spray. There was evidence that some refraction of the laser beam took place in the density gradients caused by the spray evaporating. This effect is known as beam steering. The presence of beam steering was shown by the skewing of the scattered light energy distribution that was measured by the Malvern particle sizer, which was observed during the gathering of data.

Beam steering will result in undeflected light being measured by the innermost rings of the light sensitive diodes in the Malvern particle sizer detector. This will lead to the value of SMD calculated from this data being higher than that of the spray. To quantify the effect of the beam steering several results were analysed with the data from the innermost diodes ignored. This will give a value for the spray SMD assuming that

none of the light detected at the innermost rings was diffracted from large droplets. This analysis showed the minimum bound to the SMD, assuming all the light on the innermost rings of the detector to be the result of beam steering, to be within 10% of the calculated SMD from the whole sample of the scattered light data.

The photographic work showed the persistence of a few large drops in the spray within the measurement zone. It was therefore decided to calculate the SMD from the full sample of calculated light data as some of the scattered light on the innermost rings was attributable to these large drops. As some beam steering is believed to have occurred this analysis will over predict the SMD. Thus the reported SMDs represent an upper bound to the spray size with a tolerance of -10%.

The results in Figure 56 show a large scatter in SMD between flow rates of 250 and 300 li/min. It is important to realise that this is not genuine experimental scatter, but the measurement of a genuine physical effect. It has been explained in terms of the interaction between the spray and the region of highest turbulence in the flow. Both the flow path of the spray, and the position of the most turbulent airflow are not fixed. This means some measurements record very small droplet sizes when the spray interacts with the highest turbulence air, and some record larger sizes when it does not. At higher flowrates the turbulence of the air at the VA axis is always sufficient to disperse the spray into the highly turbulent region near the outlet walls. This is why the large amount of scatter is not found at higher flowrates.

Evidence to support this explanation of the scatter comes from the measurements taken with the injector offset from the VA axis by 5mm. In this position the bulk of the spray must interact with the highest turbulence flow. These measurements do not show the scatter associated with the previous results. Furthermore they show the same value of SMD as the lowest recorded with the centrally positioned injector. This confirms that the low SMD recorded with the centrally placed injector were caused by the spray interacting with the highly turbulent region of airflow.

To completely rule out an explanation of this scatter based on beam steering measurements were taken over a period of several weeks. As beam steering is caused by spray evaporation, the magnitude of the effect will depend upon atmospheric conditions. There was no correlation between the amount of scatter in measured SMD and the temperature, pressure and humidity in the laboratory.

It seems clear that the scatter in the results is due to random elements beyond the control of the experiment. These include random fluctuation of the VA flow field and imperfect repeatability of the injector positioning and supply pressure. These small effects seem sufficient to determine whether or not the spray interacts with the most turbulent region of the airflow.

### III.ii Overview of results

The results presented in Figure 56 clearly show that excellent atomisation can be achieved at control flow rates of above 300 li/min, and good atomisation can be achieved at lower flow rates. There is however a good deal of scatter in the SMD achieved at the lower flow rates. Figure 58 shows that positioning the injector so that it is offset from the central axis of the VA removes this scatter. By offsetting the injector the bulk of the spray is certain to pass through the most turbulent region in the outlet, so ensuring the smallest possible droplets sizes are produced.

Figure 60 shows that good atomisation can be achieved across much of the VA operating regime as mixed mode flows produced fine sprays. However when supply flow was increased so that it constituted more than about 60% of the flow supplied to the VA atomisation effectiveness was reduced.

Unfortunately these positive results were obtained with an experimental set up that does not accurately represent conditions within any feasible engine design. This is because the VA outlet was fitted with an orifice plate rather than a diffuser and the measurements are taken in a large volume viewing chamber.

- The results taken under more realistic conditions were much less encouraging. Although the shorter diffuser produced sprays with SMDs as low as those measured with the orifice plate, at high control flow rates most of the spray was deposited within the long diffuser. Also the spray was deposited within the pipe outlets that were attached to the VA. Unless this problem can be overcome the excellent atomisation of sprays within the VAs is of little practical value.

### III.iii Attempts to prevent droplet deposition

The route to overcoming the spray deposition is not obvious. A simple change in the size of the VA is unlikely to provide a solution. Increasing the VA outlet diameter would mean the position of the injector was further from the walls, which

would offer a reduction in spray deposition. However to maintain VA performance the chamber height would have to be increased. This would increase the residence time of the spray within the body of the VA. The earlier work with the VGVA indicates that this would lead to spray deposition within the vortex chamber.

Some simple changes to the VA geometry were tested in an attempt to prevent droplet deposition. The injector was advanced into the chamber so that it was level with the plane of the VA outlet in the hope that this would allow greater spray penetration. However measurements with the long diffuser again showed that spray diameter did not drop below  $130\mu\text{m}$  for the range of control flows tested. This indicates that most of the spray was still deposited within the diffuser.

Another approach was to place a cylindrical gauze mesh in the VA outlet in an attempt to catch the spray before it was deposited. However this disturbed the outlet flow so that atomisation was worse at most flow conditions.

It was hoped that there was a possibility to minimise droplet deposition by timing the injection pulse to coincide with vortex spin up or spin down in unsteady flow. To investigate this the VA was tested with pulsed airflow. The results of this testing are presented in the next chapter.

Figure 62 Spray Photograph. Control Flow = 100 li/min. Orifice plate attached to VA exit

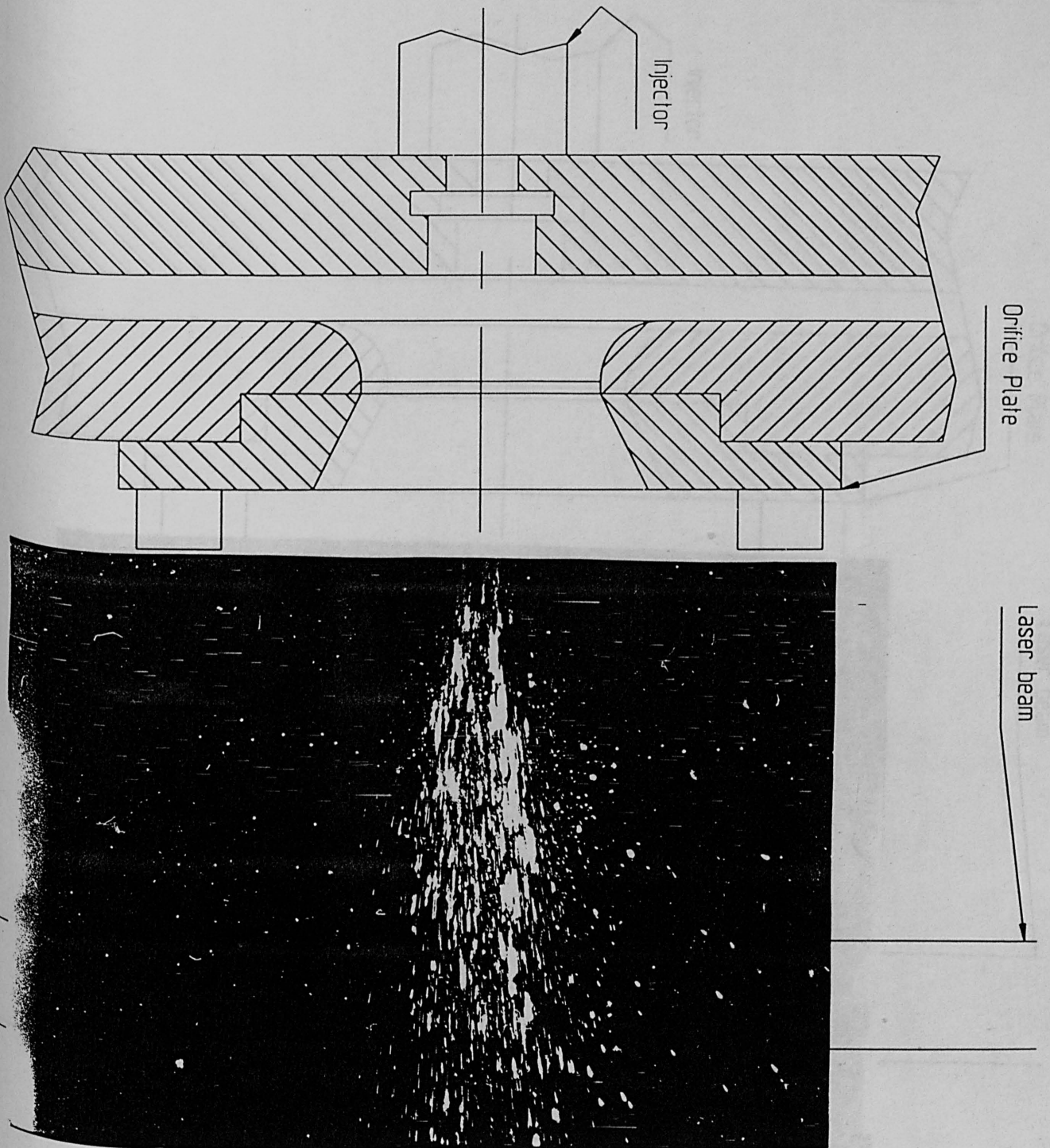


Figure 63 Spray Photograph. Control Flow = 400 li/min. Orifice plate attached to VA exit

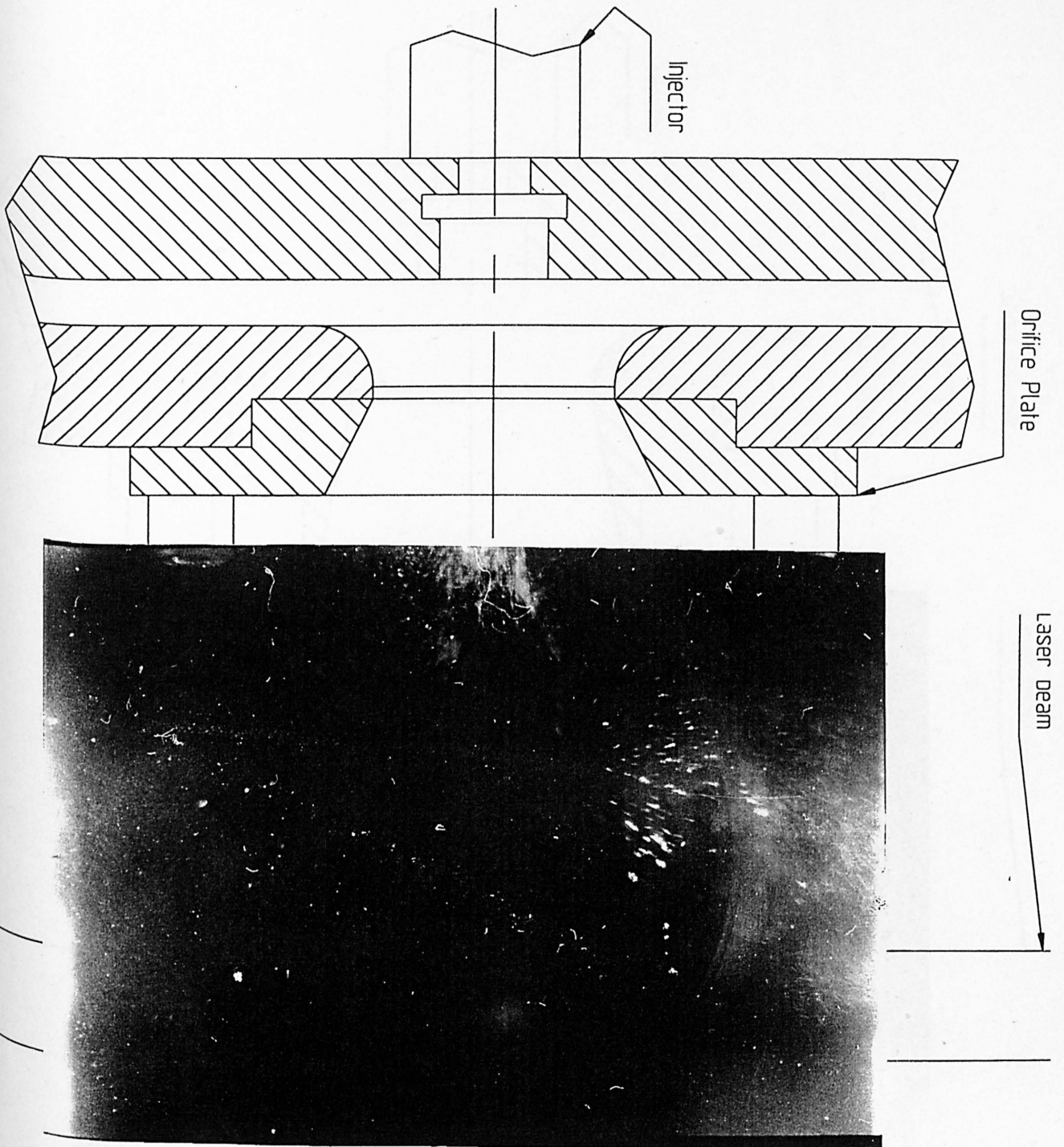


Figure 64 Spray Photograph. Control Flow = 400 li/min. Short diffuser attached to VA exit

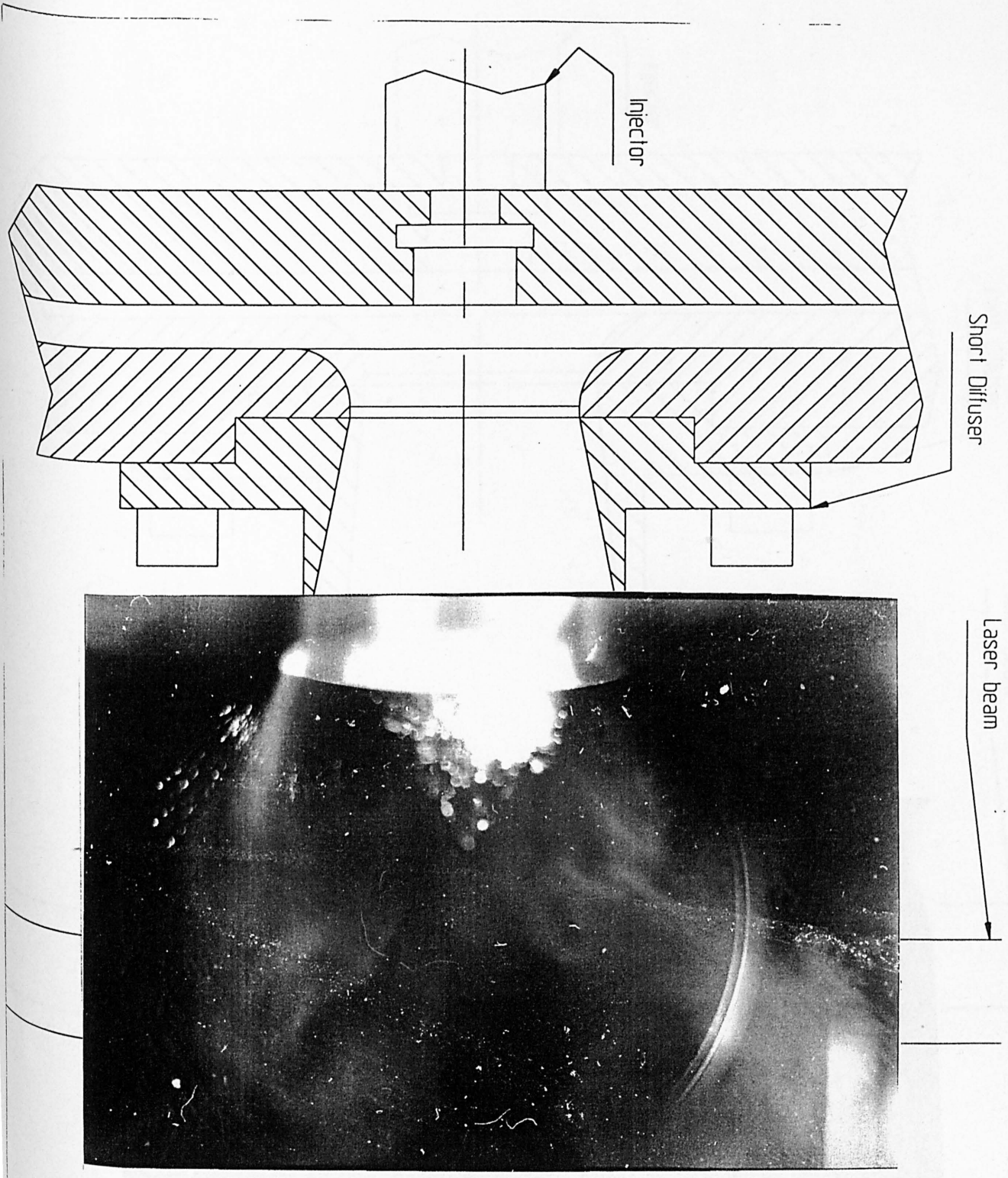
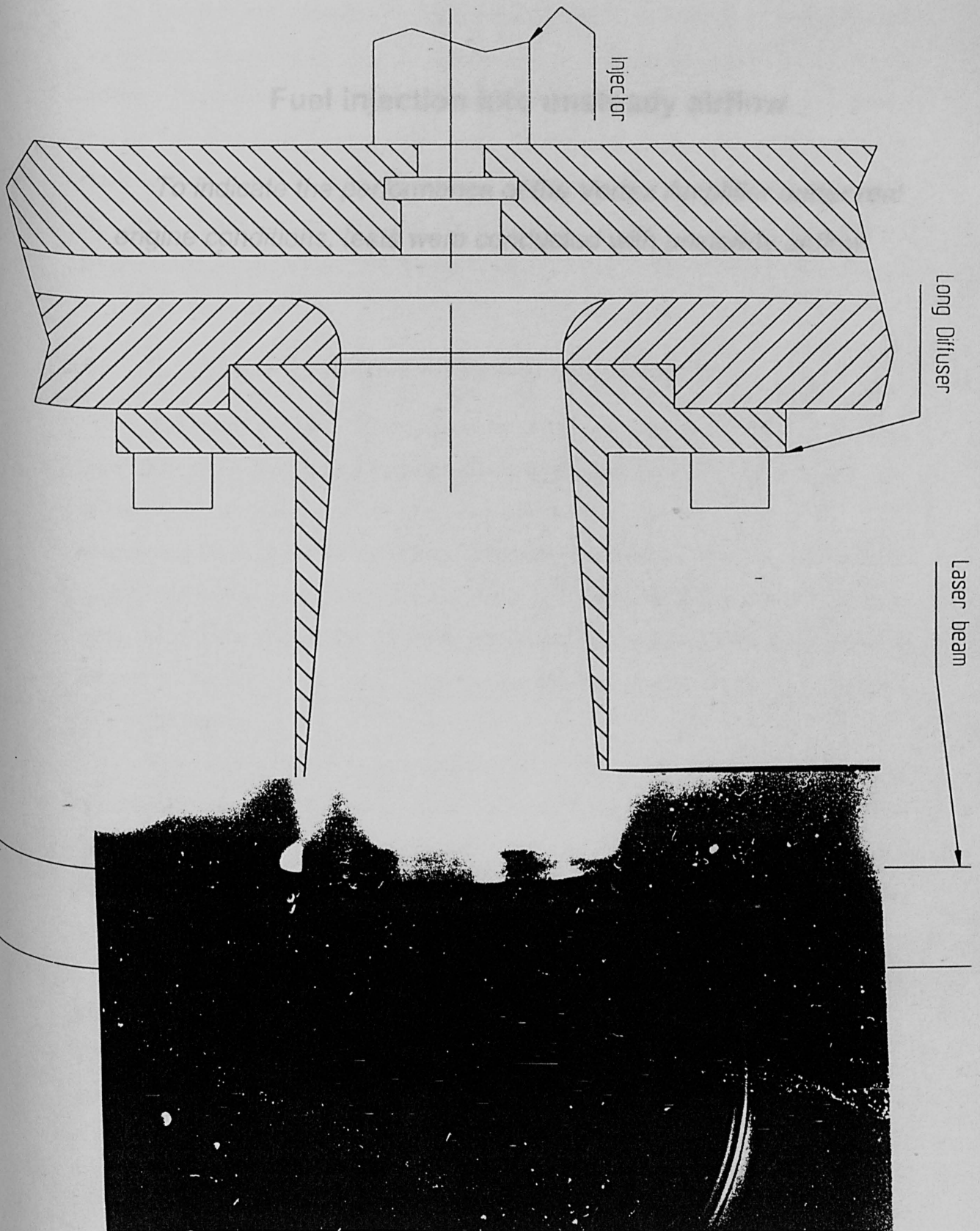




Figure 65 Spray Photograph. Control Flow 400 li/min. Long diffuser attached to VVA exit

CHAPTER 9



## CHAPTER 9

### Fuel injection into unsteady airflow

*To indicate the performance of the Vortex Amplifier under real engine conditions, tests were conducted with unsteady airflow.*

## I. Introduction

The previous chapters have presented results from numerical modelling and experiments investigating droplet behaviour in the VA under conditions of steady airflow. These have shown encouraging indications that the VA could produce sprays that are finer than those from current automotive injectors. However the flow through a spark ignition engine is obviously pulsed. Under these conditions the vortex in the chamber will take time to form. It is possible that if the 'spin up' time for the vortex is large it could adversely effect the droplet breakup. To see if this was a significant factor some tests were required to examine the effect of pulsed airflow in the VA.

## II. Test rig for pulsed flow through the VA

The steady flow test rig was altered by inserting a rotating valve that could chop the airflow into pulses. This chopping valve is shown schematically, just after opening, in Figure 66. It consisted of a rotating cylinder inside a cylindrical housing. Both the housing and the rotor had holes in them. Thus when these holes were aligned the valve allowed airflow to pass. The inlet and outlet holes were at different axial positions along the cylinder so that that the valve would open once per revolution. The holes at the inlet to the valve were much larger than the exit ones so that the flow is controlled only at the outlet.

The valve is open for approximately  $37^\circ$  of the  $360^\circ$  of the valves rotation. A typical inlet valve in a four stroke spark ignition engine would open about  $5^\circ$  before TDC of the induction stroke, and close  $45^\circ$  after BDC, a total valve opening angle of  $230^\circ$ <sup>65</sup> for every  $720^\circ$  of rotation. Figure 67 shows a comparison of the chopping valve with a typical engine inlet valve.

It can be seen that the opening profile of the chopping valve is similar in shape to that of an engine valve. As the chopping valve opens every  $360^\circ$  rather than every  $720^\circ$  the frequency of the chopping valve is twice that of an engine running at the same speed.

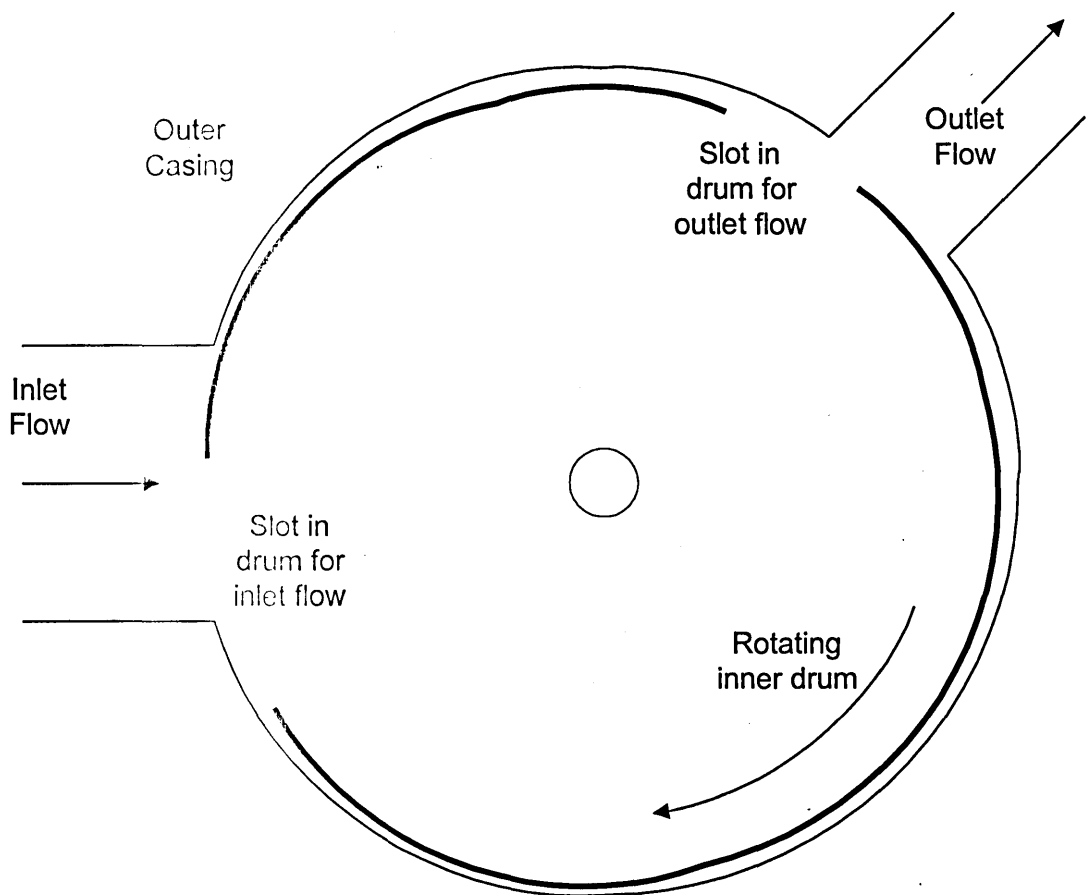


Figure 66 Schematic diagram of chopping valve

Obviously the opening angle of the chopping valve is smaller than it should be for an accurate simulation of a inlet valve. It is open for approximately 10% of the valve period, an engine valve is open for about 28% of the period. However the flow through the valve should be roughly representative of flow in an SI engine running at twice the speed.

As the primary concern of the project is the atomisation of the spray at engine idle and low power, most data was gathered with the chopping valve rotating at 400 rpm. The flow observed should correspond approximately to that in a engine intake port at the typical idle speed of an SI engine of 800 rpm.

Clearly there are considerable differences between the flow in the test rig and that that would be observed on a multi cylinder engine. The pulsed flow work only indicates trends rather than allowing accurate prediction of behaviour in an engine.

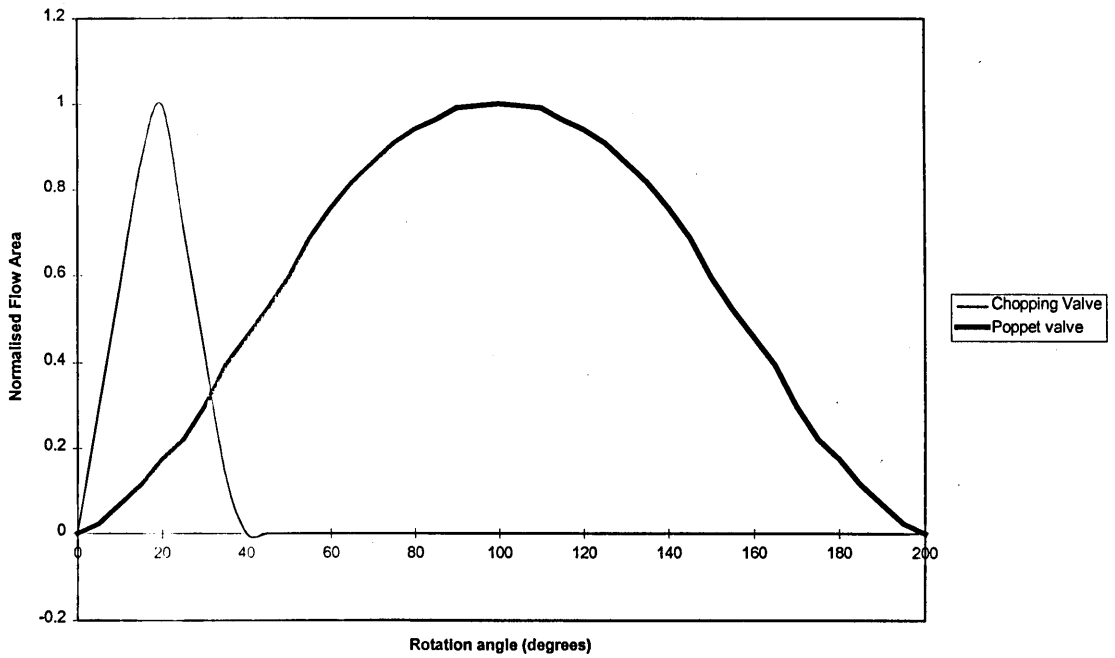


Figure 67 Comparison of chopping valve and engine inlet valve opening profiles

The test rig was instrumented to measure the pulsed flow. A magnetic pickup was installed on the chopping valve to detect the speed of rotation. The output from this pickup was fed to a digital readout that displayed the revolutions per minute, and also to the data acquisition board. This allowed the pressure readouts to be related to the position of the chopping valve.

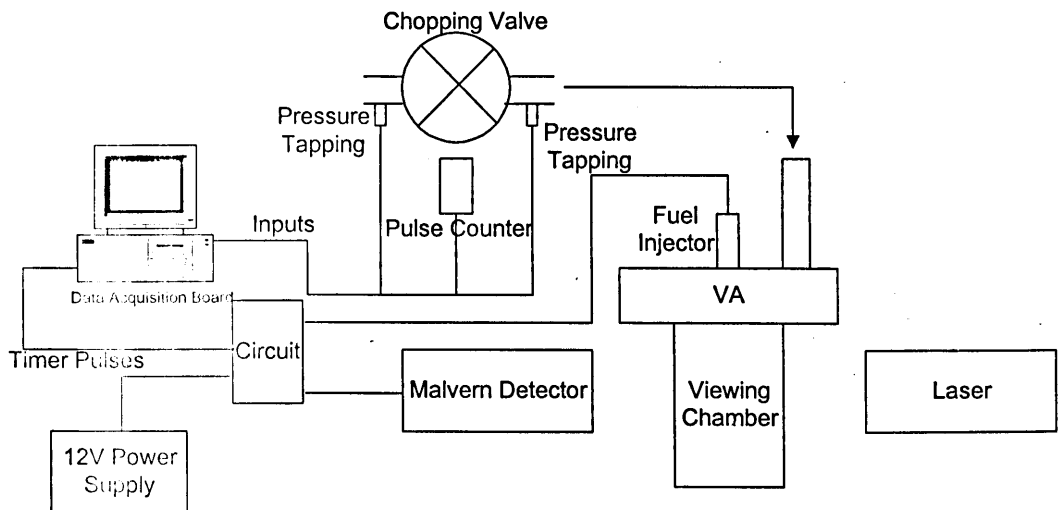


Figure 68 Schematic of test rig adapted for pulsed flow

Pressure tappings were positioned upstream and downstream of the chopping valve. These allowed access for the Druck pressure transducer. The output from this

pressure transducer can be fed to the data acquisition board, to allow the variation of pressure with chopping valve rotation to be observed.

The rotameter was left in the test rig. This was to allow the opening of the valve supplying the test rig to be set repeatably. With the chopping valve fixed in the wide open position, the throttle position could be set to give a value of steady flow, measured by the rotameter. Once the throttle position was set in this way the chopping valve could be started to begin pulsing the flow. It was very hard to set the inlet throttle position repeatably in any other way due to the large pressure drop across it.

### III. Simple Lumped Capacitance model of flow through VA test rig

To relate the drop sizes measured with pulsed flow in the VA to the steady flow results it was necessary to know how the airflow through the VA varied with time. It was decided to construct a mathematical model to describe this. Abdul-Wahab<sup>4</sup> successfully modelled flow through the VA when he used it as an engine throttle with a simple lumped capacitance model. A similar method was used in an attempt to model pulsed flow through the test rig used in the current project.

The basis of the model assumes that the flow through the chopping valve can be determined by the equation for compressible flow through an orifice, which for unchoked flow is:

$$\dot{m} = \frac{C_D A_R P_U}{\sqrt{RT_U}} \left( \frac{P_D}{P_U} \right)^{1/\gamma} \sqrt{\frac{2\gamma}{\gamma-1} \left[ 1 - \left( \frac{P_D}{P_U} \right)^{\frac{\gamma-1}{\gamma}} \right]}$$

Equation 21

In Equation 21  $C_D$  is a discharge coefficient,  $A_R$  a reference area, and the subscripts U and D refer to conditions upstream and downstream of the chopping valve respectively.

Clearly the area of the chopping valve varies as the valve rotates. When the orifice is fully open it is a rectangle of 37mm length and 13mm width. As the valve rotates the width varies between 0mm and 13mm, being closed for most of the time (see Figure 66). The diameter of the chopping valve is 80mm. If TDC (i.e. 0°, 360° etc. of

chopping valve rotation) is taken as the point where the valve is just about to open, the width of the valve,  $b$ , is:

$$\begin{aligned} b &= 80 \sin(\theta/2) & 0 < \theta \leq 18.7 \\ b &= 13 - 80 \sin(1/2[\theta - 18.7]) & 18.7 < \theta \leq 37.4 \\ b &= 0 & 37.4 < \theta \leq 360 \end{aligned}$$

Equation 22

The area of the chopping valve is thus:

$$A_R = 37 \times b \text{ mm}^2$$

Equation 23

As well as the chopping valve the test rig also contains the VA and a viewing chamber, and connecting pipework. The basic layout of the test rig is shown in Figure 69.

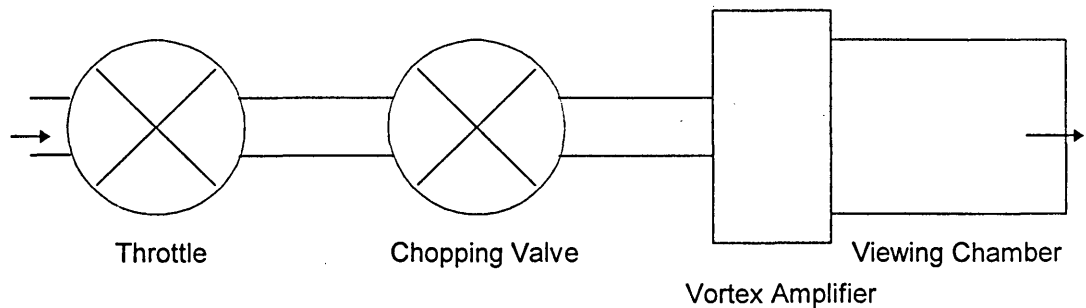


Figure 69 Schematic layout of test rig for pulsed flow

In the model of the test rig the flow through the throttle and chopping valve can be modelled with Equation 21. By treating the pipes and the viewing chambers as pure capacitances and assuming adiabatic flow the pressures can be modelled as in Equation 21.

$$\frac{dP}{dt} = \frac{\gamma - 1}{Vol} (\dot{m}_m C_p T_{in} - \dot{m}_{out} C_p T_{out})$$

Equation 24

This leaves only the VA to be modelled. A FORTRAN programme was written to solve Equation 21 and Equation 24 in the test rig with the VA modelled empirically from a curve fitted to the measured steady state control flow data. The simulation was run with a pressure upstream of the throttle of 1 bar, the viewing chamber exiting to

atmosphere and the chopping valve rotating at 400 rpm. The results from the simulation are compared to those from experimental measurements on the test rig in Figure 70.

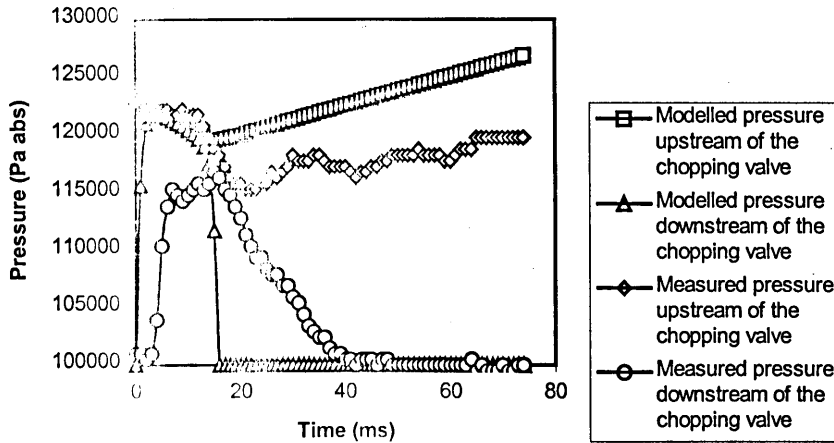


Figure 70 Comparison of measured pressures in test rig and results from lumped capacitance model

The modelled results do not give a particularly good approximation to the experimentally measured pressures. The measured pressure downstream of the chopping valve lags the predicted pressure by a considerable amount. Upstream of the chopping valve the modelled pressure recovers more rapidly than was actually the case. In addition it does not model the secondary oscillations that are a feature of the measured pressure values.

The deficiency in the model is attributable to the test rig containing some long narrow pipes which could not be accurately represented as pure capacitances. A more sophisticated model was obviously required. It was decided to use a software package that had been developed at Sheffield university that modelled pipe networks using transmission line modelling.

#### IV. Transmission Line Modelling of flow through VA test rig.

Transmission line modelling was originally developed to analyse transients in electrical networks<sup>(6)</sup>. It treats a network as transmission lines offering media through which waves travel. A flow network is a series of these transmission lines connected by flow junctions. Scattering of the waves may occur at junctions. The Sheffield University Network Analysis Software (SUNAS) models each pipe as a number of



transmissions lines. Each transmission line has its dynamic elements represented as a point resistance, capacitance or inductance. By having several transmission lines representing each pipe the model increases the distribution of the lumped dynamic elements. This improves the accuracy of the modelling. A detailed description of the formulation of the model has been published<sup>67</sup>.

The SUNAS programme requires the information about the network to be entered as a dataset. The geometry of the network is entered first by entering the number of nodes and pipes and the links between them. The length and diameter of each pipe can then be entered. Data has to be entered for each of the nodes. The boundary nodes can either be constant flow junctions or have a constant external pressure with a linear or quadratic resistance. Each internal node can be defined as either a linear, quadratic or time varying resistance.

The test rig was modelled as 6 pipes linking 7 nodes. A diagram of the network is shown in Figure 71 (all dimensions in metres).

Comparing Figure 69 and Figure 71 it is clear that the network modelling undertaken with the SUNAS software is considerably more sophisticated than the simple capacitance model. As such more accurate results are to be expected. However more complex data must be input to define the model.

The inlet throttle was modelled as a constant flowrate boundary. This was due to the fact that it was a large pressure drop (roughly 1.5 bar) across a small throat area. This meant that the flow did not vary significantly with the fluctuations in pressure downstream of the throttle.

The resistance of the VA to control flow was measured on the steady state test rig. This resistance was used in the model. The downstream boundary node for the network was the VA outlet. The pressure at the outlet was set to atmospheric.

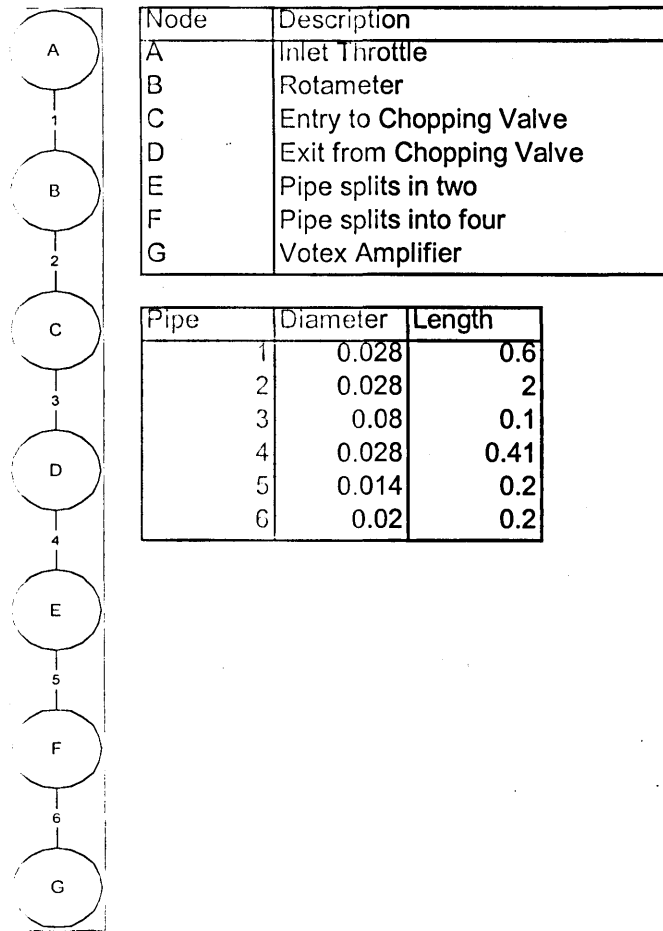


Figure 71 The pulsed flow test rig as modelled by the SUNAS programme

For simplicity, when the pipe split to enter the four separate control ports it was entered into the model as one pipe with the same flow cross sectional area as the four together. Nodes E and F were pipe splits that were assumed to have low resistances compared to the other resistances in the rig and were thus given nominal resistance values.

Estimating the rotameter resistance was not straightforward, because it varied with the flowrate through the rotameter. Pressure measurements across the rotameter, along with the volumetric flow measurements from the rotameter itself, indicated that it varied as:

$$\text{Rotameter resistance, } R = \frac{480.5}{\dot{m}^2} \text{ Pa.s/kg}$$

The average mass flow through the rotameter was fixed by the inlet boundary condition, so once this was determined the rotameter resistance could be deduced.

Unfortunately the flow through the inlet throttle was not truly constant as the pressure drop across it was insufficient to cause choking. This meant that the mass flow could not be directly estimated from the steady flow value. A considerable increase in pressure downstream of the inlet throttle occurred when the chopping valve was activated. Clearly this led to a significant decrease in the mass flow through the throttle from the steady flow value that could be measured with the rotameter. A more complex technique was required to estimate the mass flow for this boundary condition.

The pressure measurement downstream of the throttle was recorded on the test rig whilst the chopping valve was rotating. This rose during the phase of rotation when the chopping valve was closed. This pressure rise could be used to estimate the average mass flow into pipes 1 and 2 from Equation 24, assuming they behaved as capacitances. When this was done it was found that for a chopping valve rotational speed of 400rpm the pulsed and steady mass flow behaved according to the empirical relationship in Equation 25.

$$\dot{m}_{\text{pulsed}} = 1.79\dot{m}_{\text{steady}}^{1.17}$$

Equation 25

Once this equation had been derived all the required inputs to the SUNAS program had been found. When the model was run the correlation between simulated and experimental data was excellent. The results in Figure 72, which are for a steady flow rotameter setting of 4 (112.5li/min) and a rotational speed of 400 rpm, are typical. Not only does the programme model the primary pulses well it also follows the secondary pressure oscillations in the test rig.

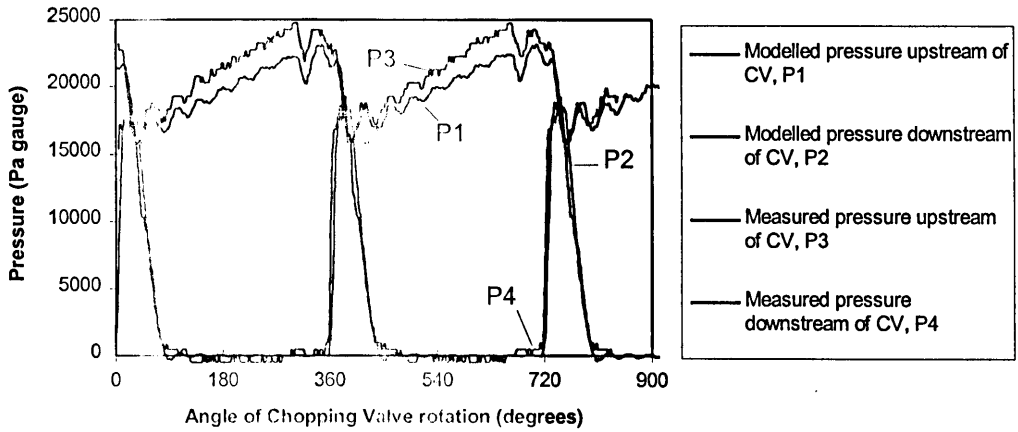


Figure 72 Comparison of measured pressures in test rig and results from TLM model

These results are an accurate representation of the pressure variation in the VA test rig. Therefore the transmission line model can be expected to accurately predict the mass flow of air through the VA for a variety of upstream pressures and chopping valve rotational speeds. This was done and some of the results are shown in Figure 73. The throttle position ‘a’ gives a steady flow of 80 li/min, and throttle position ‘b’, 112.5 li/min.

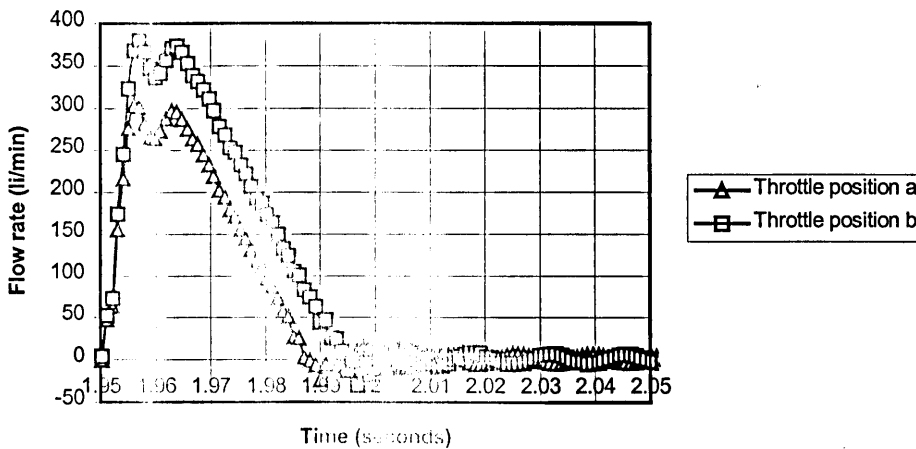


Figure 73 Air flow rates through the VA with chopping valve speed of 400 rpm (TDC=1.95s)

It can be seen that the peak air flow through the VA lasts for roughly 10ms and declines slowly. Clearly the vortex spin up time is small compared to the valve opening period. It therefore seems that at this rotational speed the effects of unsteady flow on

the flow pattern within the VA should be small. This means that the excellent steady flow atomisation should be repeated with unsteady flow.

## V. Experimental drop size measurements with pulsed airflow through the VA

To measure droplet sizes the fuel injector was triggered using the top dead centre pulse from the chopping valve. This meant that the timing of the injection pulse could be varied relative to the chopping valve opening time. The accuracy of the relative timing was estimated to be around  $\pm 3$ ms. This was mainly due to a tendency of the chopping valve speed to drift from the measured value, which was used to set the delay between TDC and the injection pulse. There was also some uncertainty in the response time of the relay driving the fuel injector.

Spray measurement results for a chopping valve speed of 400rpm are shown in Figure 74 for two throttle valve settings. The low flow setting gave a steady flow of 80 li/min, the high flow setting a steady flow of 144 li/min. The spray measurements were recorded with the injector positioned on the VA chamber axis, and with it offset by 5mm.

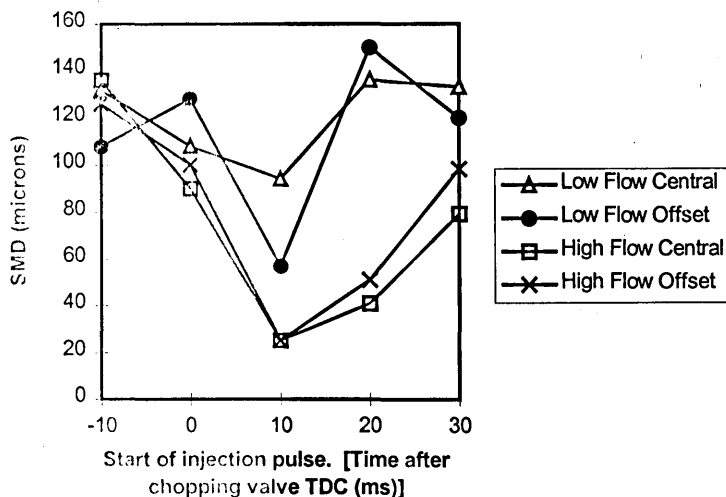


Figure 74 Measured spray SMDs in pulsed airflow

As the chopping valve opens  $4^\circ$  before TDC (about 1.7ms at 400rpm) the spray injected before top dead centre, which are similar for all four lines, should be in quiescent air. However the drop sizes are smaller than those observed for injection into

quiescent air in steady flow (210 $\mu$ m). This implies that there must be sufficient movement in the air to disrupt the largest droplets even with the chopping valve closed. This is presumably due to undamped flow oscillations.

As the injection point is moved forward with respect to TDC, the droplet sizes decrease to a minimum and then increase back toward the initial value. As would be expected smaller droplet sizes are obtained with the higher air flow rate. Figure 73 shows that the peak airflow through the VA is expected to occur between 10 and 20ms after TDC. This explains why the injection pulse that started 10ms after TDC produced the smallest droplet size. The flowrate then decreases steadily explaining the increasing droplet size.

The positioning of the injector, either upon or offset from the VA chamber axis, seemed to have only a small effect upon the droplet sizes. The general trend seemed to be for the offset injector to produce slightly larger droplets, presumably due to the sprays proximity to the walls causing more of the smaller droplets to be deposited. However at the low flow rate the offset injector produced a smaller minimum droplet size. This occurs for the injection starting 10ms after TDC, when the air flow through the VA was about 290li/min. In the steady flow tests, the centrally placed injector was found to produce a wide scatter of spray SMDs at a range of airflows between roughly 250 and 300 li/min. It was suggested that in the sprays with the larger SMDs the spray had not fully interacted with the most turbulent region of the air flow, which is off the chamber axis. This is probably the explanation for the smaller droplet size achieved by the offset injector here.

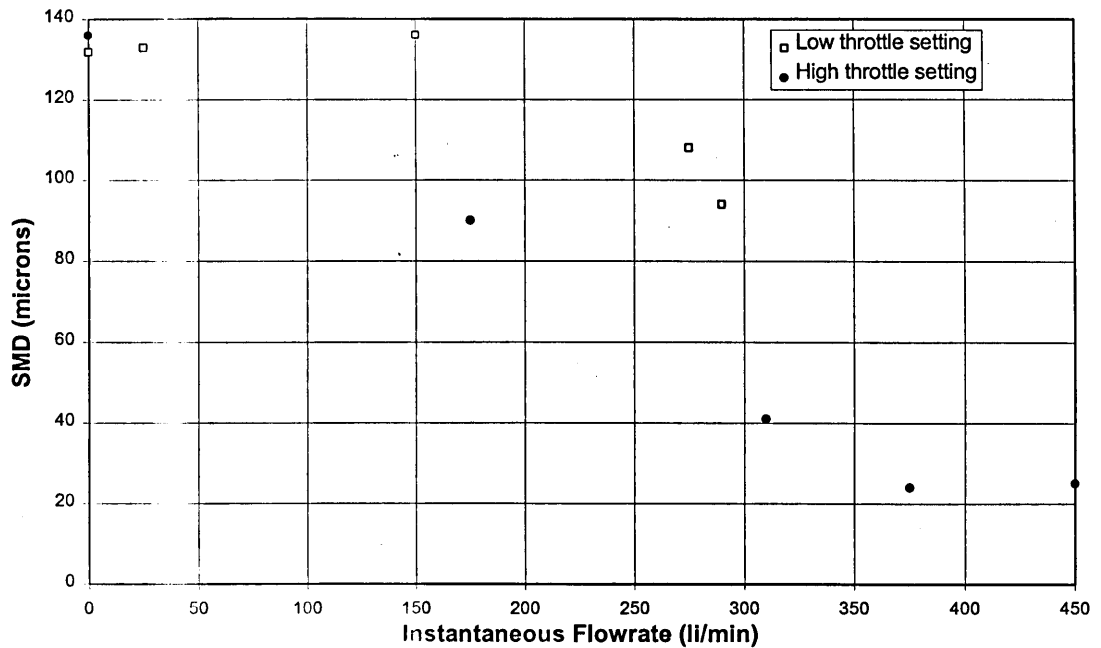


Figure 75 Measured spray SMDs vs. Predicted flowrate in pulsed flow

Figure 75 shows the measured droplet size compared with the instantaneous flowrate through the VA during injection. The air flow was calculated from the SUNAS predictions. It can be seen that the results are generally similar to the steady flow observations in Chapter 8. Again at moderate flow rates between 150 and 300 li/min a large degree of scatter is seen in the measurements.

Very small droplet sizes are again achieved at flowrates of 300 li/min or greater. This offers confirmation that the short spin up time of the vortex allows the excellent atomisation observed with steady flow to be repeated.

It was hoped that the pulsed flow through the VA might offer some advantage to prevent droplet deposition. Tests were conducted with the tube outlet and the long diffuser attached to the VA outlet. As with steady flow it seemed that the effect of droplets being flung against the walls of the outlets outweighed the particle sizing potential of the VA. Varying the injection timing so that it was prior to or after the peak air flow through the VA was not successful in preventing droplets being flung against outlet walls. No small droplets were measured passing through the tube outlet for average air flow rates during injection of greater than about 200 li/min.

## **VI. Conclusions**

VA 'spin up' time is short enough so it does not impede very good atomisation with pulsed flow. The quality of atomisation observed in the pulsed flow tests was as good as that achieved with steady flow through the VA. It also correlated with the average air flow through the VA during injection (calculated by SUNAS) in much the same way as for steady flow. However pulsed flow effects cannot be exploited to prevent droplet deposition. The problem of droplets being flung against the walls of any outlet attached to the VA exit was just as severe as with steady flow.



## **CHAPTER 10**

### **Overall Discussion**

*This chapter summarises the work described in this thesis and considers the implications of using the VA in an engine application.*

## I. Project Overview

The thrust of the project was to use a vortex amplifier to lower the emissions of Spark Ignition engines through the route of improved mixture preparation. The vortex amplifier was chosen as a mixture preparing device as it is able to produce a compact yet highly turbulent flow field. Additionally the VA has already been shown to have some ability to reduce pumping work when used as a port throttle<sup>4</sup>. If it were so employed it would be in the ideal position to provide mixture preparation for fuel metered and supplied by a multi point injection system. Combining mixture preparation and pumping work benefits from a VA would provide an attractive route to improved economy and reduced emissions.

Attempting to assess improvements in mixture preparation clearly necessitates analysing the flow of a multi-phase mixture. The flow in the outlet of a VA is highly complex and three dimensional, and is not readily amenable to numerical analysis. Due to this the work done in assessing the VA performance as a mixture preparation device has been largely experimental. Some theoretical treatment of the flow has been undertaken to clarify the experimental observations, but this has leaned heavily upon hot wire measurements of the VA flow field by King<sup>17</sup>. Most of the results presented in the project were based upon direct measurement of droplets produced in the VA by a Malvern particle sizer.

This chapter considers these results in the light of the intended use of the VA within an SI engine. The prospects for the successful implementation of a combined port throttling and spray atomising VA are assessed.

## II. Choosing a VA geometry

The initial experimental work in the project set out to establish the capacity for the vortex flow to produce finely atomised sprays. It was also designed to evaluate the effect of the VA geometry upon the droplet size produced. The results, presented in **Chapter 4**, showed that the VA could disrupt a fuel jet at levels of control flow that would be experienced in engine operation. The effectiveness of the atomisation was destroyed by the deposition of spray on the walls downstream of the injector. Thus any effect that internal VA geometry had on the spray was insignificant compared to

designing the outlet geometry to minimise the deposition. If this could be achieved then the atomisation could be exploited whilst selecting the VA geometry to give optimum control of the air flow.

In his thesis, Abdul-Wahab observed that the requirements which the VA must satisfy are:

- a) *To have as little vacuum as possible in the supply plenum (intake) during induction, so that the piston may confront less vacuum at IVO.*
- b) *At idle, the required mass of air trapped in the cylinder at IVC is that just needed for combustion to overcome total engine frictional losses. Therefore, the VA should provide the equivalent vacuum to control the charge density at IVC.*
- c) *At higher speeds, when the engine draws its maximum flow through the VA, the VA throat area must be large enough to avoid choking the flow.*

To achieve these aims is complex, as they impose different constraints on the VA flow characteristic. A design giving low control pressure ratio between the vortex state and normal state would satisfy requirement (a). However a VA sized to give the required flow at idle conditions would choke at high engine powers, and so could probably only be sized to meet one of requirements (b) and (c). This is because the control ports in a low CPR design are large and so a small sized VA would be needed to achieve the required cylinder vacuum at idle. Similarly, a high turn down ratio design should satisfy (b) and (c) but would give a considerably higher vacuum in the supply plenum. Abdul Wahab did not adequately resolve this dilemma for a 4 cylinder engine. However his work on a single cylinder engine was sufficiently promising to believe that further investigation could provide a satisfactory solution. A reasonable starting point would be a compromise geometry which maximises the 'performance index', which is

defined as the ratio of TDR/CPR. Such a geometry was used in the second phase of testing in this project, as described in Chapter 5.

There are reasonable grounds for optimism that further investigation would produce a VA based port throttling system applicable to a 4 cylinder engine. If this were so it could also take advantage of the atomisation benefits available. The independence of the atomisation effectiveness from VA geometry means that the only constraint that would be placed on the geometry of the VA so that it could combine atomisation with throttling would be that it had a low chamber height. This would prevent spray being deposited within the body of the VA. All high performance VAs have a low aspect ratio, so any VA port throttling system should meet this requirement.

It is worth noting that there is a peculiarity in the steady state performance reported by Abdul Wahab for the initial VA he designed. The geometry and performance indices of this device are summarised in Figure 76. It displayed superior steady state performance to the VAs tested in this project, and those observed in the literature by King<sup>15</sup> when compiling Figure 7, page 27. There is a significant improvement in turn down ratio over the 'optimised' design, at a lower CPR. This leads to a considerably higher performance index. However it is not believed that this performance would be repeatable. As reported by Kitsios<sup>24</sup>, and observed in Chapter 5, instability due to interaction between a VA and a test rig can significantly affect the steady state performance. As no effort was made to stabilise his test rig it is likely that the high performance observed by Abdul Wahab arose from such an instability.

|                                       | VA used by Abdul-Wahab | Optimum geometry for high performance index |
|---------------------------------------|------------------------|---|
| Chamber height/Throat radius          | 0.58                   | 0.38  |
| Chamber radius/Exit radius            | 6.4                    | 2.5   |
| Control jet area/Exit area            | 0.29                   | 0.29  |
| Reported Control Pressure Ratio (CPR) | 1.2                    | 1.3   |
| Reported Turn Down Ratio (TDR)        | 21                     | 16  |
| Performance Index (TDR/CPR)           | 17.5                   | 12.5  |

Figure 76. Comparison of VA performance.

### III. Droplet formation in steady air flows

As already mentioned in section II, and detailed in **Chapter 4** and **Chapter 8**, the VA was capable of producing very fine sprays in steady airflow. The limit to its ability to shatter droplets was determined by the level of airflow. The required flow to achieve an SMD below 50 $\mu$ m (the best available using current air shrouded atomisers) was a control flow of 320 li/min. This improved to an SMD of 25 $\mu$ m at 400 li/min (**Figure 56**, Chapter 8). The numerical modelling in **Chapter 7** showed that this excellent atomisation is due to the intense local turbulence in the exit throat of the VA.

These flowrates can easily be compared with those experienced in engine operation. During induction the peak mass flowrate of air into the cylinder of an SI engine,  $Q_{MAX}$ , is:

$$Q_{max} = A_p (V_p)_{max}$$

$A_p$  and  $V_p$  are the area and velocity of the piston respectively. The lowest air flowrates into a cylinder are experienced at idle. Typical engine speed at idle in an SI engine is 800rpm. Thus for a 400 cm<sup>3</sup> cylinder revolving at 800 rpm, the peak flow rate during induction would be approximately 1000 li/min.

It is also possible to estimate the mass flowrate into the cylinder during valve opening that would give the required idle vacuum, which is about 0.7 bar below atmospheric pressure. For a 400 cm<sup>3</sup>, 4 stroke, cylinder this is roughly 0.003 kg/s. As the density of air at 0.7 bar vacuum is 0.2kg/m<sup>3</sup>, this equates to a volumetric flowrate of

640li/min. Therefore flow through a VA used as a port throttle would be sufficient to atomise the spray effectively.

This simple analysis fails to take into account the effect of air density upon the atomisation. In Chapter 7, Equation 14 shows that:

$$d_{\max} \propto \left(\frac{1}{\rho}\right)^{1/5}$$

This implies that droplet sizes in the flow might be up to 25% bigger than that predicted from the tests in this project, which were carried out with the VA outlet discharging to atmospheric pressure. However even if this was the case, the droplet sizes produced would still be considerably smaller than those from current pintle injectors.

#### IV. Effect of pulsed airflow

It was felt that any consideration of applying a VA as a mixture preparation device would be incomplete without a study of how the pulsed airflow in a SI engine would affect the atomisation. To this end, a test rig was set up with a rotating valve, to pulse the air flow through the VA. Ideally tests would have been carried out upon a motored engine, so the results could be applied to SI engines with very high confidence. This would have enabled study of the VA atomisation throughout the range of flows encountered in engines and enabled the effect of variables such as cylinder vacuum to be studied. However the constraints of time limited the tests to the more basic study described in Chapter 9.

Although these were preliminary tests of VA behaviour, they allowed it to be established that the time constant associated with VA spin up is sufficiently small to allow spray atomisation to be achieved with pulsed flow similar in nature to that encountered in engines. The spray SMDs achieved with pulsed airflow were just as encouraging as those achieved with steady flow. The spray size achieved correlated with the mean air flow (as predicted from a transmission line model) during the injection pulse in a very similar way to the steady air flow rate in the earlier tests. This is an important result, which strengthens the case for further study of a VA atomisation system.

## V. Modelled behaviour

Models of VA behaviour based upon extensive flow field measurements [17] were described in Chapter 6 and Chapter 7. These provided insight into the processes occurring within the VA.

Chapter 7 clearly related the excellent atomisation observed in experiments to the high level of turbulence in the VA outlet. Chapter 6 analysed the motion of a droplet within the VA flow field. It highlighted the main obstacle to achieving improved mixture preparation in an engine. This was the tendency of the VA to centrifuge droplets out of the airflow and against the walls of the outlet. Guided by this work the VA tested in Chapter 8 (steady flow) and Chapter 9 (pulsed flow) was constructed with a low chamber height and no parallel section at the outlet throat. Short diffusers were fitted to it for testing and spray measurement. In spite of this no practical geometry yet tested has been able to prevent this centrifuging effect. Suggestions for other strategies that may hopefully eliminate this are contained in Chapter 11.

## VI. Reliability and Applicability of Results

The work discussed in this chapter has concentrated on conditions where only control flow is passing through the VA. In an SI engine application this would correspond to operating points around idle. This is the area to which most effort has been directed because at these operating points there is little air flow to provide atomisation. The highest control flow at which atomisation was measured on the test rig was 400 li/min, and the typical SMD at this flow rate was 25  $\mu\text{m}$ . The flow rates encountered at idle in a typical automobile SI engine would be above this (III).

Clearly the results for steady flow indicate that even at the lowest flow rates into a cylinder the VA will produce excellent atomisation. This finding can be combined with the pulsed flow results, which show that the VA has a very small spin up time. This allows steady flow results to be read across to the unsteady conditions encountered in real engines. Thus there is a high degree of confidence that the VA would produce very fine sprays in an SI engine at idle conditions.

Very little effort in the current project was directed towards studying droplet formation in the VA with combinations of supply and control flow. This decision was

made for a number of reasons. The proportions of supply and control flow passing through the VA would depend upon the strategy adopted for using the VA as a port throttle. Additionally it was felt that engine idle would be the most severe design constraint, due to the small amount of flow available for atomisation.

Some extrapolation of the engine results is possible to operating conditions above idle based on **Figure 59**, page 124 and **Figure 60**, page 125.

**Figure 60** shows the SMD of the spray produced by the VA for mixtures of supply and control flow, at a volumetric flow rate of 400 li/min. It can be seen that the SMD remains beneath 50 $\mu$ m until the supply flow increases above 50% of the mix. In an engine, flow rates will be considerably above 400li/min for operating points above idle.

**Figure 59** shows a comparison of droplet atomisation with pure supply flow and pure control flow through the VA. It can be seen that the supply flow gives significantly worse atomisation. At a flow rate of 400li/min the pure supply flow produces a droplet size of around 100 $\mu$ m. Some reduction in SMD can be expected at the significantly higher flow rates experienced at wide open throttle. However, there is no evidence that the VA would perform significantly better than current technology at high power.

These considerations mean that the excellent atomising performance of the VA at engine idle will probably extend throughout low and mid power operation. At high power no significant benefit will be experienced. However the operation of a normal automobile engine is predominantly at low to mid power where the benefits are obtained.

## **VII. Application of work to Spark Ignition engines**

The results of this project are encouraging with respect to the aim of improving mixture preparation in an SI engine with a VA. However considerable further work needs to be done to bring the project to fruition.

In particular, work needs to be done designing a practical system combining the throttling and atomisation benefits of the VA. This will involve overcoming the significant problems caused by the tendency of the VA to deposit droplets on the walls of any downstream pipework.





# CHAPTER 11

## Conclusions

## I. Summary of conclusions by chapter

The purpose of this section is to provide a brief summary of the major conclusions that have been made in this thesis.

### I.i Chapter 1

This chapter reviews the emissions problems of the Spark Ignition engine and identifies the potential to reduce emissions by improving mixture preparation. The main conclusions of the chapter are:

- Environmental concerns are leading to increasing stringent legislative controls on vehicular emissions throughout the world.
- Emissions are most severe in an engine operating after cold start due to the mixture enrichment required to ensure combustion in the engine cylinder. This problem is compounded by the fact that emissions catalysts have not achieved their light off temperature in this range of operation.
- Improvement of mixture preparation will enhance the effectiveness of any strategy adopted to reduce emissions. This is because the improvement allows a leaner mixture to burn in the cylinder improving engine economy.
- Improved mixture preparation is especially significant in the cold start regime as it reduces the amount of enrichment required to ensure combustion.
- Current injector technology is cheap and easily incorporated within an engine management system, but cannot produce sprays with SMDs below 50  $\mu\text{m}$ .
- The target droplet size for a spray to prevent fuel deposition within the intake port is roughly 10  $\mu\text{m}$ .
- Many devices have been shown to produce extremely good mixture preparation by utilising highly turbulent airflow. However none has yet found application within an SI engine.
- A vortex inducing manifold has been used to enhance mixture preparation and shown a measurable reduction in BSFC.

### I.ii Chapter 2

This chapter reviews the literature on vortex amplifiers. The main conclusions from the chapter are:

- The VA contains a compact region of highly turbulent flow at the outlet throat. This would be ideal for atomising a spray.
- A previous study has shown that a VA can be used as a port throttling device within an SI engine to reduce part load pumping work.

### **I.iii Chapter 3**

This chapter describes techniques used for spray measurement. The main conclusions are:

- The Malvern particle sizer offers a rapid and flexible method for the measurement of droplet sizes in sprays. It has been successfully applied by previous researchers.
- n-Heptane will be used to form the spray rather than gasoline to reduce evaporation of the spray.
- Refraction of the laser beam used by the Malvern particle sizer can lead to erroneous results. This effect is known as beam steering. Photographs of the spray must be taken to validate the Malvern particle sizer measurements.

### **I.iv Chapter 4**

This chapter deals with the design and testing of a variable geometry vortex amplifier. The main conclusions are:

- Photographs within the body of the VA indicate that in the control flow state the VA shatters the fuel jet effectively.
- Small droplets are flung out of the airflow and deposited on the walls of the VA chamber and outlet diffuser. This means the spray produced by the VA has a higher SMD than that produced by the fuel injector.
- The effect of VA internal geometry on spray formation is insignificant in comparison with designing the outlet geometry to minimise spray deposition.

### **I.v Chapter 5**

This chapter describes the design and steady flow testing of a new VA. The main conclusions are:

- The design algorithm developed by King provides an effective basis for designing a VA.

- VA instability can significantly affect the results obtained from steady flow tests.
- An appropriate choice of non-dimensional length to allow the scaling of results between VAs of differing geometry is  $\sqrt[3]{d_e^2 A_T}$

### I.vi Chapter 6

This chapter presents a model of droplet motion through the VA based upon hot wire velocity measurements of the airflow. The main conclusions are:

- The high tangential velocity in the outlet flow from the VA means that small droplets will tend to be centrifuged out of the airflow.
- The chamber height of the VA should be kept small, and any exit diffuser should be as short as possible.
- Some improvement in spray penetration may be obtained by injecting the spray at a position offset from the VA chamber axis.

### I.vii Chapter 7

This chapter describes a model of droplet breakup within the VA. The main conclusions are:

- The available hot wire measurements of fluctuating velocity within a VA can be applied in a model of droplet breakup in turbulent flow.
- The model predicts maximum droplet sizes of below 50  $\mu\text{m}$  can be achieved by the airflow in the VA.
- The model predicts that the most turbulent regions in the outlet (and hence the regions with the greatest atomising effect) lie off the central axis of the VA.

### I.viii Chapter 8

This chapter presents the results from the measurement of droplet sizes with steady air flow through the VA designed in chapter 5. The main conclusions are

- The VA is an extremely effective atomiser in the vortex state. At 400 li/min sprays with an SMD of 25  $\mu\text{m}$  are produced.
- There is a significant level of scatter in the results of SMD measurement for intermediate levels of control flow in the vortex state. This scatter disappears if an offset injector is used. This observation is believed to be due to the non repeatability of

spray flow path through the VA. At intermediate control flow rates it is possible that the spray will not be dispersed to the most turbulent regions of the airflow. This problem does not occur with an offset injector as it discharges spray into these turbulent regions as was shown in Chapter 7

- The low chamber height and omission of a parallel section in the outlet throat in the design of the VA prevents droplet deposition occurring within the body of the VA.

- Droplet deposition downstream of the VA remains a significant problem. The attachment of any downstream diffuser or pipe to the VA outlet causes an increase in the SMD observed at the measurement zone caused by the deposition of the smaller droplets in the spray. Longer lengths of pipe lead to complete deposition of the spray.

- Advancing the injector position into the VA body does not significantly reduce droplet deposition

- There is evidence for some beam steering effecting the Malvern particle sizer measurements. It is estimated that this could mean the results overestimate the actual spray SMD by up to 10%.

- Airflow provided by a mixture of supply and control flow still provides effective atomisation providing supply flow does not account for more than about 40 % of the total flow.

- Airflows made up of supply flow only were more effective at atomising the spray than flows containing a small proportion of control flow. This is because the swirl imparted by the control flow disperses the spray away from the region of peak velocity in the centre of the VA.

## **I.ix Chapter 9**

This chapter presents the results of tests and modelling with pulsed airflow through the VA. The main conclusions are:

- The SUNAS network analysis software allows excellent modelling of the flow through the pulsed flow test rig. This modelling was used to estimate the airflow rate.

- The droplet sizes measured with pulsed airflow correlated well with the steady flow results, based upon the instantaneous flow rate estimate by the SUNAS model.

- The VA spin up time was very short and did not affect droplet formation.

- The pulsed flow could not be utilised to reduce droplet deposition

## I.x Chapter 10

Chapter 10 considers the work in this thesis in the light of an SI engine application. The main conclusions were:

- The independence of atomisation from VA internal geometry allows the atomisation benefits to be combined with the pumping work reduction obtained from using the VA as a port throttle.
- Significant reduction in droplet deposition must be achieved if the VA is to provide an effective method of improving mixture preparation in SI engines.
- If droplet deposition can be avoided then the VA will provide excellent mixture preparation throughout low to mid power engine operation. This should substantially reduce emissions after a cold start.

## II. Overview

Progress has been made in evaluating the atomisation potential of the VA. The most significant findings of the project are:

- Extremely good atomisation has been demonstrated.
- The Malvern particle sizer is an effective and accurate method of obtaining large quantities of spray measurement data.
- The numerical models of VA behaviour in chapter 6 and 7 agree well with the experimental results and provide valuable insight into the processes occurring in the VA.
- The SUNAS network model of the pulsed flow test rig shows excellent agreement with the experimental measurements.
- Good atomisation can be achieved with pulsed flow.

The problem of droplet deposition prevents the VA from being an extremely effective route to enhancing SI engine emissions performance. Chapter 12 presents suggestions for work that might overcome this problem.

## **CHAPTER 12**

### **Recommendations for future work**



## I. Introduction

This project has demonstrated the effectiveness of the VA in producing very well atomised sprays. However the spray is rapidly deposited on the walls downstream of the injection point in any geometry that could be adopted practically in an SI engine. Most of the work suggested in this section is directed towards reducing the amount of spray flung against the walls of the diffuser and pipework downstream of the VA. This problem must be resolved if the VA is prove an effective mixture preparation device.

## II. Changing the VA diffuser geometry

All the VAs tested in the current project have either had no diffuser fitted, or have been fitted with an axial diffuser. In an engine application a diffuser would be necessary, however the spray produced by the VA tended to be completely deposited within any diffuser of practical length.

One way to address this problem would be to replace the axial diffuser with a radial one. Figure 77 shows a simple schematic of a VA fitted with a Radial diffuser. The high tangential velocities in the VA are responsible for flinging the droplets against the walls. However in the radial diffuser this problem should not arise as the flow in the diffuser is in the same direction as the tangential velocity. The axial velocity of the flow in the VA outlet might still cause droplet deposition against the walls of a radial diffuser, but as the magnitude of axial velocity is much lower than that of tangential velocity (typically the velocity ratio might be 4 to 1) in the control flow only state the problem should be significantly improved. Obviously some droplet deposition by turbulence would still occur, but the deposition of the entire spray that was observed in the axial diffuser seems less likely.

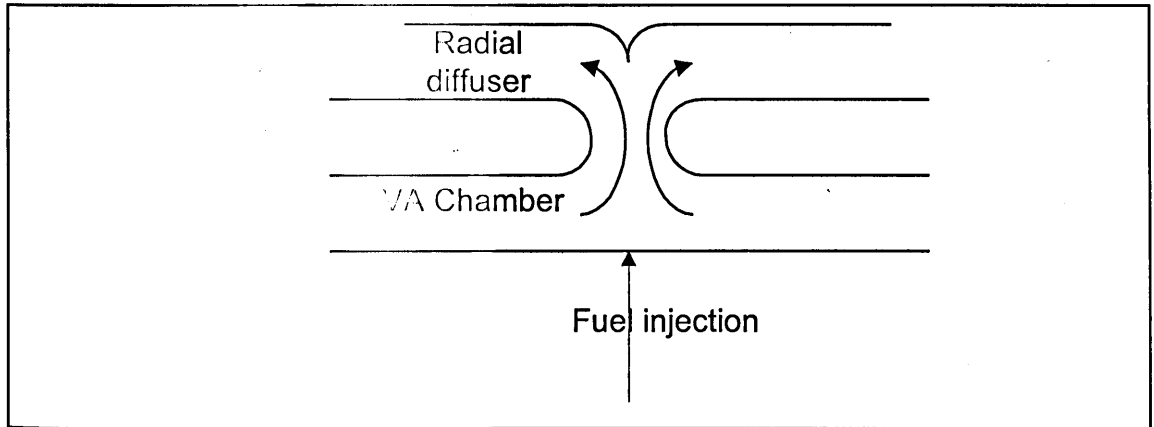


Figure 77 Schematic of a VA fitted with a Radial diffuser

Although there are considerable grounds for optimism that a radial diffuser would reduce the spray deposited on the walls there are drawbacks to the use of a radial diffuser.

Disadvantages:

- Large volume of radial diffuser introduces time lag between injector and cylinder
- Not easy to connect outlet from radial diffuser to cylinder
- Research has shown that radial diffuser increases supply flow resistance of the VA compared to axial diffuser so reducing engine performance at wide open throttle.

Clearly a considerable amount of investigation would be required to evaluate the effect of a radial diffuser both on atomisation and engine performance. This investigation would probably have to be mainly experimental with initial work directed towards establishing the range of droplet sizes carried through the diffuser without impacting.

### III. CFD analysis of two phase flow through the VA

A CFD solution for the flow of air and fuel inside an Vortex Amplifier would be very desirable. It would allow a clearer insight into the processes occurring within the VA, and could test how changes in geometry might effect those processes and thus the mixture preparation. It could allow rapid evaluation of the effect of modifications such as a radial diffuser or close coupling to an engine cylinder.

The reason that a CFD solution for the flow in the VA was not pursued within the current project was due to the extreme complexity of the task in the time available. The flow in the outlet of a vortex amplifier is notoriously hard to model. Even a single

phase model dealing with just the air flow would require around 60000 nodes and take many months to develop.

In addition to this it is desirable to know how the air and fuel interact. An accurate model for the breakup of a single droplet in turbulent flow, does not currently exist as was illustrated by the literature review in **Chapter 7**. Interfaces between CFD and spray models are complex. Some adaptation of the models in this thesis for droplet motion and breakup might possibly be successfully linked with a CFD model describing the air flow in the VA.

In light of these considerations it is clear that generating a realistic CFD model of fuel injection into a vortex amplifier would involve a major programme of work, and would have to be supported by experimental testing to provide validation of the numerical predictions. However the predictions from the model might allow rapid progress in finding a solution to the problem of spray deposition.

#### **IV. Engine Testing of VA**

It is possible that conducting engine tests using a VA as a mixture preparation device might reveal emissions and economy benefits. Although the high amount of spray deposition caused by the VA means that the injected fuel would not enter the engine cylinder as a homogenous mixture, advantages might be conferred from the high degree of spray atomisation. This is because spray evaporation rates would be very high prior to deposition. Also the size of the deposited droplets is so small that any fuel film formed should be very thin, and thus evaporated quickly. It is believed that these factors would contribute to improving the preparation of the mixture entering the cylinder, when compared with a conventional fuel injector.

An additional advantage is that this approach could be coupled with research to improve the utility of a VA as a port throttle. This combined approach might yield appreciable benefits in engine performance.

An additional option to promote evaporation of deposited droplets would be to introduce heating of the cylinder port downstream of the VA. As the VA deposits all the drops within a short length of the outlet only a small portion of the wall would have to be heated to evaporate the fuel film on the walls. This would reduce the heating of

the air drawn into the cylinder and thus reduce the impact on volumetric efficiency associated with systems that heat the entire port to promote full evaporation.

It seems clear that with port heating a VA atomising device might demonstrate a measurable advantage over a conventional fuel injector, particularly in combination with a VA port throttling system. However the maximum benefit cannot be obtained from the fine spray produced in a VA if the spray is allowed to impact with the walls. To make the VA atomising concept sufficiently attractive for adoption in SI engines a strategy to minimise droplet deposition should be adopted.

## **V. Close coupling of VA and engine cylinder.**

If the VA could be mounted directly onto the inlet valve of the engine cylinder, without any intervening diffuser or pipework, then the mixture preparation benefits of the using the VA could be tested. This testing could examine the change in the engines brake specific fuel consumption and emissions when the air was drawn into the cylinder via the control and supply ports. The fine atomisation achieved by injecting the spray into control flow should show up in significant efficiency and emissions benefits.

Although this testing would be valuable to quantify the benefit to engine performance potentially available from improved mixture preparation, it would be difficult to build a production engine to this design. This is because the cylinder head geometry would have to contain the VA, the fuel injector and the poppet valve. An additional disadvantage is that the installation of the VA, close coupled to the cylinder would probably result in some loss of ram tuning. This might be offset by using VA instability to supercharge the engine, but this is as yet an untested concept that requires validation.

## **VI. Conclusion**

Whilst this project has demonstrated the VAs considerable atomising potential the application to improved mixture preparation in an SI engine still presents several difficulties. A program of research, based on some or all of the recommendations in this chapter, is required to identify the best strategy for incorporating a VA in an SI engine.

## REFERENCES

---

- 1 Nieuwenhuis, P., Cope, P. and Armstrong, J. (1992) *The Green Car Guide*. London: Greenprint.
- 2 Hadded, O., Stokes, J. and Grigg, D.W. (1993) Low emission vehicle technology for ultra low emissions vehicle and European stage 3 emissions standards. *Proc Instn Mech Engrs.* **209** 159-170
- 3 Ashley, C. (1996) Future strategies for reducing emissions. *Automotive Engineer.* **21** No 1, 18-20
- 4 Abdul-Wahab, E.A., (1993) *Development of a vortex amplifier manifold system*. PhD Thesis. University of Sheffield.
- 5 Bland, R.J. and Saunders, R.J. (1991) *Modelling of two phase mixture flow and vaporisation in spark ignition engine intake systems*. IMechE paper C433/005
- 6 Heywood, J.B., (1988) *Internal combustion engine fundamentals*. McGraw Hill
- 7 Lenz, H.P., Fraidl, G.K. and Freidl, H., (1985) *Fuel atomisation with mixture preparation systems of SI engines*. SAE paper 885015
- 8 Kashiwaya, M. and Kosuge, T. (1990) *The effect of atomisation of fuel injectors on engine performance*. SAE900261
- 9 Nightingale, C., Tsatsami, V., (1984) Improved mixture preparation for better cold starting. *Automotive Engineer* **9** No 5 97-100
- 10 Acton and Allen. (1985) *The further modification of a vortex inducing manifold*. Sheffield University Undergraduate Project.
- 11 Chow, S.K., (1968) An Experimental Study of the Characteristics of Vortex Valves. *Proceedings of the IFAC Symposium on Fluidics*.
- 12 Syred, N. and Royle, J.K., (1972) Operating Characteristics of High Performance Vortex Amplifiers. *Fluidics Quarterly* **4**
- 13 Gebben, V.D., (1967) Vortex Valve Performance Power Index. *ASME Advances in Fluidics*.
- 14 Brombach, H., (1975) Vortex Amplifiers for Low Control Pressure Ratios. *7th Cranfield Fluidics Conference, BHRA, Bedford*.
- 15 King, C.F., (1987) The Design of Radial Vortex Amplifiers for High Performance Power Fluidics. *Journal of Dynamic Systems, Measurement and Control.* **109** 44-48
- 16 Asquith, R.W., (1973) *Performance and Characteristics of Vortex flow controllers*. PhD Thesis. University of Sheffield.
- 17 King, C.F., (1979) *Some studies of Vortex Devices*. PhD Thesis. University College, Cardiff.
- 18 Haider, H.H., (1989) *Internal static and dynamic phenomena in vortex amplifiers*. PhD Thesis. University of Sheffield.
- 19 Boucher, R.F.; Kitsios, E.E., (1984) Eulerian Transformation of Vortex Amplifier Static Characteristics. *Journal of Dynamic Systems, Measurement and Control.* **106**
- 20 Wormley, D.N. and Richardson, H.H., (1970) A Design Basis for Vortex-type Amplifiers Operating in the Incompressible Flow Regime. *Journal of Basic Engineering.* **92**
- 21 Wormley, D.N. and Richardson, H.H., (1968) *Experimental Investigation and Design Basis for Vortex Amplifiers in the Incompressible Flow Regime*. Tech Report No. DSR 70167-1, Dept. of Mechanical Engineering, Massachusetts Institute of Technology.
- 22 Tippetts, J.R., (1969) *The characterisation and uses of unvented bistable fluid amplifiers* PhD Thesis. University of Sheffield.
- 23 Wormley, D N, (1970) *A review of vortex diode and triode static and dynamic design techniques*. AGARD-NATO, Neuilly-Sur-Seine.
- 24 Kitsios, E.E., (1984) *VA Dynamics and Circuit Instabilities*. PhD Thesis. University of Sheffield.

- 
- 25 Mo, R.S., (1988) *The Dynamic Modelling and Testing of a VA of Low Aspect Ratio*. PhD Thesis. University of Sheffield.
  - 26 Anderson, W.W., (1972) *A Dynamic Model of Vortex-Type Fluid Amplifiers*. DSc thesis, Dept. of Mech. Eng., MIT.
  - 27 Grant, J., and Strong, R.E., (1973) *The Application of Power Fluidics*. Proc. Symposium of Power Fluidics for Process Control, Ins. Measurement and Control, London. April 1973.
  - 28 Balakrishnan, M.G., Mahule, K.N. and Surya Narayan. (1992) Design and development of a vortex amplifier for pressure regulation of glove boxes. *J. Vacuum Science and Technology A*. 10 No 6. 3568-3572
  - 29 King, C.F. and Syred, N. (1981) Vortex Amplifiers for Pipeline Protection. *Journal of Dynamic Systems, Measurement and Control*. 103 358-360
  - 30 Sato, K. and Syred, N. (1991) Performance Effects of a Round Bar Passing Through the Outlet of a Vortex Amplifier. *Journal of Dynamic Systems, Measurement and Control*. 113 696-701
  - 31 Kong, H. (1989) *Tuning of Intake Manifold of an Internal Combustion Engine Using Vortex Flow*. PhD Thesis. The University of Texas at Arlington.
  - 32 Bowen, I.G. and Davies, G.P., (1951) Shell Technical Note ICT 28
  - 33 Dombrowski, N. and Tyler, L.R., (1962) Brit Patent Appl. No. 31364/62 *J. Phot. Science*, 15, 40,
  - 34 Yule, A.J., Cox, N.W. and Chigier, N.A., (1978) Measurement of particle size in sprays by the automated analysis of spark photographs. Particle size analysis. Ed. Groves, Pub. Heyden, London. pp 61-73
  - 35 Jones, A.R., (1977) A review of drop size measurement - the application of techniques to dense fuel sprays. *Prog Energy Combust. Sci.*, 3 pp 225-234
  - 36 Tishkoff, J.M. (1982) Measurement of particle size and velocity in a fuel spray. Proc. ICLASS-82, pp 245-252
  - 37 McCreath, C.G., Roett, M.F. and Chigier, N.A. (1972) Technique for the measurement of the sizes and velocities of particles in flames. *J. Phys. E* 5 p 601
  - 38 Araki, K. and Moriyama, A. (1982) Simultaneous determination of size and velocity of individual droplets in water sprays. Proc. ICLASS-82 pp 267-274
  - 39 Markham, D.L. (1982) Shadowgraphic video and laser diffraction techniques for assessing drop size distributions in fuel nozzle sprays. Proc ICLASS-82 pp 293-302
  - 40 Simmons, H.C. and Lopera, D.L. (1969) A high speed spray analyser for gas turbine fuel nozzle. ASME Gas Turbine Conf., Cleveland, Mar. 1969
  - 41 Thompson, B.H. and Zinky, W.H. (1968) Holographic detection of submicron particles. *Applied Optics* 7 p12
  - 42 Bexon, R., Bishop, G.D. and Gibbs, J. (1975) Aerosol sizing by holography using the Quantimet. Quantimet No.3 (Cambridge Instruments), Nov. 1975
  - 43 Durst, F. and Umhauer, H. (1987) Local measurements of particle velocities, size distribution and concentration with combined laser Doppler particle sizing systems. LDA Symp, Technical University of Denmark, Lyngby Denmark
  - 44 Yule, A.J., Chigier, N.A., Adam, S. and Ungut, A. (1977) Particle size and velocity measured by laser anemometry *AIAA J. Energy*, 1 pp 220-228
  - 45 Farmer, W.M. (1974) Observation of large particles with a laser interferometer. *Applied Optics* 13 pp.610-622
  - 46 Swithenbank, J., Beer, J.M., Taylor, D.S., Abbott D., and McCreath C.G. (1976) A laser diagnostic for the measurement of droplet and particle size distribution. AIAA Paper No 76-69, 14th Aerospace Sciences Meeting
  - 47 Simmons, H.C. and Harding, C.F. (1981) Some effects of using water as a test fluid in fuel nozzle spray analysis. *Journal of Engineering for Power, Transactions of the ASME*. 103 pp118-123
  - 48 Williams, P.A., (1993) Laser diffraction particle sizing and spark-flash photography techniques for successful measurement of spark ignition fuel sprays. IMechE. C465/016
  - 49 King, C.F., 1978, Design of radial vortex amplifiers, PhD Thesis, University College Cardiff.
  - 50 Heywood, J.B., 1988, Internal combustion engine Fundamentals, McGraw Hill.

- 
- 51 Tennekes, H. and Lumley, J.L. (1972). A first course in turbulence. Cambridge, Mass.;London:M.I.T. Press
  - 52 Kolmogoroff, A.N., 1949, Disintegration of drops in turbulent flows. *Dokl. Akad. Nauk. SSSR* **66**, 825-828.
  - 53 Shinnar, R., (1961) On the behaviour of liquid dispersions in mixing vessels. *J. Fluid Mech.* **10**, 259-279
  - 54 Taylor, G.I., 1932. The viscosity of a fluid containing small drops of another fluid. *Proc. Roy. Soc.* **A138**, 41-48
  - 55 Hinze, J.O., 1955, Fundamentals of the hydrodynamic mechanism of splitting in dispersion processes. *A.I.Ch.E.J.* **1**, 289-295
  - 56 Kocamustafaogullari, G., Smits, S.R. and Razi, J., 1993, Maximum and mean droplet sizes in annular two-phase flow. *Int. J. Heat Mass Transfer* **37**, 955-965
  - 57 Jepson, D.M., Azzopardi, J. and Walley, P.B. (1989) The effect of gas properties on drop size in annular flow. *Int J. Multiphase Flow.* **15**, 327-339
  - 58 Levich, V.G., 1962. *Physico-chemical Hydrodynamics*, Prentice-Hall, Englewood Cliffs, NJ.
  - 59 Lopes, J.C.B. and Dukler, A.E. (1975) Droplet sizes, dynamics and deposition in vertical annular flow. University of Houston Report, NPHH-ER-4424
  - 60 Wicks, M. (1967) Liquid film structure and drop size distribution in two-phase flow. PhD Dissertation, University of Houston, Houston, Texas
  - 61 Cousins, L.B., and Hewitt, G.F. (1968) Liquid phase mass transfer in annular two-phase flow: droplet deposition and liquid entrainment. UKAEA Report, AERE-R5657
  - 62 Clark, M.M., 1987. Drop break-up in a turbulent flow-I Conceptual and modelling considerations. *Chem Eng Sci* **43**, 671-679
  - 63 Clark, M.M., 1987. Drop break-up in a turbulent flow-II Experiments in a small mixing vessel. *Chem Eng Sci* **43**, 681-692
  - 64 Jasper, J.J. (1972) The surface tension of pure liquid compounds. *Journal of Physical Chemical Reference Data.* **1** No 4, Pg 841
  - 65 Stone, R. (1992) Introduction to Internal Combustion Engines. Macmillan Press.
  - 66 Dicke, R.H. (1947) A computational method applicable to microwave networks. *J. App. Phys.* **18** October.
  - 67 Beck, S.M., Haider, H. and Boucher, R.F. (1995) Transmission line modelling of simulated drill strings undergoing water hammer. *Proc IMechE* **209** pp 419-427